

Zeitschrift: IABSE reports = Rapports AIPC = IVBH Berichte
Band: 49 (1986)
Rubrik: Theme 3: Composite light-gauge metal construction

Nutzungsbedingungen

Die ETH-Bibliothek ist die Anbieterin der digitalisierten Zeitschriften auf E-Periodica. Sie besitzt keine Urheberrechte an den Zeitschriften und ist nicht verantwortlich für deren Inhalte. Die Rechte liegen in der Regel bei den Herausgebern beziehungsweise den externen Rechteinhabern. Das Veröffentlichen von Bildern in Print- und Online-Publikationen sowie auf Social Media-Kanälen oder Webseiten ist nur mit vorheriger Genehmigung der Rechteinhaber erlaubt. [Mehr erfahren](#)

Conditions d'utilisation

L'ETH Library est le fournisseur des revues numérisées. Elle ne détient aucun droit d'auteur sur les revues et n'est pas responsable de leur contenu. En règle générale, les droits sont détenus par les éditeurs ou les détenteurs de droits externes. La reproduction d'images dans des publications imprimées ou en ligne ainsi que sur des canaux de médias sociaux ou des sites web n'est autorisée qu'avec l'accord préalable des détenteurs des droits. [En savoir plus](#)

Terms of use

The ETH Library is the provider of the digitised journals. It does not own any copyrights to the journals and is not responsible for their content. The rights usually lie with the publishers or the external rights holders. Publishing images in print and online publications, as well as on social media channels or websites, is only permitted with the prior consent of the rights holders. [Find out more](#)

Download PDF: 24.12.2025

ETH-Bibliothek Zürich, E-Periodica, <https://www.e-periodica.ch>



THEME 3

Composite Light-Gauge Metal Construction

Chairmen:

B. Kato, Japan, and T. Höglund, Sweden

Leere Seite
Blank page
Page vide

Behaviour of Steel Deck Reinforced Composite Floors

Comportement des planchers mixtes acier-béton

Tragverhalten von Stahl-Beton-Verbunddecken

Michel CRISINEL

Section Leader
Swiss Fed. Inst. Technol.
Lausanne, Switzerland

Michel Crisinel, born 1945, graduated from the Swiss Federal Institute of Technology in Lausanne in 1968 and worked for a consulting firm in Switzerland prior to his joining EPFL. He is now the research manager at the Institute of Steel Structures (ICOM) for both composite and cold-formed thin walled sheet steel structures.

Michael J. FIDLER

Senior Engineer
Cameron Taylor Partners
London, UK

Michael J. Fidler, born in 1957, graduated from University College London in 1979. He worked for four years with a consulting engineer on bridge design and spent two years at EPFL in Switzerland as a research engineer in steel structures. He currently works on the refurbishment of structures for a firm of consulting engineers.

Byron J. DANIELS

Structural Engineer
Swiss Fed. Inst. Technol.
Lausanne, Switzerland

Byron Daniels, born 1959, received his BSCE from Lehigh University in 1981. He worked as an engineer for Bethlehem Steel Corp. for two years involved with the design and repair of off-shore structures. After receiving a MSCE at the University of Texas at Austin in 1985, he is now studying the behaviour of composite floor systems for a doctoral thesis at EPFL.

SUMMARY

This paper presents a brief overview of previous studies on composite floors, employing profiled sheeting and concrete for use in buildings. Revisions to present design recommendations are proposed based upon results of a recent experimental programme conducted at EPFL. When carrying out performance testing, it is recommended that the post slip behaviour, brittle or ductile, be established. Factors of safety for these two types of behaviour and recommendations for further study are proposed.

RÉSUMÉ

Cette communication présente un aperçu des recherches effectuées à ce jour sur les planchers mixtes composés de tôles profilées recouvertes d'une dalle de béton. On y propose une révision des recommandations de calcul actuellement en vigueur, sur la base des résultats d'un programme expérimental récemment effectué à l'EPFL. On propose en particulier, lors de la réalisation d'essais de charge, de déterminer le caractère du comportement après glissement, ductile ou fragile. Des facteurs de sécurité pour ces deux types de comportement, ainsi que des recommandations pour des études à venir sont finalement proposés.

ZUSAMMENFASSUNG

Der vorliegende Bericht enthält eine Übersicht bisher durchgeführter Forschungsarbeiten auf dem Gebiete von Verbunddecken aus Profilblech mit darüber gegossener Betondecke. Aufgrund der Resultate aus einem an der EPFL durchgeführten experimentellen Forschungsprogramm wird eine Überarbeitung der bestehenden Berechnungsgrundlagen vorgeschlagen. Es wird insbesondere angeregt, bei der Durchführung von Belastungsversuchen zu untersuchen, ob das Tragverhalten nach erfolgter Relativverschiebung zwischen Profilblech und Beton duktil oder spröde ist. Für duktiles und sprödes Tragverhalten werden Sicherheitsfaktoren eingeführt. Schliesslich werden Anregungen für zukünftige Forschungsarbeiten gemacht.



1. REVIEW OF LITERATURE

For many years, engineers and designers have realised the advantages of combining profiled steel sheeting with a concrete slab to form a composite floor system. The first "modern" cold-formed composite floors were produced in the early 1950's and by the mid 1960's several manufacturers were producing a number of successful products. However, each manufacturer had to determine allowable loads through independent research.

The failure mode, most commonly occurring for typical cross sections and span lengths, is the loss of shear bonding between the profiled sheeting and the concrete slab. As a result, several research programmes were conducted to establish a design method for this mode of failure.

The first study was conducted in 1964 by Bryl [1] who proposed a design method based on allowable bending stress in an uncracked composite section, permissible bond stress and the ultimate strength of end anchorages. This method was subsequently recommended by the Swiss Institute of Steel Construction in 1973 [2].

Since 1967, several empirical equations have been proposed which have encompassed a variety of variables. The first extensive testing programme was conducted by Schuster, Porter and Ekberg which led to the development of the first of these equations [3] [4] [5]. All specimens in this test programme consisted of open trapezoidal ribs with embossments. Embossments are small indentations pressed into the webs of the profiled sheeting during the forming process. Of the 209 one way specimens tested only four failed by the flexure mode [6]. The majority failed due to shear-flexure cracking near a concentrated load. This was accompanied by a loss of shear bonding indicated by end slip in the shear span nearest the crack. End slip is defined as the relative movement between the concrete slab and the profiled sheeting at the end of the specimen.

The ultimate shear strength of a given profile is predicted by :

$$\frac{V_u s}{b d} = \frac{m \rho d}{\ell_v} + k \sqrt{f_{c,cyl}} \quad (1)$$

- V_u : maximum shear at failure obtained from tests [N],
- s : centre to centre spacing of shear transfer devices (a constant value over the length of the shear span, equal to unity for embossed sheeting),
- b : width of test specimen [mm],
- d : effective slab depth (distance from extreme concrete compression fiber to the neutral axis of the full cross section of the profiled sheeting) [mm],
- m : slope of the shear bond regression line,
- ρ : reinforcement ratio ($\rho = A_p / b d$, A_p : cross-sectional area of the profiled sheeting [mm²]),
- ℓ_v : length of shear span, the distance between an applied load and the nearest support or alternatively, the ratio of maximum bending moment to maximum shear force (for a uniformly distributed load use one fourth of the total span length) [mm],
- k : ordinate intercept of shear bond regression line,
- $f_{c,cyl}$: concrete cylinder strength at time of testing [N/mm²].

In equation (1), both m and k are constants derived from a regression analysis of the test data. This method of predicting ultimate shear bond capacity was accepted by the European Recommendations for Composite Structures in 1981 [7] and by the British Standards Institution in 1982 [8]. Also, it was adopted by the American Society of Civil Engineers in 1985 [9] and was proposed by the Commission of the European Communities (draft Eurocode 4) in 1984 [10].

Further experimental investigation was conducted by Schuster and Ling who employed both trapezoidal and rectangular profiled sheeting with embossments [11]. They found that some specimens could carry significant load after the initiation of end slip. It was assumed that "mechanical interlock" transfers shear between the slab and the steel sheeting when end slip is present. This lead to a simplification of equation (1) which is valid for both types of behaviour :

$$\frac{V_u}{b d} = \frac{m}{\lambda_v} + k \quad (2)$$

Equation (2) requires the determination of two constants, m and k , from a linear regression analysis of test data as does equation (1). Concrete strength and the reinforcement ratio have little effect on shear bond capacity. Thus, there is no significant difference between the results of equations (1) and (2) [11] [12]. In the description of the failure mechanisms, Schuster and Ling identified two components of shear bonding : mechanical and frictional. An assumed distribution of each component is proposed along the span both before and after end slip is observed [11].

In addition to the variables identified above, test programmes have been completed to study the effects of : the surface condition of the profiled sheeting [13], repeated loading [6], shoring conditions while the slab is poured [6] [13] and the thickness of the profiled sheeting [11]. Testing is required to determine ultimate shear strength for these and other variables not explicitly included in equations (1) and (2). For a manufacturer producing a range of products, the cost of such testing can be prohibitive. Seleim and Schuster proposed a semi-empirical design equation which included the thickness of the steel decking, t , [11] :

$$\frac{V_u}{b d} = \frac{k_1 t}{\lambda_v} + \frac{k_2}{\lambda_v} + k_3 t + k_4 \quad (3)$$

This is beneficial for manufacturers producing profiled sheeting with several different material thicknesses. As for equation (2), equation (3) was derived using specimens which exhibited end slip prior to failure. To use this equation, the values of k_1 , k_2 , k_3 and k_4 must be established by performing a multi-linear regression analysis of the test data.

Parsannan and Luttrell examined the ultimate load capacity of several different composite cold-formed floor specimens and also proposed a method which reduced the number of tests required [14]. This empirical equation may eliminate the need for testing if the section is similar to the data base from which it was derived. Further, Parsannan and Luttrell observed two types of behaviour after end slip was recorded. These were specimens unable to carry additional load (type 1) and specimens which had the ability to carry further load (type 2). It was observed that type 2 specimens could carry load after end slip was recorded on the second shear span. Finally, three types of shear bonding, chemical, mechanical and frictional, were identified and the relative importance of all three was proposed for both types of behaviour [14].

A comparison of design procedures, including equations (1), (2) and (3), was performed by Evans, Wright and Harding for a number of profiled sheetings produced in Great Britain [15]. Limitations and advantages of different design procedures were examined. The factors, m and k , in equations (1) and (2) were noted to have no physical meaning and thus, they cannot be related to shear bonding. At present, the need for performance testing is unavoidable due to the number of different types and the complexity of typical profiled sheetings. Based upon this review of the literature, the following objectives were established :

- confirm the load-deflection behaviour of composite floors commonly used in Switzerland,
- examine the present design procedures and propose recommendations,
- identify areas of research.

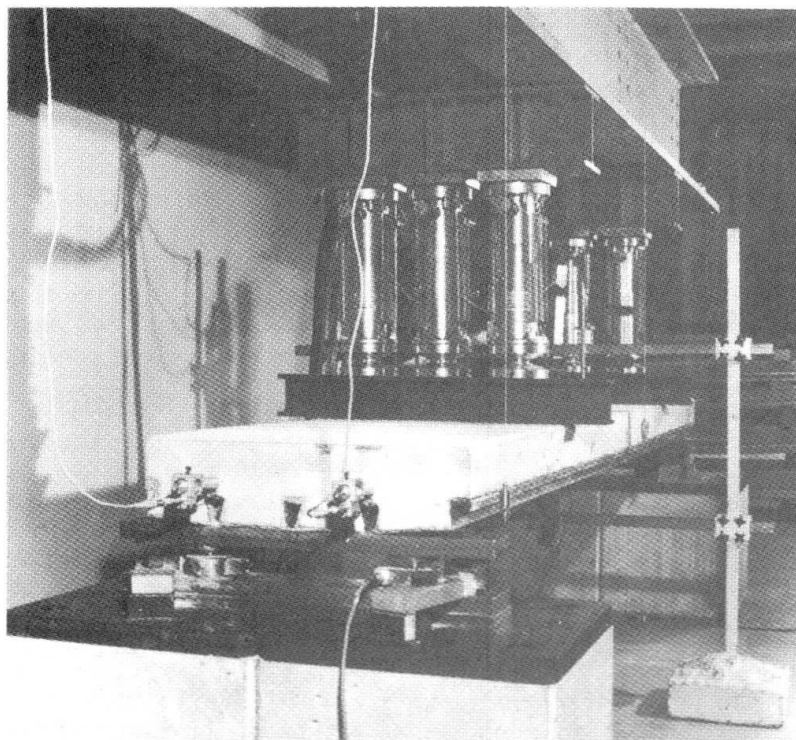


2 EXPERIMENTAL INVESTIGATION

2.1 Test specimens

Six specimens were constructed and tested to failure. Each test specimen consisted of a single profiled sheeting 3200 mm long and a concrete slab approximately 600 mm wide. These specimens were simply supported during testing; the span length was 3000 mm. Two line loads of equal magnitude, placed symmetrically about the midspan, were applied to each specimen.

Three different types of sheeting were selected according to their availability in Switzerland and for their different methods of providing shear transfer. Although



a) Test frame and instrumentation (specimen HR 51:160).

b) Specimen dimensions.

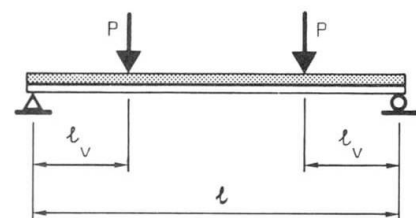


Figure 1 : Test set-up.

Table 1 : Dimensions and material properties.

CROSS-SECTION	SPECIMEN	NOMINAL VALUES [mm]					MEASURED VALUES [N/mm ²]	
		$l^*)$	$l_v^*)$	d	t	b	f_y	$f_{c,cyl}$
	MR 58:110	3000	1020	110	1.00	635	313	35
	MR 58:160	3000	780	160	1.00	635	313	35
	HR 51:110	3000	1020	110	0.91	624	305	35
	HR 51:160	3000	780	160	0.91	624	305	35
	HI 55:110	3000	1020	110	0.88	680	307	35
	HI 55:160	3000	780	160	0.88	680	307	35

*) See Figure 1 b).

several modes of shear transfer have been identified, two are commonly used [4]. These two types were included in this investigation and are :

- embossments pressed into the webs,
- a re-entrant rib geometry.

Thus, the profiled sheetings consisted of open trapezoidal ribs, dovetailed ribs and alternating open trapezoidal and dovetailed ribs. The open trapezoidal sheeting had inclined embossments on the webs of the ribs and all other profiled sheetings were not embossed. The nominal rib depths ranged from 51 mm to 58 mm and nominal material thicknesses ranged from 0.88 mm to 1.0 mm.

A minimum slab thickness of 110 mm was selected to guarantee a minimum concrete cover of 50 mm [7]. A maximum slab thickness of 160 mm was selected since it is typically used in normal construction. Concrete mix details were consistent with current concreting procedures. Thus, a pumping concrete mix was specified. The maximum aggregate size was 30 mm and 325 kg of ordinary portland cement was used per m³ of mix. A 6 mm diameter 150 x 150 mm wire mesh was placed on metal supports such that a cover depth of 25 mm below the surface of the concrete was maintained during pouring of the slab.

Shoring was placed to support the profiled sheeting at midspan until the concrete had cured. Tensile specimens, cut from the profiled sheeting, and concrete cylinders were tested according to current standards to determine material properties.

A typical test specimen is shown in Figure 1 a) and a sketch illustrating the relative positions of the supports and applied loads is provided in Figure 1 b). A summary of nominal specimen dimensions, load locations and actual material properties is given in Table 1.

2.2 Test procedure

Loads were applied using hydraulic jacks and transmitted to the specimen using 100 mm wide spreader beams. Six electric transducers were used during each test. Two transducers measured midspan deflection. At each end of the specimen, two transducers measured end slip between the concrete slab and the profiled sheeting.

All tests were displacement controlled. A midspan deflection rate of 0.2 mm/min was applied until end slip was first recorded. Thereafter a rate of 0.5 mm/min was used. At a midspan deflection of 30 mm (for the specimens tested $\ell/100$) testing was discontinued. The test set-up, hydraulic jacks and transducers are shown in Figure 1 a). A more detailed review of the test specimens and test procedure is given in [16].

2.3 Test results

The following behaviour was the same for all six specimens tested : upon initial loading, a linear load-midspan deflection curve was recorded. Subsequently, both non-linearity and reduced stiffness was observed. This reduction first occurred when small flexural cracks formed in the lower concrete fibers near midspan in the region of constant bending moment. Cracking was heard sporadically but could not be observed visually as the cracks were concealed by the profiled sheeting. End slip was not recorded at this load level. Such cracking continued to occur until a critical value of horizontal shear stress between the profiled sheeting and the concrete slab was reached. This was indicated by :

- a loud noise,
- an abrupt reduction of applied load,
- the initiation of end slip in the shear span closest to the crack.

The magnitude of initial slip was about 0.3 mm for the embossed specimens and 0.5 mm for the specimens without embossments. Initial end slip is defined as the magnitude of end slip when it is first recorded.

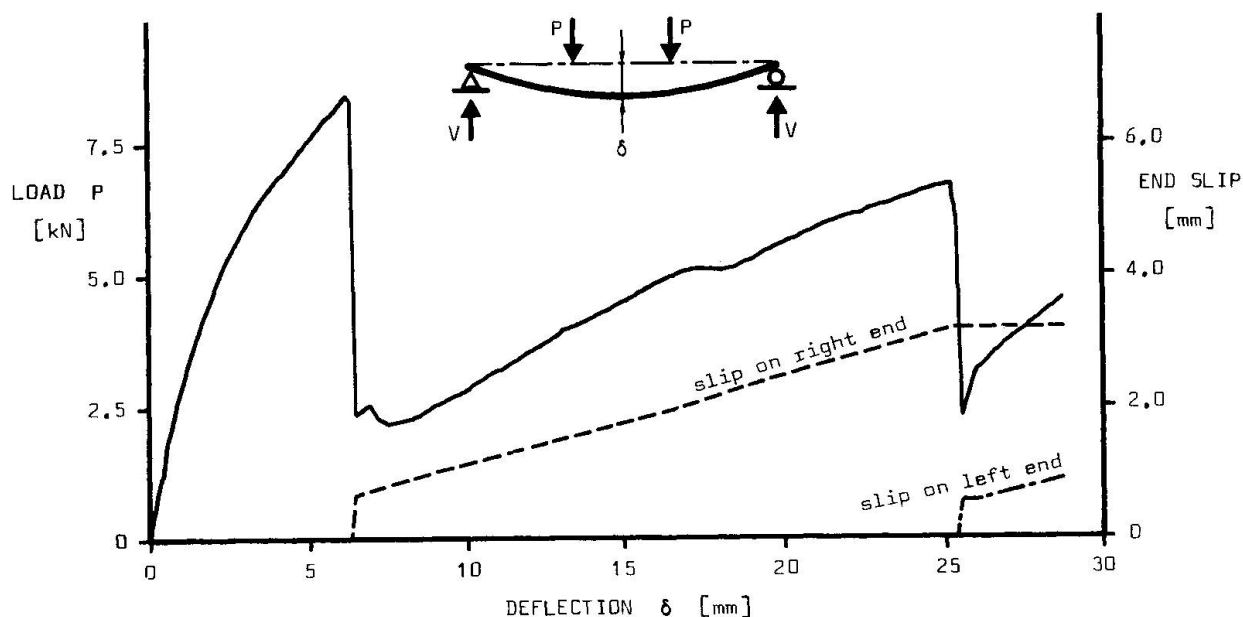


Figure 2 : Brittle behaviour (specimen MR 58:110).

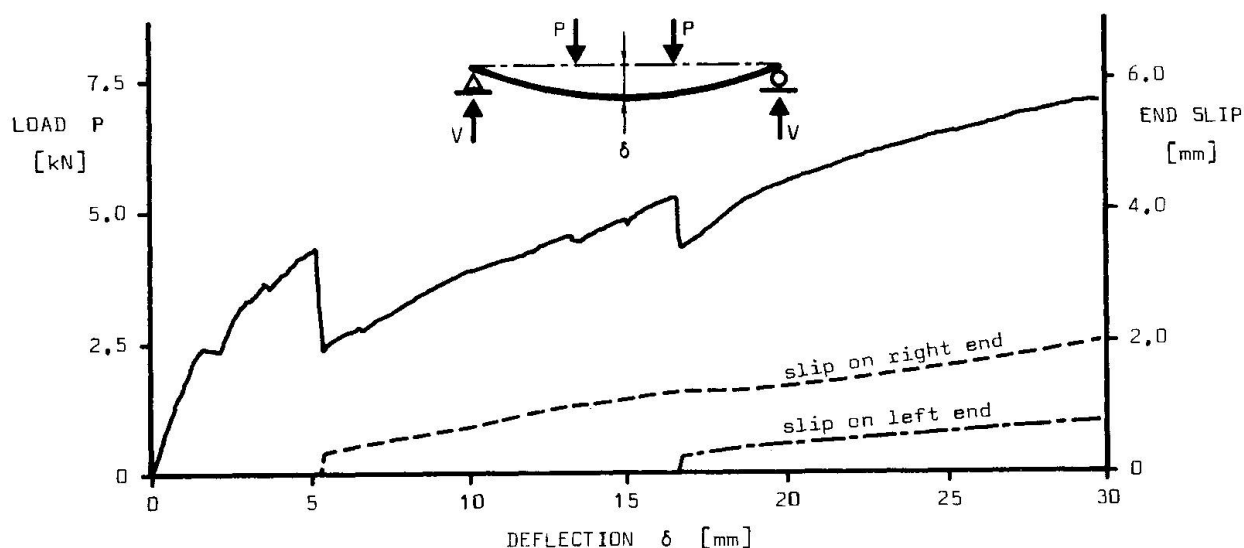


Figure 3 : Ductile behaviour (specimen HI 55:110).

After the initiation of end slip the load-deflection behaviour of the specimens varied widely. Some specimens were able to carry applied loads greater than that which initiated end slip, other specimens did not regain their previous load carrying capacity. Two of the six load-midspan deflection curves from this experimental programme are shown in Figures 2 and 3. These two specimens were chosen as they best illustrate the range of post slip behaviour observed.

3. ANALYSIS OF TEST RESULTS

3.1 Calculation of theoretical limits

Upper and lower bounds of load-deflection behaviour for each specimen was calculated. Firstly, each specimen was analysed assuming the concrete slab was

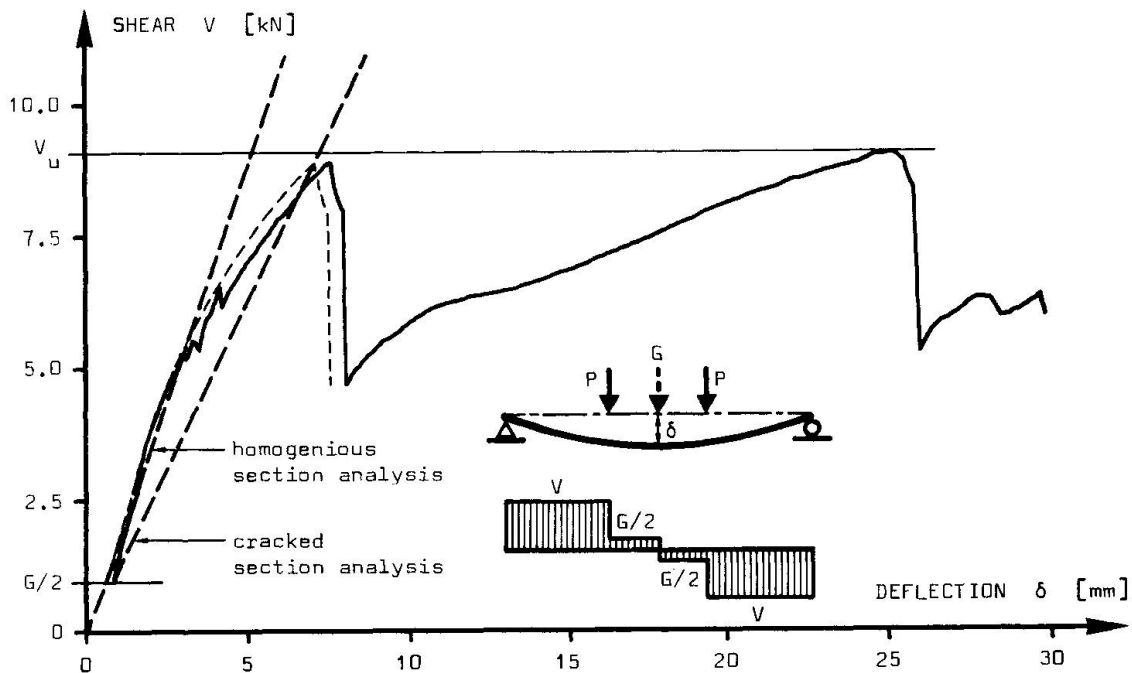


Figure 4 : Homogeneous and cracked section analysis (specimen HR 51:110).

uncracked and secondly, an analysis was performed assuming full composite interaction of the cracked section.

To compare theoretical values and test results, the initial shear and deflection due to self weight must be included. As noted earlier, shoring was inserted at midspan in order to limit the deflection of the profiled sheeting when the concrete slab was poured. After removal of the shoring, the dead weight of the concrete slab can be modelled by a concentrated load at midspan. For the static system used in this test series, the total shear in each shear span is defined as :

$$V = P + \frac{G}{2} \quad (4)$$

V : total shear in each shear span,

P : the load applied by each hydraulic jack (total applied load to the specimen : 2 P),

G : support reaction of the shoring due to the dead weight of the concrete slab.

A typical comparison between test results and these bounds is shown in Figure 4. The homogeneous section analysis closely describes the initial behaviour of the specimen whereas the cracked section analysis best describes behaviour just prior to the initiation of end slip. For all specimens tested, the shear and deflection where end slip initiated is between these two bounds.

3.2 Previous results

Design procedures which employ equation (1) are the most commonly used for classifying the behaviour of composite cold-formed profiled specimens. These procedures all require the experimental determination of ultimate load. A minimum of six test results is standard practice. Most researchers perform two groups of three tests having different span lengths and slab thicknesses. A regression analysis of these results determines the unknown constants, m and k, in equation (1) [3] [6]. These constants enable a prediction which is a straight line when plotted using the axes in Figure 5. Six lines from five studies are presented in Figure 5 [5] [6]

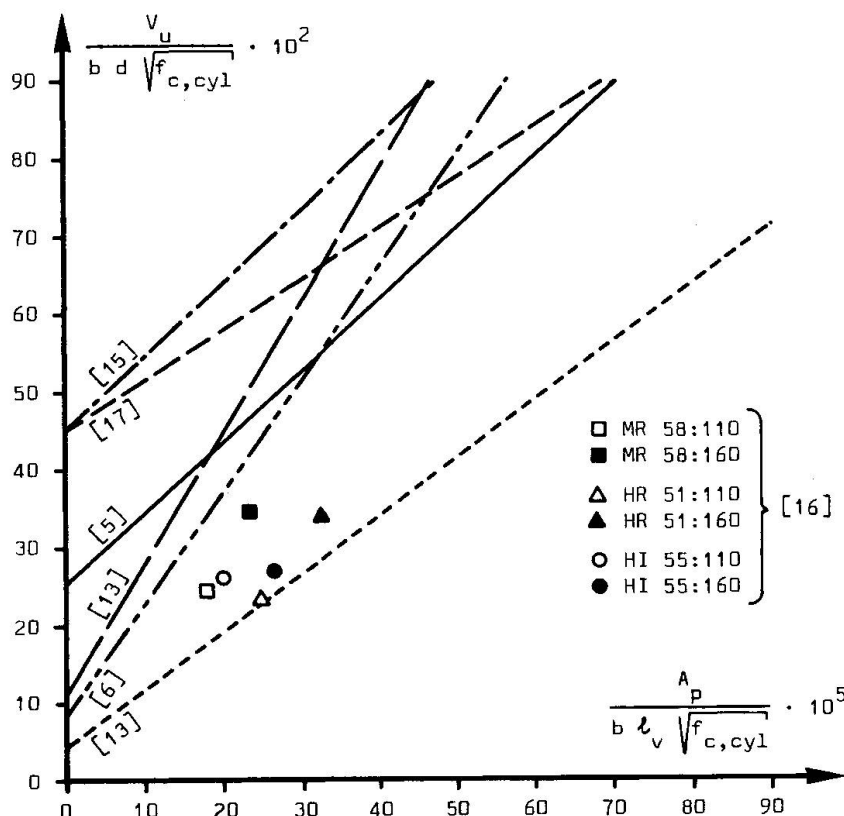


Figure 5 :

Comparison of experimental predictions using eq. (1).

V_u in [N]

$f_{c,cyl}$ in [N/mm²]

[13] [15] [17]. No systematic agreement between these predictions may be seen, except for the positive slope. Therefore, extrapolation of the lines beyond the supporting test data and application to other profiles cannot be justified.

Test results from the present study are compared with the predictions of Figure 5 using the same parameters. These results are enclosed by the upper and lower predictions.

3.3 Classification of behaviour

The ultimate shear strength predicted using equation (1) is based upon the average values of ultimate load observed during testing. This method does not take into account other parameters. For example, load capacity after end slip is recorded may vary, see Figures 2 and 3. These two types of behaviour, named type 1 and type 2 by Luttrell [14], are designated "brittle" and "ductile" in this report. This terminology was also used by Aribert and Moum [18].

Brittle behaviour (type 1) is accompanied by the initiation of end slip when the ultimate load is recorded. Ductile behaviour (type 2) occurs when the ultimate load subsequently exceeds the load which initiated end slip, and when midspan deflection is several times greater than observed at first slip.

It is useful to introduce two ratios, P_{max}/P_{slip} and $\delta_{max}/\delta_{slip}$ to quantify the "reserve ductility". Limiting ratios can be used to define ductile and brittle behaviour.

P_{max} : the ultimate load observed before a midspan deflection of 30 mm is recorded,

δ_{max} : the midspan deflection corresponding to P_{max} ,

P_{slip} : the load applied to the test specimen when initial end slip is observed,

δ_{slip} : the midspan deflection corresponding to P_{slip} .

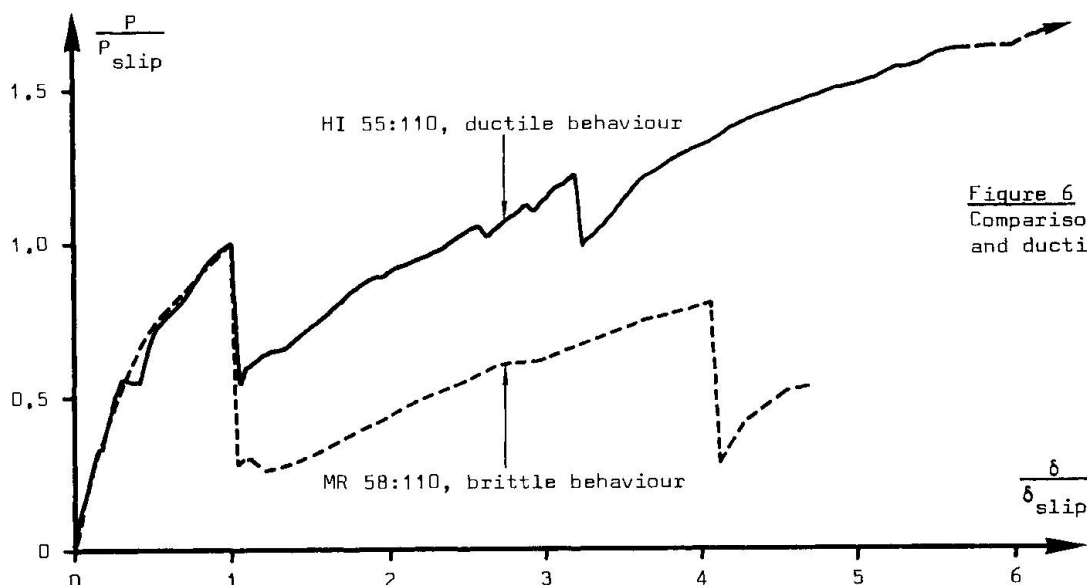


Figure 6 :
Comparison of brittle
and ductile behaviour.

Normalized load-deflection curves for brittle and ductile specimens are presented in Figure 6. They illustrate the differences in post slip behaviour between brittle and ductile behaviour. The ultimate load in the ductile specimen is 1.63 times greater than the applied load at first slip. The midspan deflection at ultimate load is 5.7 times larger than the deflection at first slip. This agrees with the results of Schuster and Ling who observed that the applied load at first slip may be between 50 and 60 % of the ultimate load [11]. Thus, the following ratios are proposed to define ductile behaviour :

$$\frac{P_{\max}}{P_{\text{slip}}} > 1.5 \quad \frac{\delta_{\max}}{\delta_{\text{slip}}} > 4.0$$

If either ratio is less than the limits given above, the behaviour is termed brittle.

4. SAFETY CONSIDERATIONS

Safety factors consist of several parts. These may be divided into two partial safety factors. One accounts for uncertainties in the strength of a component and the other accounts for variations in loading. The strength partial safety factor consists of three parts for composite profiled floors. These are :

- mode of failure,
- scatter of test results,
- warning prior to, and consequence of, failure.

Horizontal shear debonding is the dominant mode of failure. For this type of failure a partial safety factor of 1.25 is commonly accepted [10]. This partial safety factor remains the same for both brittle and ductile behaviour. Scatter between test results is treated differently by code writing organizations. A factor of 1.15 is used in this study assuming that a minimum of six tests are performed and that the test values do not vary from the regression line by more than 10 % [10]. The third part of the strength safety factor cannot be determined using statistics alone. In accordance with other structural elements, such as reinforced concrete beams, this factor was established as 1.0 for ductile behaviour and 1.25 for brittle behaviour. This corresponds to the factors of safety used in under-reinforced and over-reinforced concrete beams.

Usually, the partial safety factor for loading is taken to be 1.4 for floor systems [19]. The following overall factors of safety are then obtained :



Brittle composite floors : $\gamma_m = 1.25 \cdot 1.15 \cdot 1.25 = 1.8$

$$\gamma_f = 1.4$$

$$\gamma = \gamma_m \gamma_f = 1.80 \cdot 1.4 = 2.5$$

Ductile composite floors : $\gamma_m = 1.25 \cdot 1.15 \cdot 1.0 = 1.44$

$$\gamma_f = 1.4$$

$$\gamma = \gamma_m \gamma_f = 1.44 \cdot 1.4 = 2.0$$

γ : overall safety factor,

γ_m : partial safety factor for material,

γ_f : partial safety factor for loading.

The overall safety factor proposed by the draft Eurocode 4 is 2.0 regardless of behaviour [7]. This is the same as the factor of safety proposed for ductile specimens.

5. CONCLUSIONS

The following conclusions are limited to cold-formed composite floors which fail by loss of horizontal shear bonding through the occurrence of end slip. In addition, they apply to profiled sheetings using either embossments pressed into the webs or re-entrant web profiles.

1.- Two types of load-deflection behaviour exist, brittle and ductile.

2.- Brittle and ductile behaviour is distinguished using the two ratios P_{max}/P_{slip} and $\delta_{max}/\delta_{slip}$. The ratios defining ductile behaviour are :

$$\frac{P_{max}}{P_{slip}} > 1.5 \qquad \frac{\delta_{max}}{\delta_{slip}} > 4.0$$

If either one of these ratios is smaller than the values given above, the behaviour is termed brittle.

3.- Factors of safety which are dependent upon load-deflection behaviour can be adopted by present design methods. These factors are proposed to be :

$$\gamma = 2.5 \text{ for brittle behaviour}$$

$$\gamma = 2.0 \text{ for ductile behaviour}$$

4.- The ultimate shear strength of profiles which are not yet included in the draft Eurocode 4 design procedure (those relying upon profile shape alone to transfer shear bonding) can be included if these safety factors are employed.

5.- When equations (1) and (2) are used to predict the shear strength of a specimen, the results must be used with caution. Variables not expressly included in the equation can cause large variations in behaviour.

6. RECOMMENDATIONS

Presently, the behaviour of cold-formed profiled floors is not adequately described by design formulations. The following recommendations are made :

1.- Effect of first end slip on ultimate shear strength. Present design methods define ultimate load but do not take into account differences in behaviour. A more rational design basis which recognizes the differences between brittle and ductile behaviour should be adopted. This change will enable current design methods, for example Eurocode 4, to safely predict the ultimate shear strength of a wider variety of specimens.

2.- End anchorage. Composite cold-formed floors constructed with end anchorages, tied to the supporting steel frame, may restrict end slip. These end anchorages can take several forms :

- shear studs welded through the profiled sheeting to the supporting beams,
- cold-formed shear connectors with fasteners driven through the profiled sheeting,
- hot-rolled end angles or studs welded directly to the supporting beams.

Further research is needed in order to examine the degree of horizontal shear transfer accomplished by end restraints. Specimens which exhibit brittle behaviour may become ductile if sufficient shear capacity is added using end anchorages.

3.- Other variables affecting strength. The following variables influence the strength of cold-formed composite floors and consequently they should be considered in design formulations :

- continuous span composite floors,
- the presence of steel reinforcement,
- propping the deck prior to pouring the slab,
- surface condition of the profiled sheeting,
- repeated loadings,
- end anchorages,
- etc.

Steel deck reinforced composite construction may have applications in structures such as car parks and more recently also in bridges. This presents additional challenges since the effects of weathering and repeated loadings require additional examination.

ACKNOWLEDGMENTS

The first author wishes to express his appreciation to the staff at ICOM who contributed to the preparation of this report, in particular M.J. Fidler who conducted the tests and B.J. Daniels for his assistance in preparing the text. Partial funding for this project was supplied by grants from several manufacturers of cold-formed sheeting.

REFERENCES

- [1] BRYL, S. The composite Effect of Profiled Steel Plate and Concrete in Deck Slabs. *Acier-Stahl-Steel*, Brussels, vol. 32, no 10, 1967, pp. 453-459.
- [2] BADOUX, J.-C., CRISINEL, M. Recommandations pour l'utilisation de tôles profilées dans les planchers mixtes du bâtiment. Publication B5, Zurich, Centre suisse de la construction métallique, 1973.
- [3] SCHUSTER, R.M. Composite Steel-Deck-Reinforced Concrete Systems Failing in Shear-Bond. 9th Congress, Preliminary Report, Zurich, IABSE, 1972, pp. 185-191.
- [4] PORTER, M.L., ECKBERG, C.E. Design Recommendations for Steel Deck Floor Slabs. University of Missouri-Rolla, Third International Specialty Conference on Cold-Formed Steel Structures, vol. II, 1975, pp. 761-791.
- [5] PORTER, M. L., EKBERG, C. E., GREIMANN, L. F., ELLEBY, H.A. Shear-Bond Analysis of Steel-Deck-Reinforced Slabs. *Journal of the Structural Division*, New York, vol. 102, no 12, 1976, pp. 2255-2268.
- [6] PORTER, M. L., EKBERG, C. E. Compendium of ISU Research on Cold-Formed Steel-Deck-Reinforced Slab Systems. Bulletin 200-78263, Iowa State University, Engineering Research Institute, 1978.



- [7] European Convention For Constructional Steelwork (ECCS). Composite Structures. London, The Construction Press, 1981.
- [8] Structural Use of Steelwork in Building, Part 4 : Code of practice for design of floors with profiled sheeting. British Standard BS 5950, London, British Standard Institution, 1982.
- [9] Specifications for the Design and Construction of Composite Slabs and Commentary on Specifications for the Design and Construction of Composite Slabs. Technical Council of Codes and Standards Division, New York, American Society of Civil Engineers, 1985.
- [10] Composite Steel and Concrete Structures, First Draft. Eurocode 4, Brussels, The Commission of the Europeans Communities, 1984.
- [11] SCHUSTER, R. M., LING, W. C. Mechanical Interlocking Capacity of Composite Slabs. University of Missouri-Rolla, Fifth International Specialty Conference on Cold-Formed Steel Structures, 1980, pp. 387-405.
- [12] SELEIM, S. S., SCHUSTER, R. M. Shear-Bond Capacity of Composite Slabs. University of Missouri-Rolla, Sixth International Specialty Conference on Cold-Formed Steel Structures, 1982, pp. 511-531.
- [13] PORTER, M. L., EKBERG, C. E. Coating Effects of Cold-Formed Steel Deck Slabs. University of Missouri-Rolla, Fifth International Specialty Conference on Cold-Formed Steel Structures, 1980, pp. 369-386.
- [14] PRASANNAN, S., LUTTRELL, L. D. Flexural Strength Formulations for Steel-Deck Composite Slabs. Morgantown, West Virginia University, 1984.
- [15] EVANS, H. R., WRIGHT, H. D., HARDING, P. W. Composite Floors : Comparisons of Performance Testing and Methods of Analysis. IABSE Reports, vol. 48, Zurich, 1985, pp. 219-225.
- [16] CRISINEL, M., FIDLER, M. J., DANIELS, B. J. Flexure Tests on Composite Floors with Steel Sheeting. Publication ICOM 158, Ecole Polytechnique Fédérale de Lausanne, 1986.
- [17] LONG HUNG, H., FULOP, A., MOUM, C. Planchers à bacs collaborants, recherche expérimentale. Annales de l'Institut Technique du Bâtiment et des Travaux Publics, Paris, no 363, 1978, pp. 86-105.
- [18] ARIBERT, J.-M., MOUM, C. Efficacité de la connexion dans les planchers mixtes de bâtiment. IABSE Reports, vol. 48, Zurich, 1985, pp. 227-236.
- [19] Norme SIA 161 : Constructions métalliques. Zurich, Société suisse des ingénieurs et des architectes, 1979.

Long Span Composite Slabs

Planchers mixtes à grande portée

Verbunddecke mit grossen Spannweiten

Jan STARK

Civil Engineer
Institute TNO, Univ. of Technol.
Rijswijk, the Netherlands



Jan Stark, born in 1939, received his civil engineering degree at the Delft University of Technology. He is deputy director of the Institute TNO for Building Materials and Building Structures and lectures at the Eindhoven University of Technology. Jan Stark is a member of a number of national and international professional committees.

SUMMARY

In this paper specific design aspects of long span composite slabs, with deep steel sections and relatively small ribs, are discussed. Results are given of a numerical study on the rotational capacity of such sections, leading to conclusions on the applicability of plastic analysis. A simplified method is given for the calculation of the ultimate moment. A prototype of a new special steel deck element for use in ground floors in housing is presented. This element provided with insulation is designed to span up to 5,50 m without temporary support.

RÉSUMÉ

Cette communication traite des aspects spécifiques du dimensionnement des planchers mixtes à grandes portée, à profil de grande hauteur et à petites nervures. Les résultats d'une étude numérique sur la capacité de rotation de tels profils sont présentés, ainsi que les conclusions sur la possibilité de leur appliquer une analyse plastique. Une méthode simplifiée de calcul des moments ultimes est proposée. Le prototype d'une plaque nervurée en acier pour planchers mixtes de maisons d'habitation est présenté. Cet élément, comportant une isolation thermique, est dimensionné pour franchir une portée de 5,5 m sans étai intermédiaire.

ZUSAMMENFASSUNG

In diesem Aufsatz werden Entwurfsaspekte von Verbunddecken mit grossen Spannweiten behandelt, die mit hohen Stahlblechprofilen und relativ schmalen Betonrippen ausgestattet sind. Es werden Ergebnisse einer numerischen Studie über Rotationsfähigkeit dieser Querschnitte mitgeteilt, die Schlussfolgerungen über die Anwendungsmöglichkeit der Plastizitätstheorie zulassen. Eine vereinfachte Methode zur Berechnung der Biegetragfähigkeit wird gegeben. Ein Prototyp eines neuen Deckenelementes für die Anwendung in Wohnhäusern wird präsentiert. Dieses mit Isolierung versehene Element wurde für Spannweiten bis 5,5 m entworfen.



1. INTRODUCTION

Two very important advantages of structural steel for buildings are simplicity and speed of construction. To exploit these advantages optimally, the design of the floor construction should fit within the total concept of the structural steel design. For office and apartment buildings an efficient structural solution is to use steel frames spaced at distances of 5-6 m. and composite floors directly spanning from main beam to main beam without secondary girders. The use of temporary supports (props) under the steel sheet in the construction phase should be avoided. This leads to sheets with deep profiles, relative small ribs and a minimal concrete cover (see f.e. Fig. 3). However, there are hindrances for the use of these types of floors:

- According to some standards the height of the compression zone of the concrete may not exceed a certain maximum f.e. half the effective depth of the slab;
- The use of simple plastic design for the determination of the moment capacity is not generally permitted for deep decks. A more complicated non linear flexural strain analysis is then required;
- As the ribs are shallow, the vertical shear is more often critical. The design rules for the determination of the vertical shear capacity in most standards are overconservative. The contribution of the steel sheet for the vertical shear is normally neglected, which is obviously not correct especially for deep decks with unproped construction.

This paper presents results of a study undertaken as a contribution to level the first two hindrances.

For long spans other forms than trapezoidal profiled sheets are also possible. As an example, a prototype for such a special designed deck element for ground floors in housing will be presented.

2. ROTATION CAPACITY IN POSITIVE BENDING

If a reinforced concrete slab is "over-reinforced" the rotation capacity may be too small. This is caused by premature crushing of the concrete before the reinforcement yields. Therefore, the amount of reinforcement should be limited. In concrete codes this is achieved indirectly by setting a maximum for the height of the compression zone of the concrete. Often the same rule is also adopted or referred to in specs for the design of composite slabs. For example BS 5950 - Pt 4 [3] states: 'Unless the slab has compression reinforcement, the depth of the stress block for the concrete should not exceed $0.5 d$.' However, intuitively can be expected that with the same reinforcement ratio^s the rotation capacity of the considered composite cross-sections is more favourable compared with reinforced concrete. This is based on the following facts:

- The bending strength of the profiled steel sheet (reinforcement) itself is considerable, especially in case of deep decks for long spans;
- The self weight of the structure is carried by the sheet alone leading to considerable stresses in the sheet before composite action is effective;
- The yield stress (strain) of sheet material is normally smaller than for rebars.

To verify whether this holds true a numerical parameter study is carried out. With a special developed computerprogram based on non linear flexural strain analysis moment-curvature relations have been determined for a number of cross-sections. The basic assumptions of the calculations are:

- Plane sections remain plane after bending;
- Concrete in tension is neglected;
- After composite action is effective the interaction is complete (no slip);
- The stress-strain relation for steel is as shown in Fig. 1a;
- For the stress-strain relation for concrete two cases are considered as shown in Fig. 1b:

- . a bilinear diagram, according to the Dutch Concrete Code, with a maximum strain of $\epsilon_u = 3.5 \text{ ‰}$;

because the numerical calculation should simulate physical tests as close as possible, a more realistic stress-strain diagram with a falling branch is also considered. This diagram is based on physical tests given in [4].

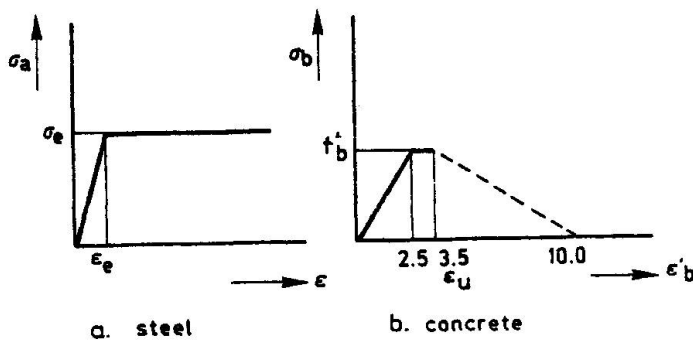


Fig. 1 Stress-strain relation for steel and concrete

In Fig. 2 the effect of the height of the concrete cover h_b on the strain- and stress-distribution is illustrated qualitatively. Two cases are shown:

- h_b is sufficient great to cause yielding of the sheet over the full height;
- h_b is so small that the height of the compression zone x exceeds h_b . The steel is still partial elastic when $\epsilon_b = 3.5 \text{ ‰}$.

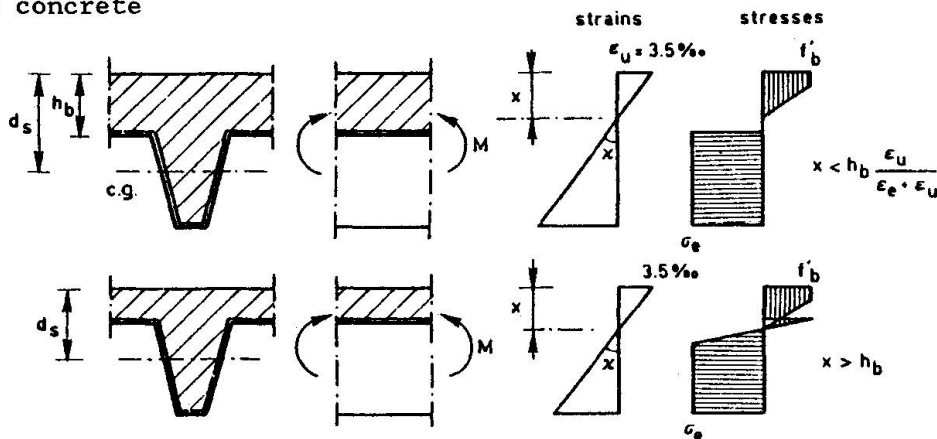


Fig. 2 Strain- and stress distributions

The parameter calculations have been carried out for the three sheet profiles shown in Fig. 3. The following parameters have also been varied:

- The concrete cover is varied from 50 to 150 mm;
- The concrete strength $f'_b = 14, 18$ and 24 N/mm^2 ;
- The yield strength of the sheet: $\sigma_e = 280, 320$ and 500 N/mm^2 ;
- The method of construction: propped resp. unpropped.

In fig. 4 the calculated moment-curvature relations for floor type II, with $f'_b = 18 \text{ N/mm}^2$ and $\sigma_e = 500 \text{ N/mm}^2$, are given for different heights of the concrete cover h_b . This is a rather extreme case with a relative low concrete strength and an unusual high yield strength of the steel sheet. The results for other cases are similar. Remarkable is that at maximum moment the concrete strain is greater than 3.5 ‰ as indicated in Fig. 4. This means that although the concrete strength decreases (falling branch in σ - ϵ diagram) the moment still increases. Very important is the fact

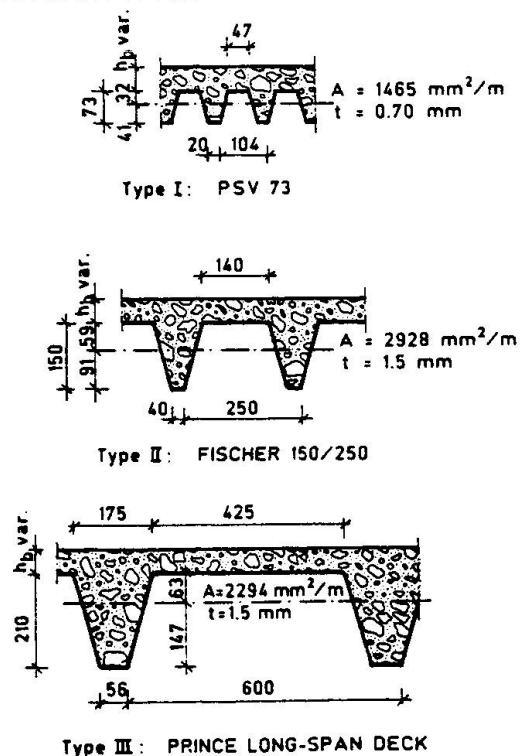


Fig. 3 Considered cross-sections



that both the curvature at $\epsilon'_b = 3.5\text{‰}$ and the curvature at M_{\max} are greater for the smaller values of h_b . For the case given in Fig. 4 is $x > h_b$ for $h_b < 80\text{ mm}$. This leads to the conclusion that from the point of view of rotation capacity, there seems to be no reason to put restrictions on the application of deep sections with minimal concrete cover. This conclusion should be confirmed by experimental evidence. In Fig. 5 the calculated moment-curvature diagrams are given for two cases with propped and unpropped construction. The ultimate moment in both cases is independent of the construction method as can be expected on theoretical basis [2]. The deformation capacity is greater for unpropped construction.

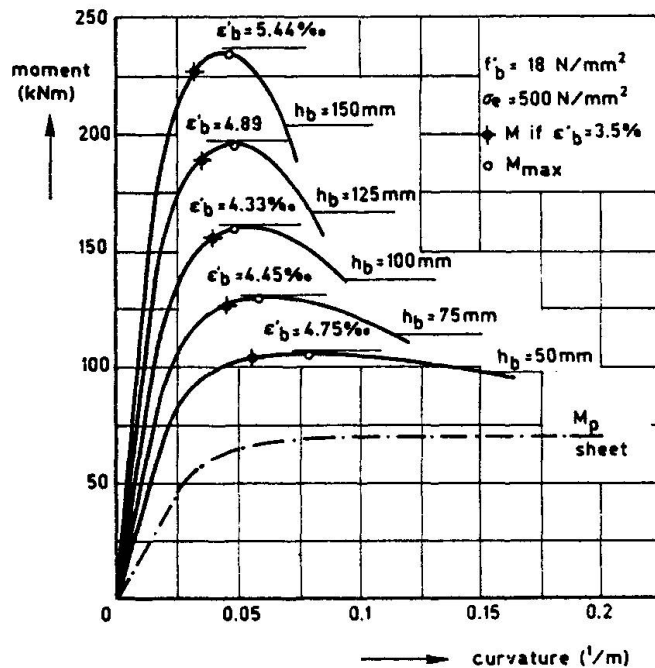


Fig. 4

Effect of variation of concrete cover h_b on moment-curvature relation

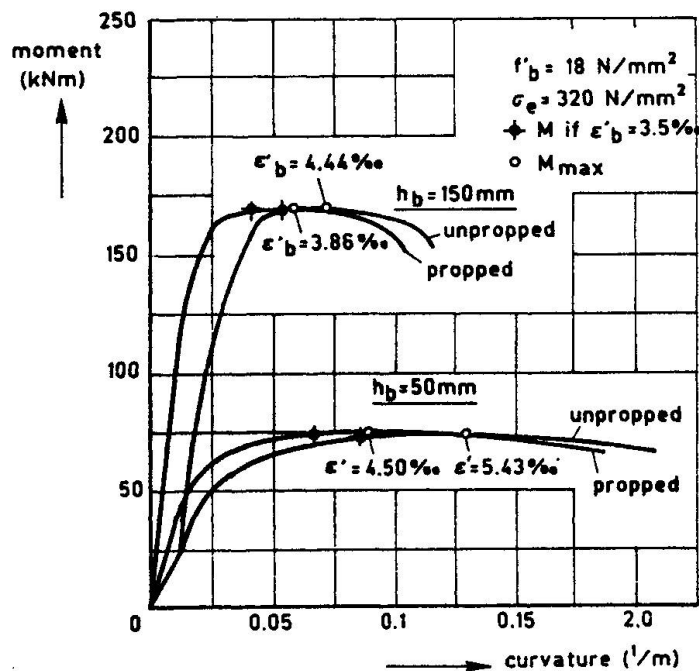


Fig. 5

Illustration of the influence of the construction method

3. SIMPLIFIED CALCULATION METHOD FOR ULTIMATE MOMENT

Use of non linear flexural strain analysis as described in paragraph 2 is not suitable for allday practical design work. Therefore a simplified method is developed. Two simplifications are introduced (see Fig. 6). The structural form is simplified by neglecting the concrete rib and a second simplification is that both steel and concrete are assumed to be ideal plastic materials. For steel this is a usual assumption. For concrete the difference between reality and idealisation is greater. To compensate for the effect of this unsafe idealisation, the design stress of the concrete f'_b is reduced with a factor k .

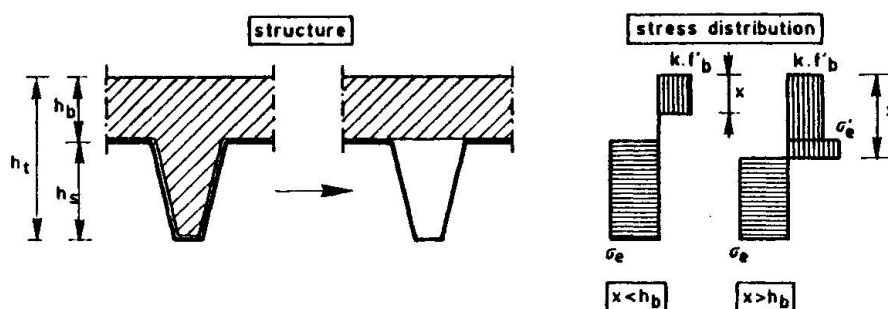


Fig. 6

Assumptions
for simplified
calculation
methods

There are two possible cases to be considered, depending on the height x of the compression stress block. For the type of floors under consideration practically ever is $x > h_b$. Although much simplified now, the calculation for this case is still elaborate. Therefore, a further simplification is introduced.

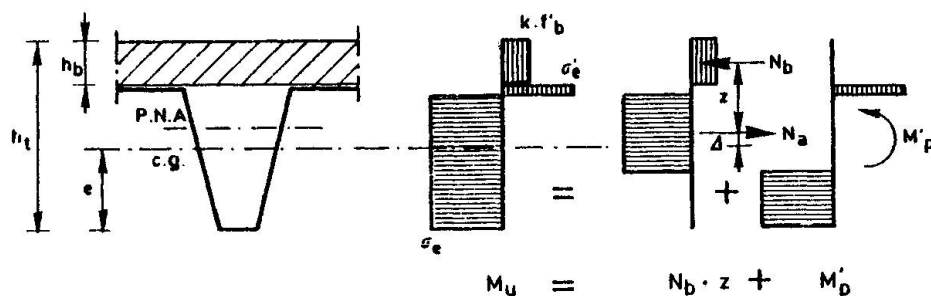


Fig. 7

Model for
further
simplification

As shown in Fig. 7 the stress distribution is split into two parts leading to two components of the ultimate moment. From equilibrium follows that the normal force in the sheet is equal to N_b . In this case $N_b < A\sigma_e$ so the steel section can resist an additional so called reduced plastic moment M'_p . The value of M'_p can be determined from the yield contour for combined effect of N and M on the cross-section. The yield contours have been calculated for 8 different types of sections. It has been found that the curves form a narrow band as shown in Fig. 8.

The curves can be approximated by the expression:

$$M'_p = 1.25 M_p \left(1 - \frac{N_a}{A\sigma_e} \right)$$

where: M_p is the unreduced plastic moment.

The only unknown value is now the lever arm z . If $N_a = A\sigma_e$ ($x \leq h_b$) the line of application N_a goes through the centre of gravity. However, for smaller values of N_a the line of application shifts from the centre of gravity to the plastic neutral axis as illustrated in Fig. 9. If, as a very simple approximation is assumed that this shift is linear proportional to $N_a/A\sigma_e$ the distance e_{px} from



N_a to the bottom fibre follows from the expression:

$$e_{px} = e_p - (e_p - e) \frac{N_a}{A\sigma_e}$$

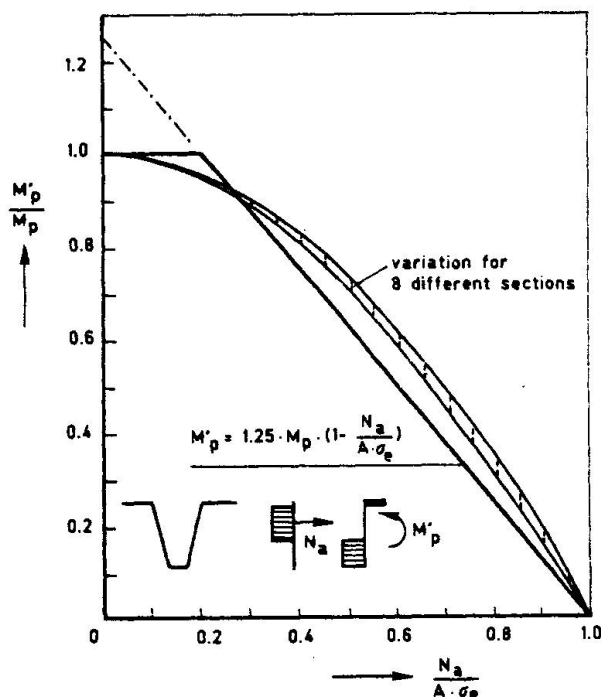


Fig. 8

Yield contours for combined effect of N and M on profiled sections

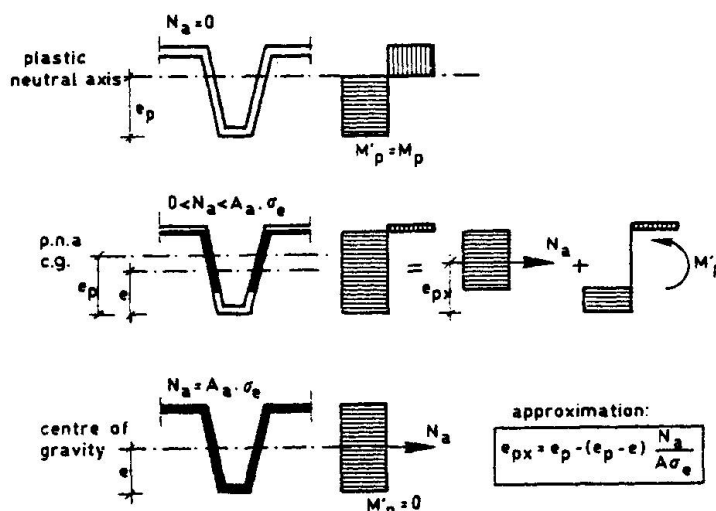


Fig. 9 Position of the tensile stress resultant N_a for various values of M .

The value of M_u can now be calculated with the following expressions:

$$M_u = N_b * z + M'_p$$

where: $z = h_t - 0.5 h_b - e_p + (e_p - e) \frac{N_b}{A\sigma_e}$

$$M'_p = 1.25 M_p \left(1 - \frac{N_b}{A\sigma_e}\right) \leq M_p$$

$$N_b = k f'_b h_b b$$

For the cases given in par. 2 the values of M_u have been calculated for $k = 1.0, 0.9, 0.8$ and 0.7 . These values were compared with M_{\max} as determined with the non linear flexural strain analysis. The following conclusions could be drawn:

- a value of $k = 0.8$ gave the best average correspondence;
- for $k = 0.8$ the average difference between M_u and M_{\max} was -1.6% and the standard deviation 1.5% .

A NEW FORM OF DECK ELEMENT

As a common effort of the Dutch steel and concrete industry a project is started to investigate possible use of composite decks in housing, especially for ground floors. This application requires some special properties:

- the possible span should be 5.50 m;
- no temporary supports;
- the element should be provided with thermal insulation;
- special attention should be paid to corrosion resistance.

Although use of trapezioded sheets described in the previous paragraphs is possible, ideas for new forms have also been developed. Just as an illustration of such a possible new form in Fig. 10 and 11 an impression is given of a prototype of a new deck element.

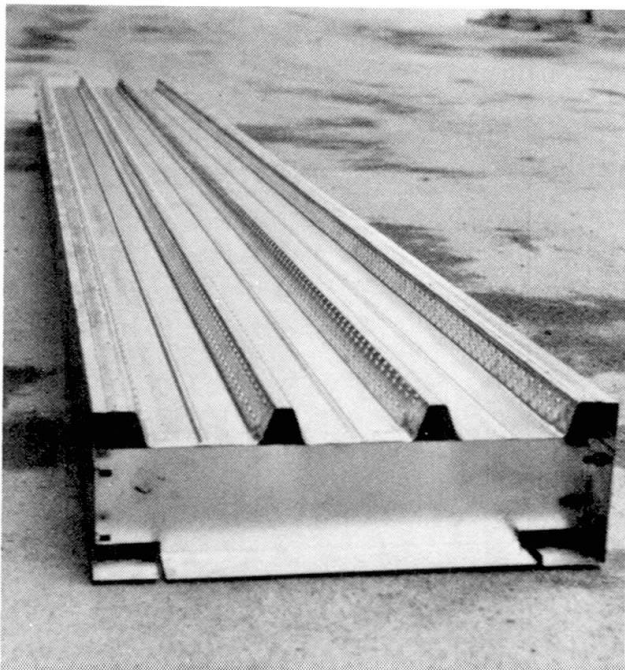
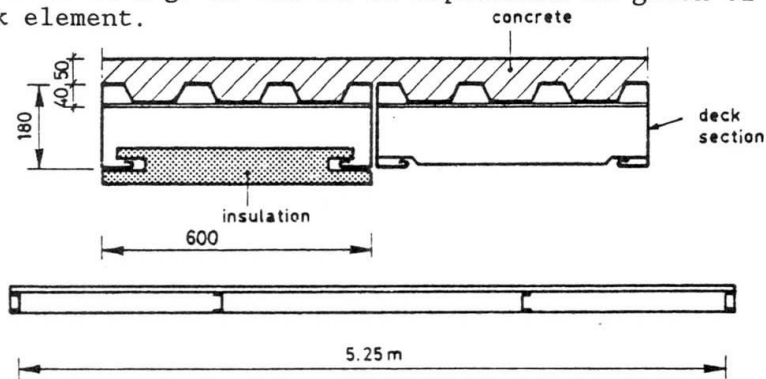


Fig. 10 Prototype of deck element



The basis is an existing trapezoidal profiled sheet with a height of 40 mm. The webs are provided with two rows of burls to provide shear connection. Properties of this type of shear connection are given in [2]. By using a wider sheet than normal, two edge members can be formed. These edge members should provide strength and stiffness for this long span under dead weight and construction loads. To support the corrugations of the sheet and distribute loads in transverse direction, two intermediate transverse profiles are provided as shown in Fig. 10. A test programme is underway to determine the structural properties and of course also the economical feasibility is investigated.



Fig. 11 Composite deck element under test loading (field test)

ACKNOWLEDGEMENT

The numerical parameter study described in this paper has been carried out by S.J. Boonstra and D. Verschuren as point of the final project for a structural engineering degree at the University of Eindhoven.

REFERENCES

1. BOONSTRA S.J., VERSCHUREN D., Composite decks (in Dutch). Eindhoven Technical University, Report BKO-KO-S-85-02, April 1985.
2. STARK J.W.B., Design of composite floors with profiled steel sheet. Proc. of the 4th Intern. Spec. Conf. on Cold-Formed Steel Struct., University of Missouri-Rolla, 1978.
3. BS 5950 - Part 4, Structural use of steelwork in building - code of practice for design of floors with profiled steel sheeting, BSI, 1981.
4. MIER J.v., Strain-softening of concrete under multiaxial loading conditions. Ph.D. Thesis, Eindhoven University of Technology, Sept. 1984.

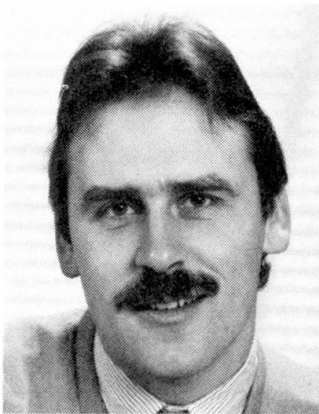
Light Gauge Structural Panel for Composite Flooring

Plateau porteur en acier formé à froid pour planchers mixtes

Leichtbausystem für Verbunddeckenkonstruktionen

Jonathan A. RAMSDEN

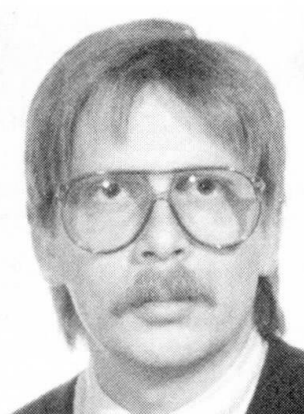
Development Manager
Engdahls AB
Kalmar, Sweden



Jonathan Ramsden has been involved in research into composite flooring at the Swedish Institute of Steel Construction since 1981. Having completed his doctors' degree he is currently employed by a Swedish steel fabricator as research and development manager.

Anders SEGERLIND

Development Engineer
Dobel AB
Borlänge, Sweden



Anders Segerlind, civil engineer, was employed for the first 4 years after his degree by a firm of consulting engineers. Since 1982 he has been employed by Dobel AB, manufacturers of coated light gauge metal products for the Building Industry as development engineer.

SUMMARY

This paper describes the background to and the testing of a new Swedish composite flooring system, which offers up to 7,5 m span, complete composite action, 2 hours fire resistance without additional reinforcement, and a finished soffit ready for painting. The floor has been tested on two sites in Stockholm and has created considerable interest in the Swedish Construction Industry.

RÉSUMÉ

Cet article relate le développement et les essais d'un nouveau système de plancher mixte suédois qui permet de franchir des portées jusqu'à 7,5 m, dont l'interaction acier-béton est complète, dont la résistance au feu sans armature supplémentaire est de 2 heures et dont la face inférieure peut être facilement peinte. Le plancher a été testé sur deux chantiers à Stockholm et a suscité un intérêt considérable dans l'industrie suédoise de la construction.

ZUSAMMENFASSUNG

Der Artikel beschreibt Hintergründe und Versuche zur Entwicklung eines neuen schwedischen Verbunddeckensystems, das Spannweiten bis zu 7,5 m zulässt. Das System ermöglicht vollständige Verbundwirkung, 2-stündigen Feuerwiderstand ohne zusätzliche Bewehrung und eine anstrichfertige Unterseite. Das System wurde auf zwei Baustellen in Stockholm erprobt und hat in der schwedischen Bauindustrie bedeutendes Interesse gefunden.



1 BACKGROUND

Composite flooring is often associated with steel frames. Steel frames in Sweden are, due to the absence of an alternative flooring system, often constructed with a pre-fab concrete slab floor, spanning between 6 and 12 metres. Secondary beams are therefore seldom used. Floor thicknesses in Sweden vary between 150 and 300 mm, due to limitations on construction height imposed by Town Planning Legislation. Limited floor to floor height and longspan flooring then leaves little room for a traditional primary-secondary beam system in the floor structure.

Unreinforced composite floors generally have low resistance to fire. Being as composite beams are seldom used in Sweden, the floor slab must be capable of withstanding Code fire requirements without relying upon the advantages gained by using composite beams. The composite floor must be able to fulfil the A 60 class, A = incombustible, 60 = fire resistance of 60 mins. (ISO 834) approved for pre-fab composite slabs over a span of 6 metres.

A thin steel sheet subjected to fire will suffer an extremely rapid increase of temperature unless the energy input can be diverted or absorbed by some other material. Concrete is an excellent thermal energy absorbent due to its high specific heat capacity and may therefore be used to minimize the temperature in the sheet steel panel by embedding as much of the sheet panel as possible into the concrete topping. The sheet steel will then serve as tensile reinforcement even at elevated temperatures. It is of course possible to introduce extra reinforcement as a measure by which to increase the fire rating of a composite floor. This is, however, a step back and the steel decking then tends to become an expensive way of providing formwork for a traditional in-situ concrete floor.

2 PROTOTYPE NO. 1

The three conditions mentioned previously, i.e. long span, finished ceiling surface and high resistance to fire, must be fulfilled if a composite flooring system is to succeed on the Swedish market. With these criteria in mind a sheet panel, denoted here as prototype no. 1, was developed at the Swedish Institute of Steel Construction, and tested at the Royal Institute of Technology, Dept. of Steel Structures.

2.1 Basic Concepts

The standard basic dimension for modular design in Sweden is 100 mm but most designs are based on multiples of 600 mm. The visible lined pattern created by the underside of a proposed sheet panel must combine with a multiple of 600 mm, which means that a flat bottom flange of 300 mm should be a reasonable compromise between economic sheet use, acceptable deflection and modular compatibility.

The edge stiffener on the upper flange not only gives a considerable increase in pre-composite load capacity compared to that of an unstiffened flange, but even eases the fitting together of the panels on site. No screws are necessary in order to create a safe working platform. The panels are held together just above the bottom flange by a stitch fold joint. The stiffened upper flange of the panel effectively prohibits vertical separation between the steel panel and the concrete topping, hardened concrete that flows between the panels and acts as a shear connector, ensuring composite action.

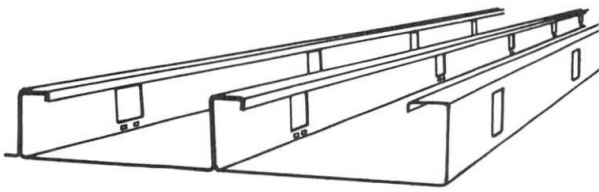


Fig 1 Prototype no. 1

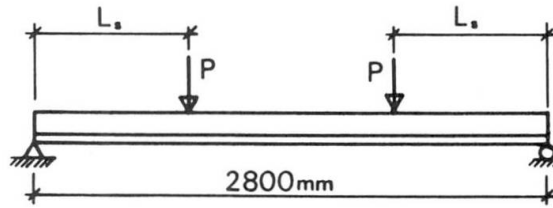


Fig 2 Sketch of the test set-up

2.2 Experimental Investigation

An experimental investigation into the function and strength of prototype no. 1 was carried out. The test specimens were 3x300 mm wide and 3000 mm long with either a 120 or 160 mm concrete topping, grade K25 (nominal cube strength 25 N/mm²). The investigation was conducted in accordance with the recommendations in the Swedish Code for Light Gauge Metal Structures (2). The method is based on the results obtained through experimental investigation at Iowa University, Iowa, USA and is characterized by slip between the metal sheet and the concrete at ultimate loading.

2.3 Results

The results from testing show that the sheet panels performed as expected, that is to say performed in a similar way to that of a compatible reinforced concrete slab. The test specimens did however bring to light two major defects.

The most serious defect was that the panels leaked during the pouring of the concrete, leaving drops of cement paste that had adhered to the underside of the panels (the visible surface of the panels). This defect is of an aesthetic nature and has nothing to do with structural mechanics, but is of great importance if such a flooring system is to offer a finished ceiling surface.

The second defect was caused by the large proportion of the hole in the web in relation to the web itself. The hole substantially weakens the panel, especially when approaching yield loads, which is clearly demonstrated in fig 3.

The combination of these two defects indicated that the basic concept was good, but that the hole should be replaced by some other medium in order to counteract the shear forces in the panel web/concrete interface.



Fig 3 Panel deformation at ultimate load

3 PROTOTYPE NO. 2

The results achieved from the testing of prototype no. 1 awoke the interest of Dobel AB of Borlänge, Sweden whereby a joint project was started, based on a revised version of Prototype no. 1, hereafter referred to as Prototype no. 2.



3.1 Basic Concepts

The only way to ensure that no seepage occurs between the panels is to refrain from perforating them. If the webs are provided with embossments instead of holes, the embossed web surfaces will combine to act as shear connectors, being as the top flange overlap ensures that the adjoining webs are completely flush and are embedded in the concrete topping. The embossed webs should then act in a similar fashion to that of ribbed reinforcement bars. The web embossment pattern chosen consists of three rows of indentations 12 mm x 6 mm, 3 mm high and 6 mm between each row.

The stitch fold joint was replaced by self-drilling screws, which can be quickly and effectively fitted by means of a special adapter fitted to a variable-speed electric hand-drill. The fitting of self-drilling screws requires a horizontal working surface which was achieved by the introduction of a "shelf" 20 mm wide, 25 mm above the bottom flange. The revised concept with embossed web, shelf and self-drilling screws, became prototype no. 2 and is shown in fig 4.

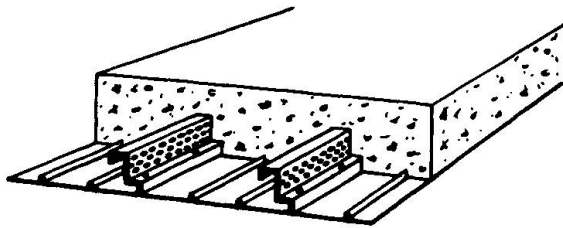


Fig 4 Sketch of prototype no. 2

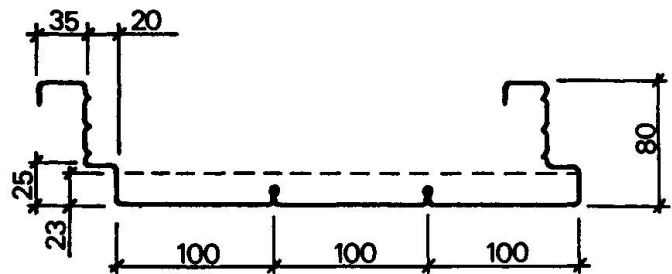


Fig 5 Section data

4 SHEAR LOAD CAPACITY

The shear load capacity of composite flooring with a regular, continuous pattern of embossment is determined by means of formula (4.1) which is stipulated in The Swedish Code for Light Gauge Metal Structures, StBK-N5 (2) and explained in (3).

$$V_d = \frac{0.8 \, b d}{\gamma_n} \left(\frac{m q d}{L_s} + k f_{ct} \right) \quad (4.1)$$

4.1 Test details, frame

The test frame was basically the same as that shown in fig 2 and consists of a simply supported composite slab, 900 mm (three panels) wide subjected to two equal knife-edge loads at a distance of L_s from each support respectively. Deflection was measured in the centre of each slab on each side. Two deflection gauges were placed at each end of the slab in order to measure the amount of slip between the concrete slab and the steel panels.

The test series consisted of the following seven tests, each test being repeated three times to check consistency:

Table 1 The test series, shear load capacity

Denomination	L (mm)	H (mm)	L (mm)	d (mm)	Number of tests	L/H
H 130-390	1650	130	390	107	3	3
H 130-780	2300	130	780	107	3	6
H 130-1170	3400	130	1170	107	3	9
H 200-600	2300	200	600	177	3	3
H 200-1200	3400	200	1200	177	3	6
H 300-900	3400	300	900	277	3	3
H 300-1800	4700	300	1800	277	3	6

4.2 Test results

The results from the tests were plotted in the design diagram in the Swedish Code (2) (The Porter-Schuster semi-empirical design method).

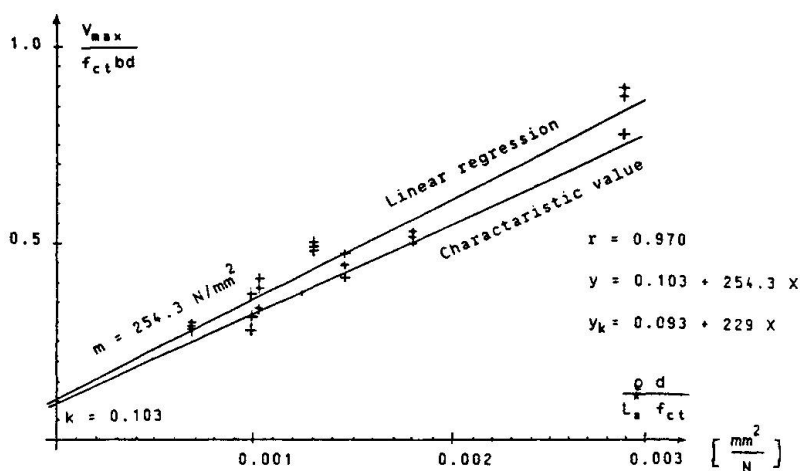


Fig 6 The plotted regression line giving the coefficients m and k

The regression line determined in fig 6 fits the equation

$$y = 0.103 + 254.3 x \quad (4.2)$$

The regression line for design is determined by a 10 % reduction in the values in equation (4.2), being as 21 tests had been carried out. The equation for the design curve is then

$$y = 0.093 + 229 x \quad (4.3)$$

$$k = 0.093 \quad (4.4)$$

$$m = 229 \text{ N/mm}^2 \quad (4.5)$$

for the composite panel BLK 300/80

The equation for the calculation of the shear capacity of composite flooring using the panel BLK 300/80 is, after the substitution of $m = 229 \text{ N/mm}^2$, $k = 0.093$ and $\rho = A_s / bd$

$$V_d = \frac{0.8 d}{\gamma_n} \left(229 \frac{A_s}{L_s} + 0.093 b f_{ct} \right) \quad (4.6)$$

4.3 Bending moment capacity

The bending moment capacity of fully composite flooring with profiled steel sheeting is given in StBK-N5 section 34:265 (2). Formula (4.7) applies to under-reinforced slabs.



$$M_d = A_s f_{ty} d \left(1 - \frac{\rho f_{ty}}{2 f_{cc}} \right) \quad (4.7)$$

and formula (4.8) to over-reinforced slabs

$$M_d = f_{cc} b d^2 \eta (1 - 0.5 \eta) \quad (4.8)$$

where

$$\eta = 0.5 \left(\sqrt{4\beta + \beta^2} - \beta \right) \quad \text{and} \quad \beta = \frac{E_s A_s \epsilon_{cu}}{f_{cc} b d} \quad (4.9)$$

The slab is classified as under-reinforced when $\rho < \rho_b$ and as over-reinforced when $\rho > \rho_b$ where

$$\rho_b = \frac{h_s f_{cc}}{d f_{ty}} \frac{1}{(1 + f_{ty} / 700)} \quad \text{and} \quad \rho = \frac{A_s}{b d} \quad (4.10)$$

When producing theoretical design data for the panel BLK 300/80 it was found by Anders Segerlind (4) that formula 4.4 did not give sufficiently correct design values for the under-reinforced slab, presumably due to the fact that the formula is directly derived from equivalent reinforced concrete formulae, which do not take the height and the stiffness of the sheet web into consideration. A new design model was established which divided the panel section into a number of sub-sections, each of which was theoretically allowed to plasticise in turn until a balance in stresses was obtained in the compression (concrete) and tension (steel) zones. This model is shown in fig 7.

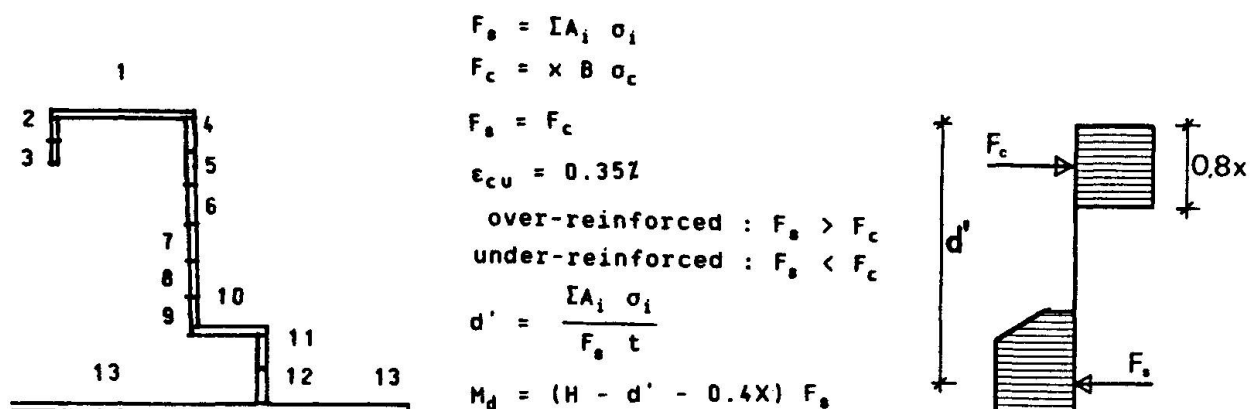


Fig 7 The sub-divided panel for the calculation of the moment capacity of the under-reinforced panel section.

This new design model gave considerably improved design values which correlate well with the test results obtained, see Table 2.

4.4 Theoretical deflection of the cracked slab

The handbook "BYGG" part I section A24:35 gives the deflection of a simply supported slab subjected to two downward point loads that are of an equal distance, L_s , from each support as

$$y = \frac{P L_s (3L^2 - 4L_s^2)}{24 EI} \quad (4.11)$$

The moment at midspan is

$$M = P L_s \quad (4.12)$$

and the curvature of the slab

$$\frac{1}{r} = - \frac{d^2 y}{dx^2} = \frac{M}{EI} \quad (4.13)$$

the substitution of (4.13) and (4.12) into (4.11) give

$$y = \frac{1}{r} \frac{(3L^2 - 4L_s^2)}{24} \quad (4.14)$$

If the effects of creep are ignored then the curvature of a concrete slab is given in (1) p. 34 as

$$\frac{1}{r} = \frac{\sigma_s}{E_s d(1-x/d)} \quad (4.15)$$

This straight line is shown in fig 8.

4.5 Theoretical deflection of the uncracked slab

The curvature of the slab is given in (4.15). Where the height of the compression zone, x , is

$$x = \frac{(\alpha-1)A_s d + 0.5bH^2}{(\alpha-1)A_s + bH} \quad (4.16)$$

and the second moment of area of the uncracked composite section is given in (1) p 36 as

$$I_{id} = \frac{bH^3}{12} + bH(x-H/2)^2 + (\alpha-1)A_s (d-x)^2 + \alpha I_s \quad (4.17)$$

The flexural stress in the concrete as shown in (1) p. 36 is

$$\sigma_{cb} = \frac{M}{I_{id}} (H-x) \quad (4.18)$$

$$\frac{1}{r} = \frac{\sigma_{cb}}{E_s d(1-x/d)} \quad (4.19)$$

which may be substituted into (4.14). An example of the resulting straight line is shown in fig 8.

4.6 Calculation of the load at which the first crack occurs

Section 4.4.2 in (1) gives

$$M_{max, test} = PL_s + qL^2/8 \quad (4.20)$$

and 4.18 rewritten gives

$$M_{max, material} = \frac{\sigma_{cb} I_{id}}{H-x} \quad M_{max, test} = M_{max, material} \quad (4.21)$$

which gives

$$P_{crack} = \left[\frac{\sigma_{cb} I_{id}}{H-x} - qL^2/8 \right] \frac{1}{L_s} \quad (4.22)$$

which is shown in fig 8.

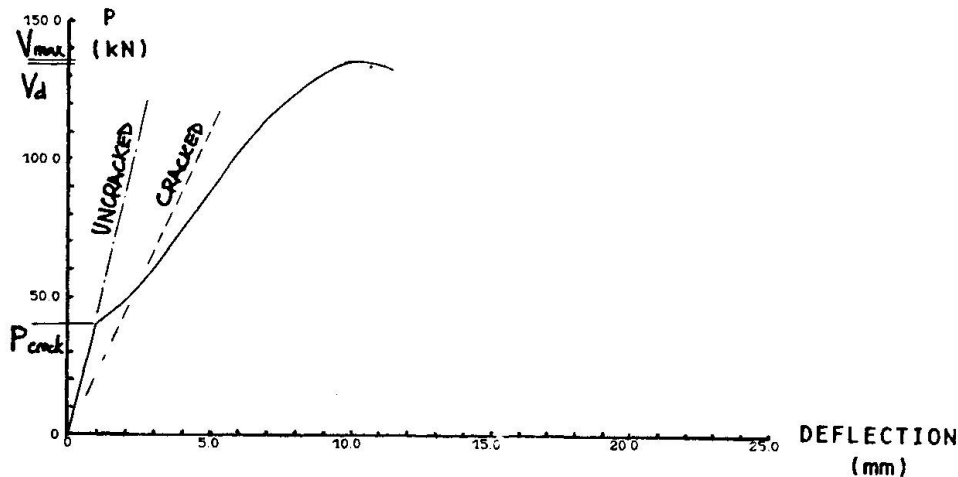


Fig 8 An example of the load deflection curve from testing

4.7 Conclusion

The regression line for the calculation of the coefficients k and m in formula (4.1) shows excellent consistency and may therefore be taken as a reliable basis for the calculation of the shear capacity of a concrete slab using the Dobel BLK 300/80 sheet steel composite panel. The ratio between V_{max} (the maximum load values during testing) and V_d (the design values for shear capacity using formula (4.6)) is shown in table 2 below where the highest value is 0.755, giving a minimum of a 32 % safety margin in design before the introduction of material and load reduction factors. The safety margin in design is then in the order of 35-45 %, which is more than sufficient, perhaps even conservative. The corresponding values for moments, M_{max} and M_d are shown for the cube strength measured in the tests. M is calculated according to Segerlind's design table (4), which includes a material load factor. The design strength of the sheet steel was at a nominal value of $f_{ty} = 350 \text{ N/mm}^2$. In reality (that is to say during testing) $\gamma = 1.0$ and $f_y = 390\text{-}400 \text{ N/mm}^2$.

Table 2 Test values and design values for shear and bending

Test	V_{max}	f_{ct}	V_d	V_d/V_{max}	M_{max}	Cube strgth	M_d	M_d/M_{max}	Fail mode
	(N) ($\times 10^3$)	(MPa)	(N) ($\times 10^3$)		(Nmm) ($\times 10^6$)	(MPa) ($\times 10^3$)	(Nmm) ($\times 10^6$)		
H130-390	177.0	2.16	120.9	0.683	69.0	37.8	54.1	0.784	SPLIT
H130-780	93.0	2.16	68.3	0.734	72.5	37.8	54.1	0.746	SPLIT
H130-1170	85.4	2.15	50.6	0.592	99.9	37.6	54.0	0.541	BEND
H200-600	185.7	2.26	140.3	0.755	111.4	40.4	115.0	1.032	SHEAR
H200-1200	120.6	2.02	80.7	0.669	144.7	34.4	112.5	0.778	BEND
H300-900	253.8	2.08	156.9	0.618	228.4	35.7	187.0	0.819	SHEAR
H300-1800	148.4	2.07	97.6	0.658	267.1	35.5	187.0	0.700	BEND

Tests H130-1170, H200-1200 and H300-1800 failed in bending. See fig 9. Tests H130-390 and H130-780 failed by the slab splitting along the line of the upper flange of the panels as shown in fig 9. This form of failure may easily be remedied by placing additional reinforcement at right-angles to the direction of the panels in areas of high shear. As may be seen in table 2 the load values at failure are far higher (+ 30 %) than the calculated values without load factors so that addition reinforcement is not really required. It is however

reassuring to note that additional reinforcement at right angles to the panels could increase the shear capacity of the panels even further. This is a possible area for continued research.

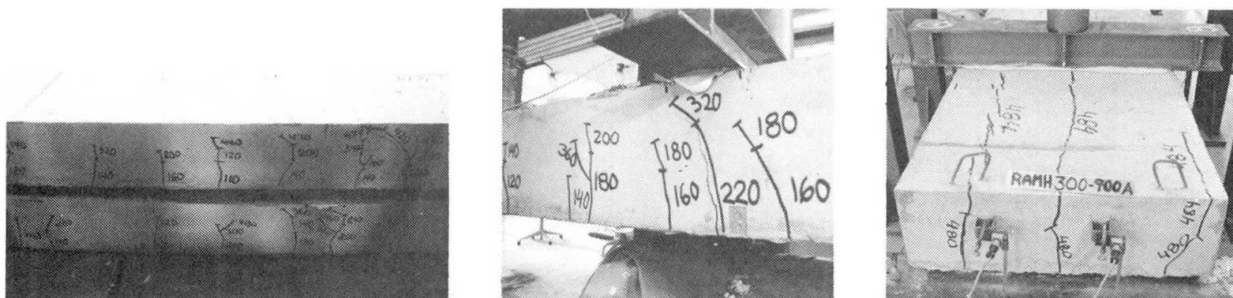


Fig 9 Bending failure

Shear failure

Failure due to splitting

5 FIRE PERFORMANCE

The BLK 300/80 composite panel was designed to withstand 60 minute standard fire (ISO 834). Fire tests were carried out at the National Testing Station in Borås in Jan 1985 in order to verify the preliminary computer calculations. The time - temperature curves for the computer analysis and the actual results obtained during testing are shown in fig 10. These results may be used for calculation in the fire engineering design of the BLK 300/80 composite slab. The results obtained from such an analysis vary from case to case, but it may generally be concluded that a 200 mm thick slab spanning 6 m without support restraint will sustain a working office load of 2 kN/m^2 for 90 mins and a reduced load of $1,8 \text{ kN/m}^2$ for 120 mins. Complete fire engineering design tables and details are available from Dobel AB.

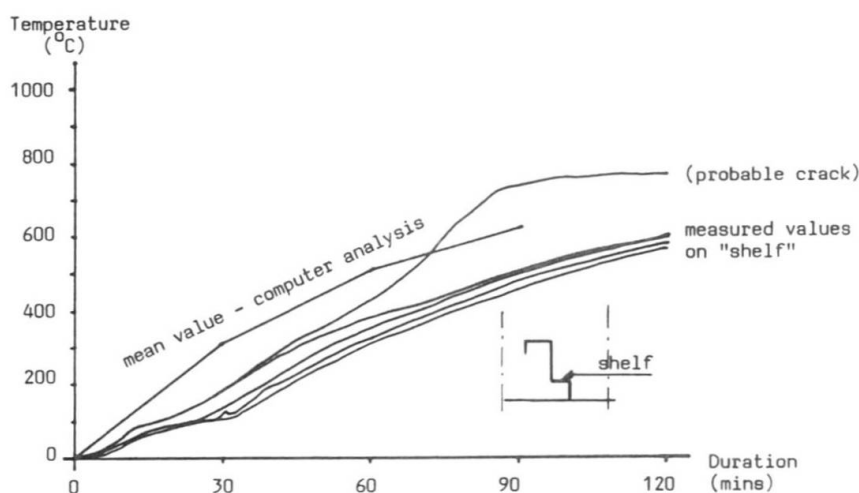


Fig 10 An example of the theoretical and test temperatures in the composite slab

**SYMBOLS**

A_s	Crosssectional area of tensile reinforcement
B	Width of test specimen
b	Width of panel
d	Depth of compressive reinforcement
E_c	Modulus of elasticity of concrete
E_s	Modulus of elasticity of steel
f_{cc}	Cylinder strength of concrete
f_{ty}	Tensile yield strength of steel
H	Total height of test specimen
h	Effective height from neutral axis of tensile reinf.
I	Second moment of area
L	Span
l	Length
M_d	Design value of strength with respect to bending moment
M_u	Ultimate value of strength with respect to bending moment
P_d	Design load
P_u	Theoretical ultimate load
q_D	Self weight per unit of length
q_L	Live load per unit of length
t, t_{nom}	Thickness of sheet incl zinc, coating, etc.
t_{core}	Thickness of steel within the sheet
x	Depth of compression zone
y	Deflection of test specimen
ϵ_{cu}	Ultimate strain in concrete
σ_s	Strain in steel reinforcement
σ_{ch}	Calculated compressive strength due to bending

REFERENCES

- (1) Ramsden, J. A., "Light Gauge Structural Elements for Composite Flooring. Part One: Background Prototype and Preliminary Investigation". Report 103:6 from the Swedish Institute of Steel Construction, Stockholm, Sweden 1984.
- (2) The Swedish Code for Light Gauge Metal Structures. StBK-N5. Publ 76 from the Swedish Institute of Steel Construction, Stockholm, Sweden 1982. (English translation from Swedish original).
- (3) Ramsden, J. A., "Samverkansbjälklag av tunnplåt och betong - inventering och nulägesrapport". Report 103:3 from the Swedish Institute och Steel Construction, Stockholm, Sweden 1982. (Swedish)
- (4) Segerlind, A., Unpublished report on the calculation of the ultimate design values of composite panel BLK 300/80. Dobel AB, Borlänge, Sweden, 1984. (Swedish)
- (5) BBK 79. (The Swedish Code for Concrete Structures) Stockholm 1979. (Swedish)
- (6) Betonghandbok, Konstruktion (The Swedish Concrete Design Manual) Stockholm 1980. (Swedish)
- (7) Eurocode 4. Composite steel and concrete structures. First Draft October 1984.

Shear Strength of Unwelded Shear Connectors for Composite Beams

Résistance au cisaillement de connecteurs non soudés
pour construction mixte acier-béton

Scherfestigkeit von ungeschweissten Schubverbindungen für Verbundträger

Colin K. JOLLY

Lecturer
Univ. of Southampton
Southampton, UK

Stuart S. J. MOY

Lecturer
Univ. of Southampton
Southampton, UK

Ashraf M. EL-SHIHY

Assistant Lecturer
Zagazig University
Zagazig, Egypt

Colin Jolly, born 1950, obtained his Civil Engineering Master's degree and Doctorate at Southampton University. For four years he was involved in the design of concrete water-retaining and building structures. His research interests are in cementitious composites, the in-service monitoring of structures, and composite construction.

Stuart Moy, born 1945, obtained his Civil Engineering degree and Doctorate at Nottingham University. He has worked in the aircraft industry and on the design and construction of cooling towers and nuclear pressure vessels. His research interests are in cooling tower analysis and composite construction.

Ashraf El-Shihy, born 1955, obtained his Civil Engineering degree at Cairo University and his Master's degree at Southampton. He is currently undertaking research in composite construction at Southampton.

SUMMARY

This paper describes push-out tests to determine the strength of several fixings used to provide the shear connection between composite slabs and composite beams. The research investigates the effect of varying the pattern of the fixings, the type and orientation of the profiled sheeting, the concrete strength and steel beam size.

RÉSUMÉ

Cet article décrit les essais de type «push-out» effectués en vue de déterminer la résistance de différents moyens de connexion entre les planchers mixtes avec tôle profilée et les poutres métalliques. L'étude traite de l'influence de l'écartement des fixations, du type et du sens porteur de la tôle profilée, de la résistance du béton et de la dimension de la poutre métallique.

ZUSAMMENFASSUNG

In diesem Referat werden «push-out»-Versuche beschrieben, in denen die Tragfähigkeit von mehreren Befestigungsvorrichtungen bestimmt wird, welche die Schubkräfte zwischen Platte und Träger des Verbundelementes übertragen. In der Forschungsarbeit werden die Auswirkungen untersucht, wenn das Muster der Befestigungsvorrichtungen, die Art und Orientierung der im Querschnitt dargestellten Verkleidung, die Festigkeit des Betons und die Dimensionen des Stahlbalkens verändert werden.



1. INTRODUCTION

Composite slabs of profiled steel sheet permanent shuttering and concrete provide for construction of spans up to three or four metres without additional support from beams. On large contracts, or in bridges, where spans in excess of 10 metres can be required, welded shear connectors provide economic composite beams. The aim of this research, into the use of unwelded shear connections, is to bring the economic advantages of composite beam construction to the intermediate span beams which are more common on smaller construction contracts. In addition, the results show the contribution of the unwelded fixings used to locate the profiled steel sheeting during construction to the shear resistance of composite beams with through-deck welded shear connectors.

Unwelded shear connectors have already been used in the construction of some buildings in the U.K., for example self-drilling, self-tapping screws for a hospital in Oxfordshire, and shot-fired fixings for a multi-storey car park and other small buildings in South Wales. In general, each application has had to be justified by beam load tests.

The advantages of using unwelded shear connectors are that it avoids the requirement for expensive three-phase welding equipment and trained operatives on smaller sites, or where only modest beam spans are used.

These methods of fastening are less weather-dependent, and should be attractive in developing countries where skilled staff are at a premium.

2. THE TEST PROGRAMME

2.1 Test variables

This paper describes the results obtained from push-out tests on four proprietary fixings which may be suitable for providing shear connection in composite beams. The push-out tests were based on the standard dimensions quoted in CP117 [1] for concrete cast directly onto the steel beam. The concrete area was increased, when necessary, to coincide with integer multiples of the pitch of the steel decking profiles. The aim was to ascertain the behaviour of the connections under a wide range of likely practical conditions. Consideration was therefore given to the following wide range of variables;

- the number and pattern of the different fixings,
- the type of profiled sheeting (dovetailed and trapezoidal sections),
- orientation of the profiled sheeting,
- type of concrete (normal weight and lightweight aggregate),
- size of the steel beam section.

A summary of the tests is given in table 1. Variations made to each of these parameters will be described in more detail.

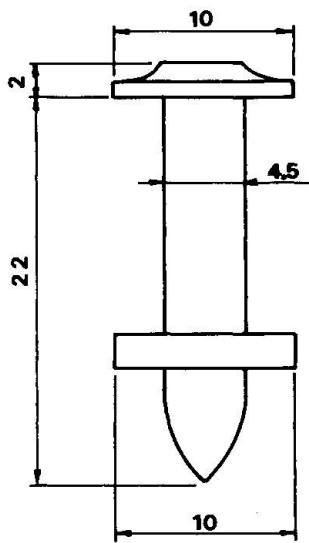
2.2 Fixings

The four types of fixing used as shear connectors in the tests are;

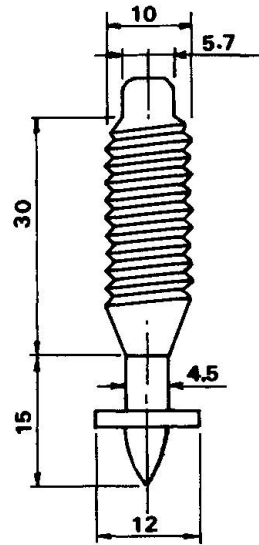
- shot-fired threaded studs,
- shot-fired nails,
- an angle bracket fixed by two shot-fired nails,
- self-drilling, self-tapping screws.

Each of these connections is shown in figure 1.

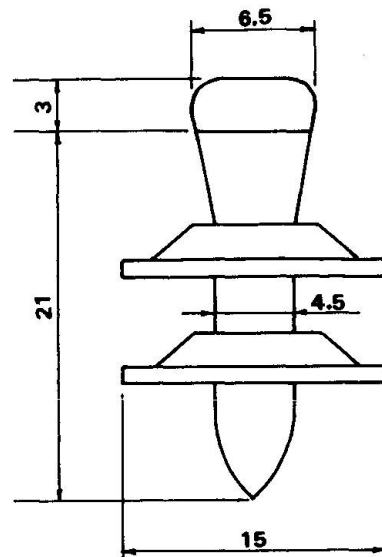
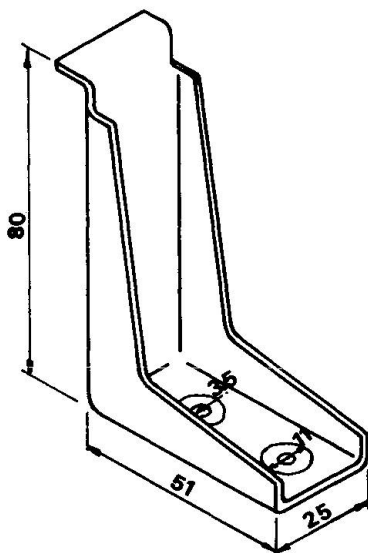
Seven different patterns of connection were used for each of the profile types. The cross-sectional dimensions of each profile influenced the choice of these patterns, which varied from two fixings per face to eight fixings per face in the push-out test (see figure 2).



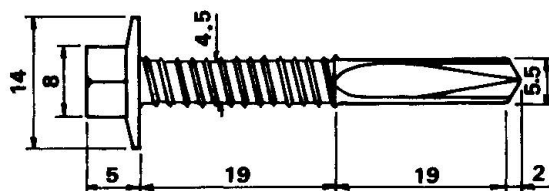
Shot-fired nail



Shot-fired threaded stud

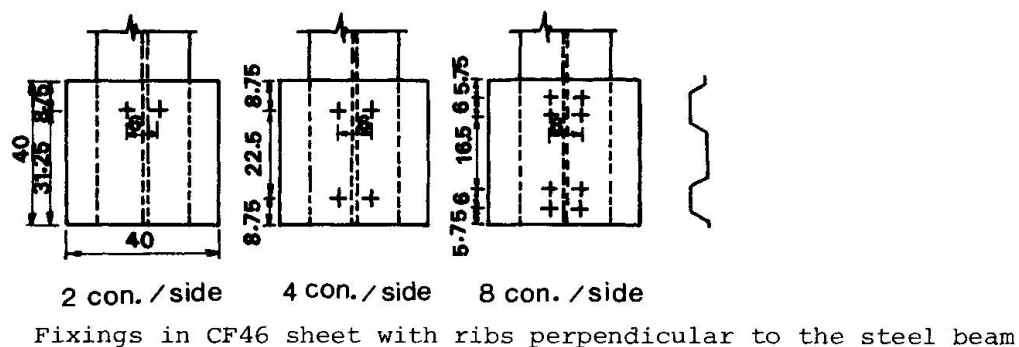
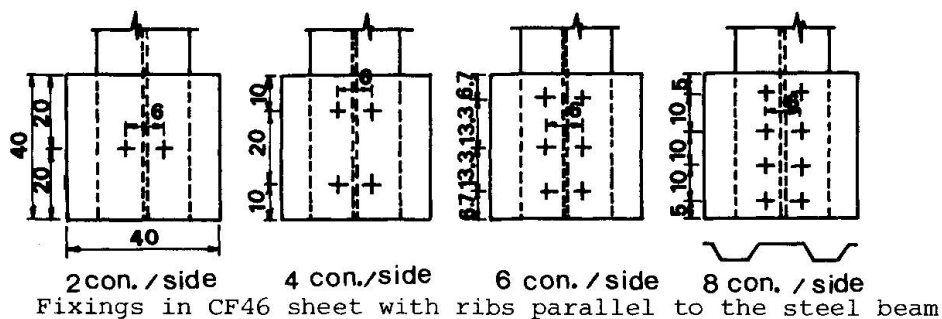
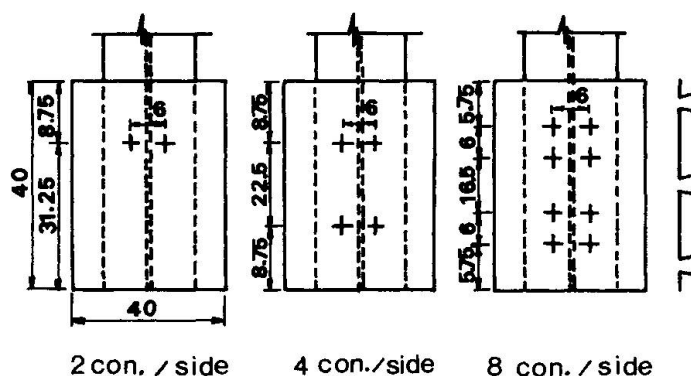
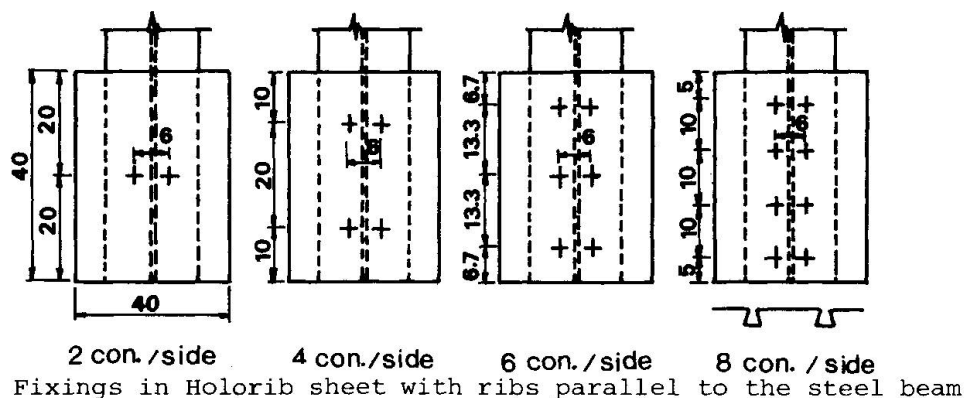


Angle bracket shear connector and detail of the shot-fired nails used to fix it



Self-drilling, self-tapping screw

FIGURE 1. TYPES OF FIXING.



Dimensions in centimetres

FIGURE 2. FIXING PATTERNS FOR PUSH-OUT TESTS.

2.3 Profiled Steel Sheeting

Two types of profiled steel sheeting were used in the tests: Holorib, produced by Richard Lees Ltd., and CF46 produced by Precision Metal Forming Ltd. The thinnest available gauge of each type of sheeting was used, since shearing or tearing of the sheeting are the only likely effects contributing to any failure mechanism. The results should, if anything, give conservative strengths for the thicker sheeting which is available.

2.4 Orientation of the profiled sheeting

Composite slabs are most commonly designed as one-way spanning. The ribs of the sheeting are then orthogonal to the supporting beam which is likely to be designed to act compositely. Some degree of two-way action of the slab is inevitable when there is a trimming beam around the slab. Use of the profiled sheeting was therefore investigated in both orientations.

2.5 Types of concrete

Lightweight aggregate concrete is now common in the U.K. for composite slab/composite beam construction due to the enhanced fire protection provided and the reduced self-weight of members. Three types of concrete were used.

- Normal weight concrete with a target characteristic strength of 40 N/mm². The solids content was in the ratio 1:2.36:4.03 (by weight), with a free water : cement ratio of 0.6. The mix had a 20 mm slump and density of 2350 kg/m³.

- Structural lightweight concrete, also with a target strength of 40 N/mm². In this mix 'Lytag' with a maximum size of 10 mm was used as the only coarse aggregate. The solids ratio was 1:2.5:1.59, with a water : cement ratio of 0.75. The density of this mix was 1950 kg/m³.

- Lightweight concrete with a target strength of 25 N/mm². Pumice aggregate graded from 15 mm to dust was the sole aggregate in this mix, for which the solids ratio was 1:2.09. A plasticising admixture was added to the water to compensate for the high absorbency of the pumice. The water : cement ratio was 0.65 and the resulting density was 1450 kg/m³.

2.6 Size of steel beam

Work-hardening or crystalline phase changes due to heating were considered possible during the installation of the fixings. Any such effects would vary with the thickness of flange to be penetrated. Therefore three different sizes of steel I-beam were used to provide flange thicknesses ranging from 9.7 mm to 12.8 mm. The sections were;

- 305 x 103 UB25,
- 356 x 171 UB45,
- 406 x 178 UB60.

3. RESULTS

3.1 Failure modes and maximum shear strengths

There were four main modes of failure.

- Shearing of the connectors, when few connectors were used.
- Shearing of the concrete at the plane connecting the tops of the profiles.
- Separation of the concrete from the profiled sheeting.
- Tearing of the profiled sheet under the fixing heads.

When the failure was by shearing of the connectors, the average ultimate shear strengths obtained were 19.25 KN per shot-fired threaded stud, 11.8 KN per shot-fired nail, 20.25 KN per nail used to fix the angle bracket, and 14.38 KN per self-drilling, self-tapping screw.



3.2 The effect of test variables on failure mode and strength

In cases where failure was due to shearing of the fixing itself, less than a 5% reduction in shear strength per fixing was measured when the fixing density was increased. The self-drilling, self-tapping screws were almost twice as ductile as the shot-fired fixings, at equal loads. When failure was by shearing of the fixing or tearing of the sheet, the type of profiled sheeting had little effect. However, when the other failure modes predominated, the CF46 was strongest when orthogonal to the beam, and Holorib strongest when parallel to the beam.

The orientation of the sheeting had little effect when few fixings were used, with failure resulting from shearing of the fixings. When more fixings were used, shearing of the concrete occurred with the Holorib sheeting at shear stresses in excess of 0.92 N/mm^2 (0.59 N/mm^2 in pumice concrete) whereas separation was more likely with the CF46 sheeting at a shear stress above 0.49 N/mm^2 (0.42 N/mm^2 in pumice concrete). Higher shear stresses were required to produce concrete shear or separation failures when longer fixings were used. The longer fixings also produced slightly higher ultimate strengths when the sheeting ribs were parallel to the beam.

Strength results were almost identical when the normal weight and structural lightweight concrete were used. The very light pumice concrete showed signs of aggregate crushing in some tests. The flange thickness of the steel I-beams had no significant effect on the ultimate shear strengths.

4. CONCLUSIONS

Of the four types of fixing tested, only the shot-fired nails showed a tendency to tear through the sheeting. The low shear strength of these nails makes them of little use as independent shear connectors, though they make a useful contribution in conjunction with welded shear studs. The advantages of the self-drilling, self-tapping screws are greater ductility and security of fixing. Ease of fixing is the advantage of the shot-fired stud, but the greatest shear capacity is obtained with the angle bracket and its nail fixings.

Concrete shear failure and separation from the sheeting reduce the potential shear capacity of all these fixings when used independently, but steps could be taken to prevent these failure modes. Density of fixings and sheeting orientation would then have little effect on the shear strength.

Lightweight aggregate concrete should be avoided unless a structural lightweight mix is used, incorporating sand to prevent local crushing. Fire-rating and overall cost currently favour the use of lightweight coarse aggregate. Provided the fixings can penetrate the flange, any steel section can be used.

Full-scale beam tests are currently under way to justify the use of the push-out test results in composite beams incorporating the use of unwelded fixings as shear connectors.

REFERENCE

1. BRITISH STANDARDS INSTITUTION, CP117, Code of Practice for Composite Construction in Structural Steel and Concrete. BSI, London.

Test No.	No. of fixings	Type of sheet	Rib direction	Type of concrete	Type of beam	Test No.	No. of fixings	Type of sheet	Rib direction	Type of concrete	Type of beam
AN1	6	HR	PP	N	S1	CP3	4	HR	NN	P	S1
AN2	4	HR	PP	N	S1	CNS1	8	PMF	PP	N	S2
AN3	4	HR	NN	N	S1	CNS2	8	PMF	NN	N	S2
AN4	8	HR	NN	N	S1	CNS3	4	PMF	PP	N	S2
AN5	6	HR	PP	N	S3	CNS4	4	PMF	NN	N	S2
AN6	4	HR	PP	N	S3	CPS1	8	PMF	PP	P	S2
AN7	4	HR	NN	N	S3	CPS2	4	PMF	PP	P	S2
AN8	8	HR	NN	N	S3	CPS3	4	PMF	NN	P	S2
AN9	8	HR	PP	N	S1	CL1	8	HR	PP	L	S3
AN10	8	HR	PP	N	S3	CL2	8	HR	NN	L	S3
AN11	6	HR	NN	N	S1	CNS1M	4	HR	PP	N	S1
AN12	6	HR	NN	N	S3	DN1	4	HR	PP	N	S1
AP1	6	HR	PP	P	S1	DN2	8	HR	PP	N	S1
AP2	4	HR	PP	P	S1	DN3	4	HR	NN	N	S1
AP3	4	HR	NN	P	S1	DN4	8	HR	NN	N	S1
AP4	8	HR	NN	P	S1	DN5	4	HR	PP	N	S3
AP5	6	HR	PP	P	S3	DN6	8	HR	PP	N	S3
AP6	4	HR	PP	P	S3	DN7	4	HR	NN	N	S3
AP7	4	HR	NN	P	S3	DN8	8	HR	NN	N	S3
AP8	8	HR	NN	P	S3	DP1	4	HR	PP	P	S1
AL1	4	HR	PP	L	S3	DP2	8	HR	PP	P	S1
AL2	4	HR	NN	L	S3	DP3	4	HR	NN	P	S1
AL3	8	HR	PP	L	S3	DP4	8	HR	NN	P	S1
ANS1	6	PMF	PP	N	S2	DP5	4	HR	PP	P	S3
ANS2	4	PMF	PP	N	S2	DP6	8	HR	PP	P	S3
ANS3	4	PMF	NN	N	S2	DP7	4	HR	NN	P	S3
ANS4	8	PMF	NN	N	S2	DP8	8	HR	NN	P	S3
APS1	6	PMF	PP	P	S2	DL1	4	HR	PP	L	S3
APS2	4	PMF	PP	P	S2	DL2	4	HR	NN	L	S3
APS3	4	PMF	NN	P	S2	DL3	8	HR	NN	L	S3
APS4	8	PMF	NN	P	S2	DNS1	4	PMF	PP	N	S2
AN1F	4	HR	PP	N	S1	DNS2	8	PMF	PP	N	S2
APS1F	4	PMF	PP	N	S1	DNS3	4	PMF	NN	N	S2
BN1	6	HR	PP	N	S1	DNS4	8	PMF	NN	N	S2
BN2	8	HR	NN	N	S1	DPS1	4	PMF	PP	P	S2
CN1	8	HR	PP	N	S1	DPS2	8	PMF	PP	P	S2
CN2	8	HR	NN	N	S1	DPS3	4	PMF	NN	P	S2
CN3	4	HR	PP	N	S1	DPS4	8	PMF	NN	P	S2
CN4	4	HR	NN	N	S1	DN1F	4	HR	PP	N	S1
CP1	8	HR	PP	P	S1	DPS1F	4	PMF	PP	N	S1
CP2	4	HR	PP	P	S1						

Key	A...Shot-fired threaded studs	NN Ribs perpendicular to the beam
	B...Shot-fired nails	PP Ribs parallel to the beam
	C...Angle bracket shear connector fixed by two shot-fired nails	N Normal weight concrete
	D...Self-drilling, self-tapping screws	P Pumice lightweight concrete
		L Lytag lightweight concrete
	HR Holorib sheet	S1 UB25 steel beam
	PMF CP46 sheet	S2 UB45 steel beam
		S3 UB60 steel beam

TABLE 1. SUMMARY OF THE TESTS



Test No.	f_{c28}^2 (N/mm ²)	Failure Load (KN)	Load per connector (KN)	Failure mode	Test No.	f_{c28}^2 (N/mm ²)	Failure load (KN)	Load per connector (KN)	Failure mode
AN1	40.5	205	17.1	C	CP3	24.9	80	10.0	C
AN2	42.0	155	19.38	S	CNS1	37.6	333	20.81	SEP
AN3	38.0	162	20.25	S	CNS2	42.8	305	19.06	SEP
AN4	42.0	190	11.88	C	CNS3	36.3	170	21.25	S
AN5	43.0	230	19.16	C	CNS4	42.8	160	20.0	P
AN6	38.0	155	19.38	S	CPS1	24.0	214	13.38	C
AN7	43.0	155	19.38	S	CPS2	24.0	160	20.63	S
AN8	43.0	215	13.44	C	CPS3	24.4	133	16.63	SEP
AN9	40.5	230	14.38	C	CL1	39.7	310	19.38	S
AN10	40.5	270	16.9	SEP	CL2	39.7	245	15.31	C
AN11	40.4	155	12.92	C	CNS1M	35.7	235	14.69	SEP
AN12	40.4	185	15.42	C	DN1	37.2	115	14.38	S
AP1	25.6	180	15.0	C	DN2	37.2	210	13.13	S
AP2	25.6	115	14.38	SEP	DN3	41.5	124	15.5	S
AP3	25.6	101	12.63	C	DN4	41.5	185	11.56	C
AP4	25.6	135	8.44	C	DN5	41.5	115	14.38	S
AP5	25.6	165	13.75	SEP	DN6	37.2	214	13.38	S
AP6	25.6	132	16.5	SEP	DN7	41.5	120	15.0	S
AP7	25.6	101	12.63	C	DN8	38.5	200	12.5	C
AP8	25.6	135	8.44	C	DP1	25.0	130	16.25	S
AL1	39.7	155	19.38	S	DP2	25.0	165	10.31	C
AL2	39.7	124	15.5	C	DP3	25.0	130	16.25	C
AL3	40.0	245	15.31	C	DP4	25.0	120	7.50	C
ANS1	40.6	215	17.92	SEP	DP5	26.3	110	13.75	SEP
ANS2	40.6	160	20.0	S	DP6	26.3	156	9.75	SEP
ANS3	35.5	144	18.0	S	DP7	25.0	118	14.75	C
ANS4	35.5	255	15.94	SEP	DP8	26.3	130	8.13	C
APS1	24.0	135	11.25	SEP	DL1	40.0	100	12.5	S
APS2	24.0	85	10.63	SEP	DL2	40.0	140	17.5	S
APS3	24.1	130	16.25	SEP	DL3	40.0	220	13.75	S
APS4	24.1	200	12.5	SEP	DNS1	37.6	110	13.75	S
AN1F	35.7	140	17.5	S	DNS2	36.3	160	10.0	SEP
APS1F	23.6	135	16.88	SEP	DNS3	36.6	100	12.5	S
BN1	41.4	125	10.42	P	DNS4	36.6	200	12.5	SEP
BN2	40.4	190	11.8	P	DPS1	25.1	92	11.5	S
CN1	41.4	345	21.56	SEP	DPS2	25.1	100	6.25	SEP
CN2	41.4	265	16.56	C	DPS3	24.6	105	13.13	SEP
CN3	38.5	160	20.0	S	DPS4	24.6	140	8.75	SEP
CN4	38.5	132	16.5	C	DN1F	35.7	135	16.88	S
CP1	24.9	275	17.19	C	DPS1F	23.6	100	12.5	SEP
CP2	24.9	150	18.75	S					

Key C Shearing of the concrete
 S Shearing of the connectors
 SEP Separation between the steel and the concrete
 P Pulling out of the concrete

TABLE 2. SUMMARY OF THE RESULTS

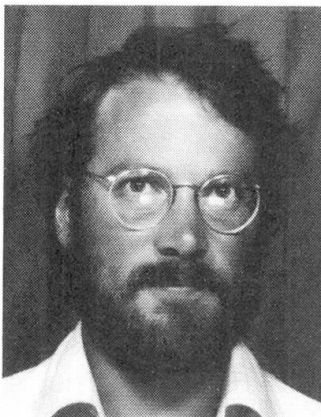
Behaviour of Profiled Sheetting during Composite Floor Construction

Comportement des tôles profilées lors du bétonnage des planchers mixtes

Verhalten von Stahlblechen während der Herstellung von Verbunddecken

Howard D. WRIGHT

Lecturer
University College
Cardiff, UK



Howard Wright, born 1952, obtained his Degree at Sheffield University, GB. He has worked for the Electricity Board and the Boots Co P.L.C. as a structural engineer before joining the lecturing staff at University College, Cardiff in 1982.

H. Roy EVANS

Prof. of Struct. Eng.
University College
Cardiff, UK



Roy Evans, born 1942, obtained his degree at University College, Swansea. Following a period with Freeman Fox and Partners he joined the staff of University College, Cardiff in 1969, where he is now Professor of Structural Engineering and Head of the Department of Civil and Structural Engineering.

SUMMARY

The behaviour of profiled steel sheeting under wet concrete loading is considered in this paper. Simple analysis techniques give acceptable prediction of centreline deflection but do not attempt to model the edge deformation. Such deformation is of consequence when imperfect lap or crimp joints are formed between sheets. A folded plate analysis method is developed and compared to experimental results. The analysis is then used to predict the edge deformation lap joint deformation and crimped joint deformation of profiled steel sheets subject to wet concrete loading.

RÉSUMÉ

Cette contribution concerne le comportement des plaques nervurées de planchers sous l'action du béton frais. Un simple calcul statique donne une bonne estimation de la flèche médiane de tels systèmes, mais ne permet pas de modéliser la déformation des bords des plaques. De telles déformations sont importantes lorsque les recouvrements ou les emboîtements latéraux sont imparfaits entre les plaques nervurées. Une méthode basée sur l'analyse des structures plissées a été développée, dont les résultats sont comparés aux essais. Cette analyse permet de calculer les déformations aux bords libres, aux recouvrements et aux emboîtements des plaques nervurées soumises au poids du béton frais.

ZUSAMMENFASSUNG

Das Verhalten von Profilblechen unter der Last von frischem Beton wird in diesem Aufsatz untersucht. Eine einfache statische Berechnung führt zu einer brauchbaren Bestimmung der Verformungen in der Mittellinie, eignet sich aber nicht als Modell für die Verformung der Kanten. Solche Verformungen müssen berücksichtigt werden, wenn unvollständige Überlappungs- oder Faltstöße zwischen den Blechen vorkommen. Eine Methode der Faltwerte wird angewandt und mit Versuchsergebnissen verglichen. Die Methode wird dann benutzt, um die Kantenverformungen bei Überlappungs- und Faltstößen von Profilblechen unter Frischbeton-Last zu ermitteln.



1. INTRODUCTION

In this paper the structural behaviour of profiled steel sheeting under load will be investigated with specific reference to the loading likely to occur during the construction of a composite floor slab. Installation of such a slab is carried out by laying lengths of profiled steel sheeting over supporting floor beams. The sheeting is normally fixed to the floor beams with self tapping screws or shot fired pins and connected along the longitudinal edges by screws or rivets. The resulting surface is then concreted.

The wet concrete exerts a pressure loading normal to each plate as the concrete may be assumed liquid at this stage. This pressure varies; between top and bottom flanges of the profile due to the increased depth of concrete, along the span due to the presence of ponding (see Fig. 1(a)) and occasionally across the sheet if there is reduced edge support (see Fig. 1(b)).

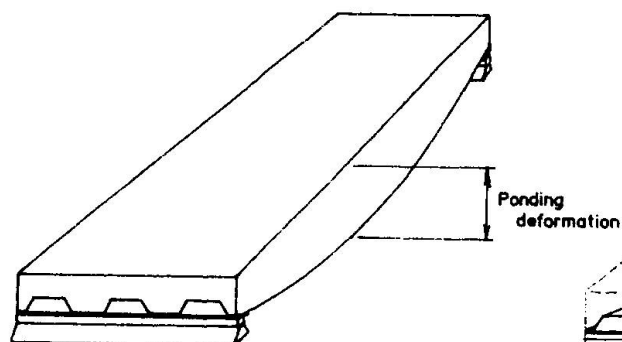


Fig. 1a

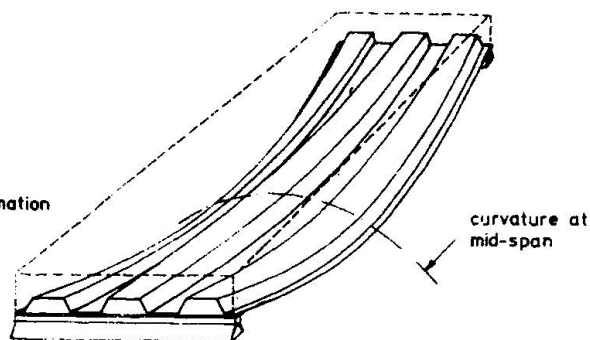


Fig. 1b

2. ANALYSIS FOR DESIGN

The application of simple beam theory gives good agreement with test results. The A.I.S.I. Specification for the Design of Cold Formed Steel Structural Members¹ uses this technique and adopts an effective width approach to plate buckling. This method provides a simple design solution for the complex behaviour of plate buckling. Its integration into the simple beam approach gives rise to the need for iteration and this makes the analysis tedious.

Despite the tedium of analysis and conservatism involved with stiffener design the A.I.S.I. code has become a model for both the British Code of Practice BS 5950 Pt² and the European recommendations on profile steel sheet design.

3. COMPARISON OF CODE PREDICTIONS AND TEST RESULTS

The A.I.S.I. code, British Code and European Recommendations have been used to evaluate the load deflection response of four typical profiles and the results have been compared to those of an experimental investigation.

The tests were carried out on samples of sheeting between 700mm and 800mm wide. The load was applied as a uniform pressure over the whole sheet by means of an air bag acting against a restraint frame. Deflections were measured by dial gauges at midspan and on the centreline only.

A typical load deflection plot for one of the profiles is given in Fig. 2 and superimposed are the plots evaluated by the A.I.S.I./ British Code and the European Recommendations. Reasonable agreement between experimental and predicted values is noted. However, since such sheets are to be mass produced, a more accurate analysis is required.

The results of a more accurate analysis capable of looking, not only at central

pitch behaviour, but also at unsupported edge and longitudinal joint behaviour in the linear and post-buckling range is now presented.

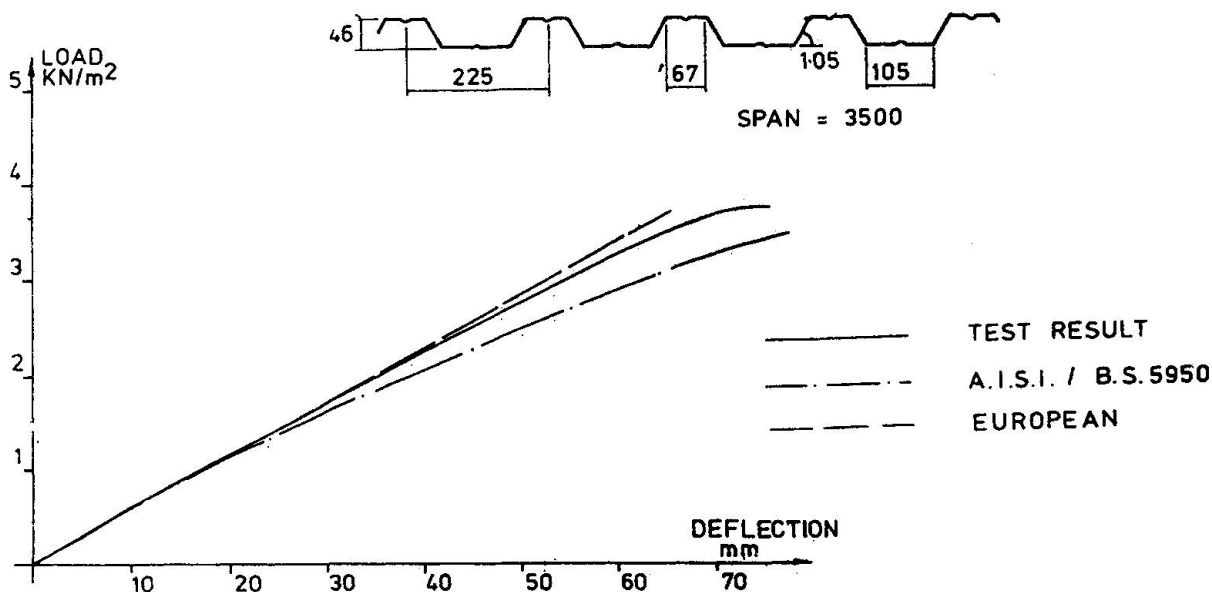


Fig. 2

4. ANALYSIS USING FOLDED PLATE METHODS

There are three possible analysis methods that could give a more accurate prediction of behaviour, viz. finite element, finite strip and folded plate methods. The last of these offers significant advantages for this situation and is adopted for the investigation in this paper.

The introduction (see Fig.1) cited loading and deformation characteristics of profiled steel sheeting that cannot be modelled by simple beam methods. The more complex folded plate methods can predict deformation under such loading. To demonstrate this, the application of the method to a typical representative profile⁴ will be described and the results compared to analysis using the simple beam method.

a) Free Edge Effects

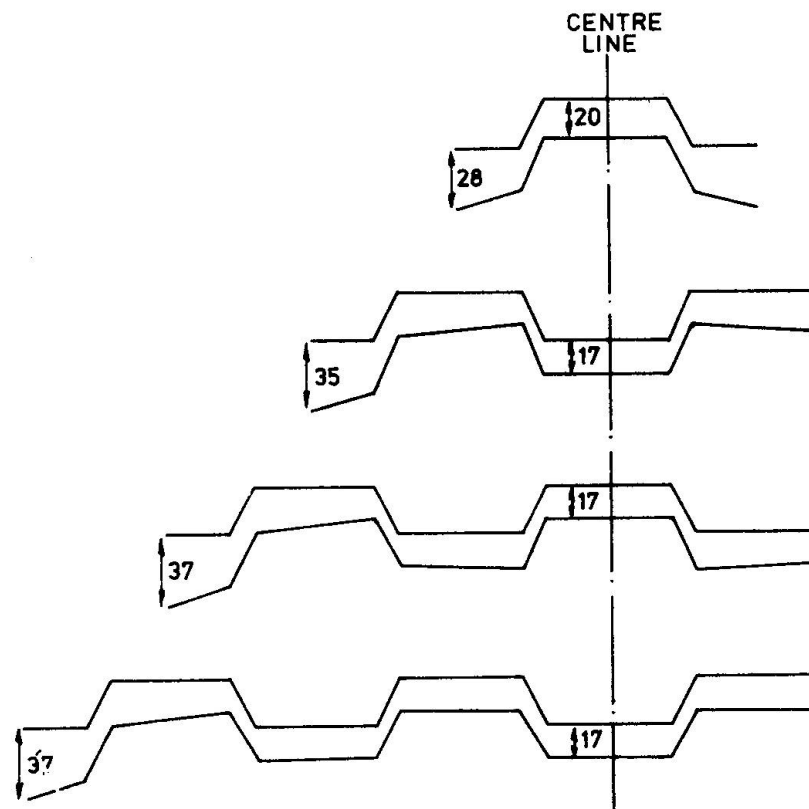
Even if the additional load due to lateral distortion and ponding is not taken into account profile edges will still distort more than the central pitches even under a uniform pressure distribution. To investigate this, folded plate analysis was used to predict the deflected shape of one, two, three and four pitch samples of a 3m span of the model profile subject to a uniform pressure of 2 kN/m² on each plate. The results of these analyses are shown in Fig. 3.

b) Edge Deformation of Lapped and Crimped Joints

Current codes of practice use the simple beam method to predict the deformation of entire floor areas. In the analysis it is assumed that the joints between adjacent profiled sheets are continuous and uniform vertical deflection results. In reality, the longitudinal joints between sheets may be lapped or have crimped upstands. These joints may not support the edge fully and the deflected shape of the floor may resemble that shown in Fig. 4.

The folded plate analysis developed for prediction of unsupported edge effects can be used to investigate the deformation pattern of joints. Figure 5 shows a typical lap joint with elemental plates numbered. It is assumed that the deformation of this joint will produce only one contact edge between the sheets and that this occurs along fold lines. The degree of connectivity between the nodes representing the folds may be adjusted to simulate real conditions.

This connectivity for a lap joint may be itemised as follows :



Mid-span deformation for 3m span samples carrying 2 kN/m^2 .

Fig. 3

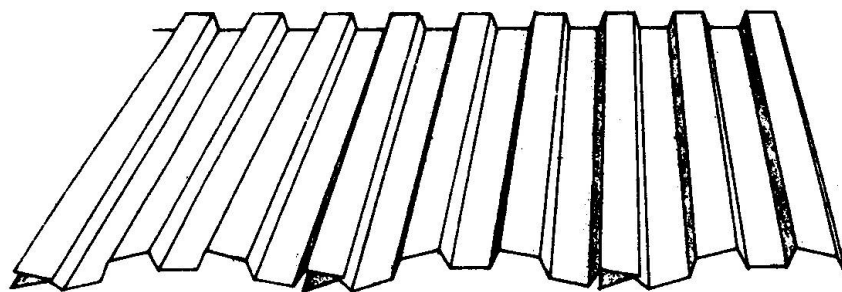


Fig. 4

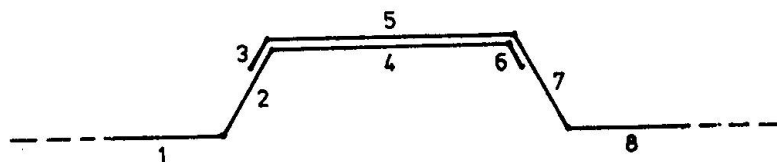


Fig. 5

- a) Longitudinal connectivity:- There will be only slight frictional forces between the two sheets along the span and therefore complete freedom may be allowed.
- b) Lateral connectivity:- This will depend on the keying effect of the two sheets. If they lap closely then no movement will occur and lateral movement will be restrained. If they lap loosely or relative vertical movement occurs before loading then there may be complete lateral freedom.
- (c) Vertical connectivity:- The upper lap will normally carry load and deflect onto the lower lap. Consequently there is complete connection between nodes in the vertical direction.
- (d) Rotational connectivity:- The two sheets are capable of free rotation and no rotational fixity is assumed.

Assuming this pattern of joint connection the folded plate analysis was used to determine the deformation of the lapped joint. It was found that considerable variation occurred when lateral connectivity was assumed fixed or free. If the lap between sheets is riveted then lateral movement is fully restricted and the joint becomes more stiff than the adjacent pitches. If the lap is left unconnected then considerable rotation and deformation occurs. These patterns of behaviour are shown in Fig. 6.

An alternative method of jointing is the crimped upstand joint shown in Fig. 7. This joint, when well formed, provides complete connectivity in all directions, but often the crimping may not be perfect and this will allow rotational freedom between sheets. It is also possible that uneven loading of a badly crimped joint may cause the two sheets to separate completely before loading. In this latter case the sheets act completely separately. The deformation predicted by folded plate methods for each of these conditions is shown in Fig. 7.

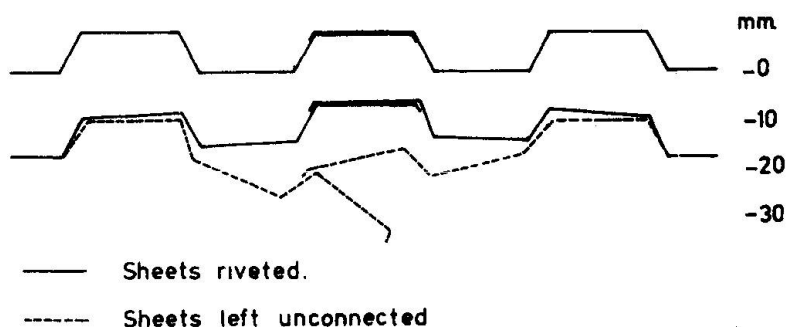


Fig. 6

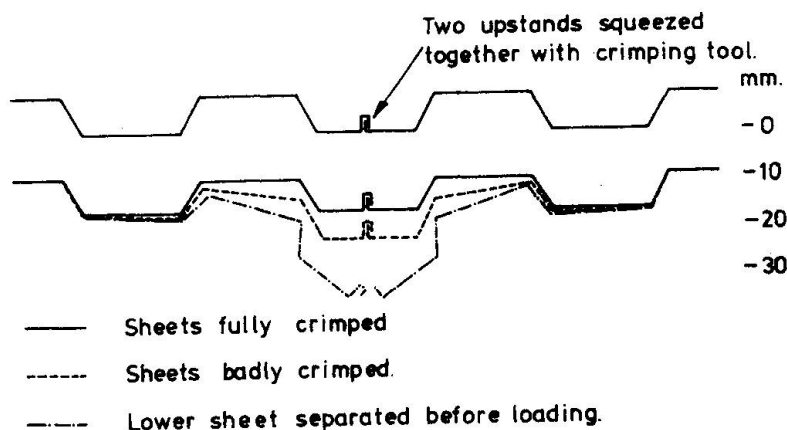


Fig. 7



The behaviour of both lapped and crimped joints has been shown to depend on the degree of connectivity between the sheets. It must also depend on the geometry of the sheet and upstand if used. Only one geometry has been investigated here and this has not been confirmed by test. However, test verification of the folded plate method has been undertaken for a free edge model and this is now described.

5. THE EFFECTS OF WET CONCRETE LOADING

As described in the introduction, wet concrete finished to a level surface gives rise to a non-uniform pressure distribution on the sheeting. The effects of this distribution can, conveniently, be split into three parts. Firstly, the effects due to the variation of pressure with depth, secondly, the effects of ponding and, thirdly, the effects of edge distortion of the sheeting.

a) The Effects of Variable Pressure Loading

During the casting operation the load of wet concrete acts as a liquid and the pressure on individual plates varies with depth of concrete. This fact is ignored when simple beam methods, where a uniform vertical pressure is assumed to act over the entire sheet, are used. The normal nature of pressure loading is also ignored by the simple beam method. The angled webs are subject to a vertical and a lateral load component of which only the vertical component, is used in the simple beam analysis.

Variable pressure is conveniently catered for by careful specification of the input data in the folded plate analysis.

b) Ponding Deformation

Ponding has been shown diagrammatically in Fig. 1. The European recommendations give guidance on the calculation of ponding deformation by adding an equivalent uniformly distributed load to simulate the ponding load. The equivalent load is determined from the mid span deflection under nominal concrete depth. An additional depth of concrete equal to 0.7 times this deflection is the resulting equivalent ponding load.

The use of equivalent uniformly distributed loads to simulate ponding is unnecessary with the folded plate method. Uniformly distributed loads are simulated, in this method, by the summation of harmonics of a sine wave. The first harmonic is identical in form to the assumed deflected shape. Consequently, when the deflection under a uniformly distributed load has been found the folded plate analysis can be repeated for the first harmonic only, thus giving a theoretically accurate distribution of ponding load. However, under this load further deflection ensues and subsequent first harmonic analyses are required to iterate to an acceptable convergence.

c) Lateral Distortion

As the folded plate computer program requires input data for each individual plate, the lateral distortion of an unsupported edge subject to ponding load is modelled automatically.

6. TEST VERIFICATION OF PONDING AND LATERAL DISTORTION ANALYSIS

A test was devised specifically to monitor the ponding and edge deformation of a profiled steel sheet loaded in a manner similar to that caused by wet concrete.

A 3.5 m long sample of "P.M.F. Ltd. CF 46 composite profile" was simply supported on roller bearings to give a clear span of 3.422 m. Timber formwork was then erected around the sample. Fine builders sand was then spread over the profile and finished to a level surface. Sand, rather than wet concrete, was used as it is a more manageable medium. Mid span deformation was measured at ten points across the sheeting with dial gauges.

Figure 8 shows the results of this test in comparison to the analysis developed in the previous Section. The accuracy of the analysis for the centreline profile deformation is shown and the edge deformation is also shown to be very close.

The centreline deflection of the profile was also calculated in accordance with the European recommendations to include the effects of ponding. This method also proved accurate, predicting the deformation within one millimetre of the folded plate and experimental value. It must be pointed out, however, that the European

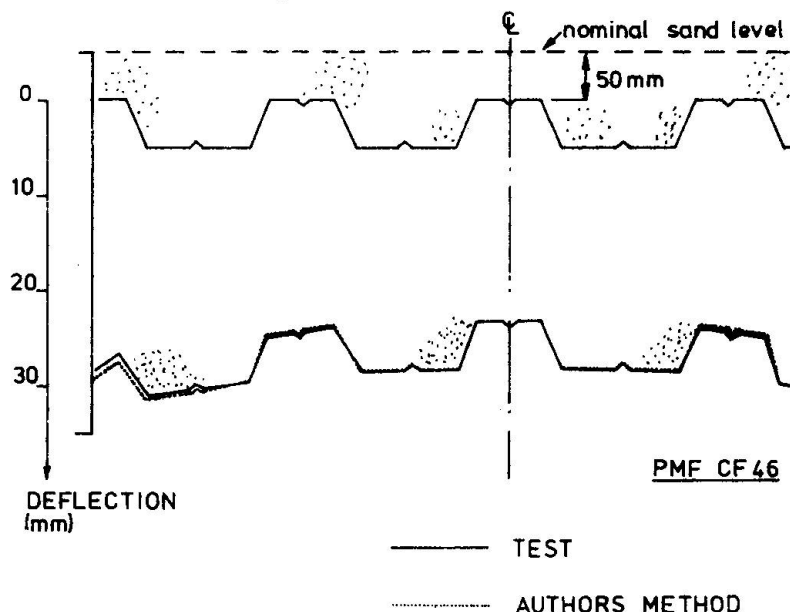


Fig. 8

recommendations cannot evaluate the very significant edge deformation.

The edge deformation in the test was sufficient to cause buckling in the outer plates. Considering the density of sand (14 kN/m^3) in comparison with wet concrete (24 kN/m^3) leads to the conclusion that the deformation under wet concrete would have been considerable. An analysis for the wet concrete case showed an edge deformation of 52 mm which was over 25% greater than that predicted by the European recommendations.

7. CONCLUSIONS

The development of a folded plate analysis method for the prediction of deflection of profiled steel sheeting has been described in this paper.

The deformations of profiled steel sheets have been predicted for free edges, lapped joints and crimped joints. The close comparison between the analysis and a test on a free edge specimen confirms the validity of these predictions. The observed and predicted deformation patterns indicate the large errors that can arise from using the simple beam method.

REFERENCES

- 1 AMERICAN IRON AND STEEL INSTITUTE, Cold-Formed Steel Design Manual, 1968.
- 2 B.S.5950 : Part 4 : 1982. Structural Use of Steel in Building. Code of Practice for Design of Floors with Profiled Steel Sheeting.
- 3 EUROPEAN RECOMMENDATIONS FOR STEEL CONSTRUCTION. ECCS-TC7, The Design of Profiled Steel Sheeting, 1983 CONSTRADO.
- 4 CONSTRADO, Steel Framed Multi-Storey Buildings. Design Recommendations for Composite Floors and Beams using Steel Decks. Section 1 Structural. Oct. 1983.

Leere Seite
Blank page
Page vide

Colonnes tubulaires à parois minces remplies de béton

Betongefüllte Hohlprofilstützen

Concrete Filled Thin-Walled Tubular Steel Columns

Jacques RONDAL

Chargé de Cours
Université de Liège
Liège, Belgique



Jacques Rondal est né en 1944. Il est ingénieur civil des Constructions et Docteur en Sciences Appliquées de l'Université de Liège. Spécialisé en Stabilité des Constructions et en Optimisation des structures, il est auteur de plus de 100 publications scientifiques.

Jean MOUTY

Dir. Techn. et Adm.
COMETUBE
Levallois, France



Jean Mouty est né en 1932. Il est Ingénieur ENSAM et s'est spécialisé dans l'emploi des tubes en acier dans la construction. Il est membre de la S/C XV E de l'IIS, de la Commission 8 de la CECM et président de la Commission Technique du CIDECT.

RÉSUMÉ

Les colonnes en profils creux remplis de béton constituent une solution économique dans les immeubles multi-étagés. En cas d'utilisation de profils à parois minces, le béton joue un rôle favorable dans le voilement local des parois. Le but de cette contribution est de présenter une méthode de calcul des colonnes constituées de profils creux en acier, de sections carrées, à parois minces, remplis de béton.

ZUSAMMENFASSUNG

Betongefüllte Hohlprofilstützen stellen für mehrstöckige Gebäude oft eine wirtschaftliche Lösung dar. Wenn dünnwandige Hohlprofile benutzt werden, wirkt sich der Beton beim örtlichen Ausbeulen der Wandung günstig aus. Das Ziel dieses Beitrags ist die Vorstellung einer Berechnungsmethode für dünnwandige, betongefüllte, quadratische Stahlhohlprofile.

SUMMARY

Concrete filled tubular steel columns are often an economical construction procedure for high-rise buildings. When the walls of the profiles are thin, the concrete has a positive effect on the local buckling phenomenon. The aim of the present paper is to propose a design method for concrete filled thin-walled square hollow steel columns.



1. INTRODUCTION.

Les colonnes en profils creux remplis de béton, qui combinent harmonieusement les qualités spécifiques de l'acier et du béton, constituent une solution particulièrement économique pour les colonnes de bâtiments multi-étagés.

Dans de nombreux cas, on est amené à choisir, comme profil tubulaire en acier, des formes carrées plutôt que des profils circulaires afin de simplifier les assemblages des poutres aux colonnes.

Lorsque les parois des profils en acier deviennent relativement minces, il peut y avoir apparition, dans les parois des colonnes, du phénomène de voilement local qui entraîne une diminution de la charge de ruine de la colonne par rapport au phénomène de flambement. Cette interaction entre voilement local et flambement global dans les profils tubulaires à parois minces de formes carrées ou rectangulaires a fait l'objet d'une recherche, menée par COMETUBE et l'Université de LIEGE, qui a permis de proposer une méthode simple et précise de calcul de la charge de ruine des poteaux et poutres-poteaux à parois minces [1].

Le but de cette contribution est d'étendre la méthode au cas des profils à parois minces, de section carrée, remplis de béton. La méthode proposée permet un calcul simple et précis d'un tronçon court constitué d'un profil creux de forme carrée, à parois minces, remplis de béton. Comme il a été montré dans [1], il est aisé, une fois calculée cette charge de tronçon court, de passer au calcul des poteaux longs.

2. CHARGE DE RUINE D'UN TRONÇON COURT.

La charge de ruine d'un tronçon court constitué d'un tube de forme carrée, à parois minces, rempli de béton est donnée par [2, 3] :

$$N = N_A + N_B \quad (1)$$

avec

$$N_A = \bar{N}_V \cdot A \cdot f_y \quad (2)$$

où A est la section d'acier, f_y est la limite élastique de l'acier et \bar{N}_V est le coefficient de réduction au voilement local, et

$$N_B = B \cdot f_{ck} \quad (3)$$

où B est la section de béton et f_{ck} est la résistance caractéristique du béton sur cylindre.

Pour un tube carré, dont les dimensions sont précisées à la figure 1, les sections d'acier et de béton sont données par :

$$A = 4at - 4t^2 - (4 - \pi)(r^2 - r_{int}^2) \quad (4)$$

$$B = (a - 2t)^2 - \pi \cdot r_{int}^2 \quad (5)$$

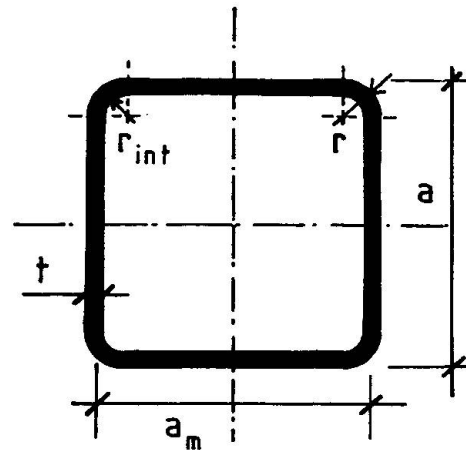


Figure 1 - Notations.

3. COEFFICIENT DE VOILEMENT POUR UN TUBE CARRE.

Selon [1], le coefficient de voilement \bar{N}_V peut, pour un tube carré non rempli de béton, être calculé à l'aide d'une équation de type AYRTON-PERRY :

$$(1 - \bar{N}_V) (1 - \bar{N}_V \cdot \bar{\lambda}_V) = \beta (\bar{\lambda}_V - \bar{\lambda}_{V0}) \bar{N}_V \quad (6)$$

avec :

$$\bar{\lambda}_{V0} = 0,8 \quad (7)$$

et $\beta = 0,35$ (tubes finis à chaud)

$\beta = 0,67$ (tubes finis à froid).

Sous forme directe, la relation (6) donne (figure 2) :

$$\bar{N}_V = \frac{1}{2\bar{\lambda}_V} \{ 1 + \beta (\bar{\lambda}_V - \bar{\lambda}_{V0}) + \bar{\lambda}_V - \sqrt{[1 + \beta (\bar{\lambda}_V - \bar{\lambda}_{V0}) + \bar{\lambda}_V]^2 - 4\bar{\lambda}_V} \} \quad (8)$$

Dans les formules (6) et (8), l'élancement relatif est donné par :

$$\bar{\lambda}_V = \sqrt{\frac{f_y}{\sigma_{crv}}} = \frac{a_m}{1,9 t} \sqrt{\frac{f_y}{E}} \quad (9)$$

où σ_{crv} est la contrainte critique de voilement d'une paroi.

Lorsque le tube est rempli de béton, le phénomène de voilement est bridé pour la présence du béton. En effet, si les deux faces qui se déforment vers l'extérieur ne sont pratiquement pas influencées par le béton, il n'en est pas de même des deux faces qui tendent à se déformer, lors du voilement local, vers l'intérieur de la section [4].

Ces dernières se comportent comme des plaques sur une fondation élastique. A l'aide des relations établies par SEIDE [5], il est aisé de montrer, pour le cas d'une fondation agissant uniquement lors d'une "compression", que la rigidité du béton est telle que l'on peut donner au coefficient de voilement la valeur $k = 5,33$ au lieu de la valeur $k = 4$ habituellement utilisée pour les plaques à côtés simplement appuyés. Il est dès lors aisé de calculer, pour les côtés se déformant vers l'intérieur du profil, une largeur de voilement réduite par la présence du béton et donnée par :

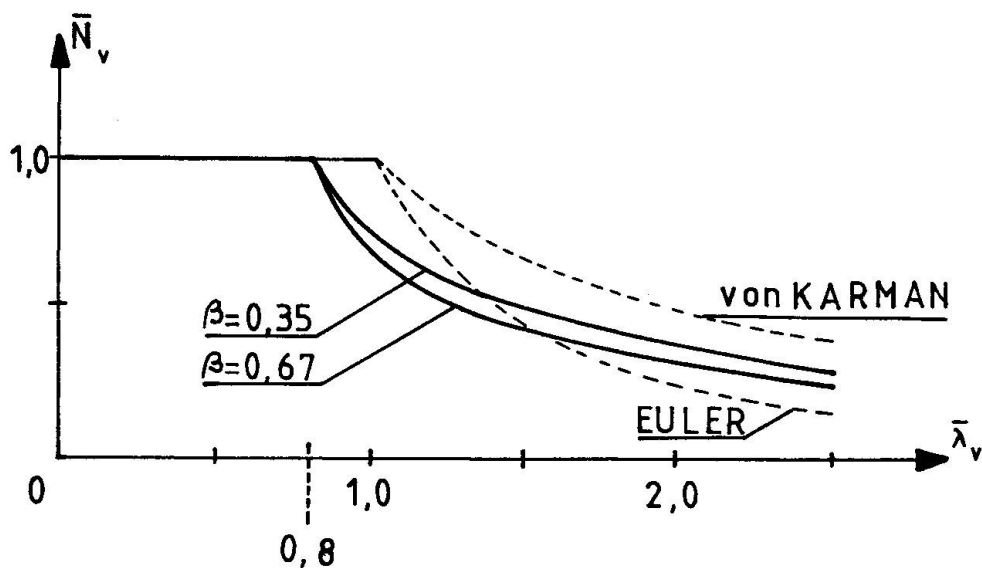


Figure 2 - Courbes de voilement.

$$4 \frac{\pi^2 E}{12(1 - \nu^2)} \left(\frac{t}{a_m}\right)^2 = 5,33 \frac{\pi^2 E}{12(1 - \nu^2)} \left(\frac{t}{b_m}\right)^2 \quad (10)$$

soit :

$$b_m = 0,866 a_m \quad (11)$$

On en vient ainsi à remplacer le profil initial par un profil rectangulaire équivalent (figure 3).

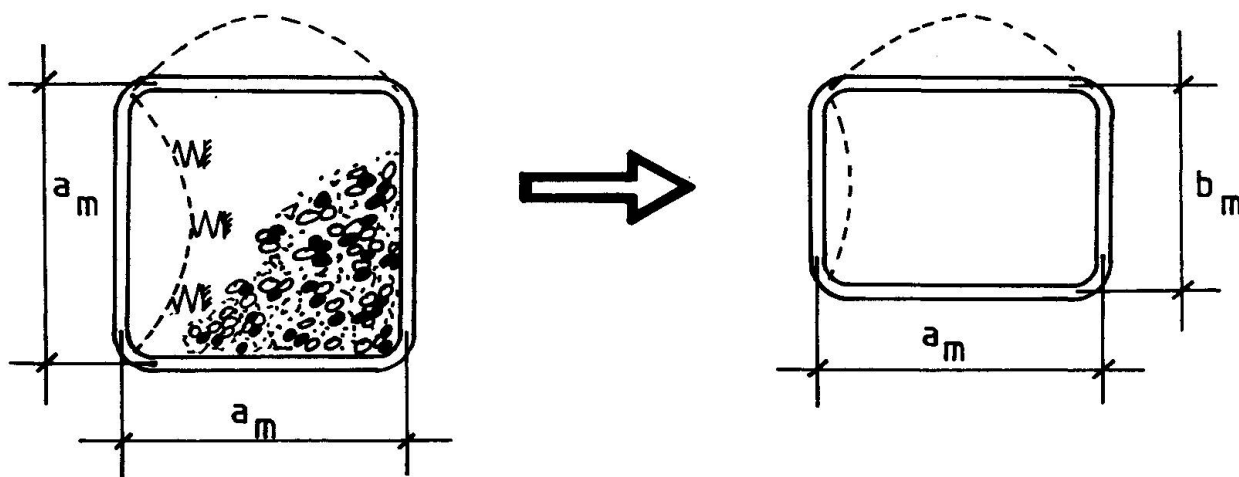


Figure 3 - Profil rectangulaire équivalent.

Comme il a été montré dans [1], les faces ne voilent pas simultanément dans un profil rectangulaire et les petites faces jouent, pour les grandes faces, un rôle d'encastrement partiel. Ce comportement peut être pris en compte à l'aide d'un coefficient d'encastrement qui dépend du rapport des dimensions du profil [1].

$$\mu = \frac{6,8 - 3 (b_m/a_m)^2}{7,8 - 3 (b_m/a_m)^2} \quad (12)$$

ce qui permet de définir les élancements relatifs des parois du profil creux :

$$\bar{\lambda}_{V(a_m)} = \mu \frac{a_m}{1,9 t} \sqrt{\frac{f_y}{E}} \quad (13)$$

$$\bar{\lambda}_{V(b_m)} = \frac{b_m}{1,9 t} \sqrt{\frac{f_y}{E}} \quad (14)$$

A l'aide de la relation (8), il est aisé de calculer les coefficients de voilement des faces, soient $\bar{N}_{V(a_m)}$ et $\bar{N}_{V(b_m)}$ et de définir un coefficient de voilement de la section donné par :

$$\bar{N}_V = \frac{\bar{N}_{V(a_m)} + \bar{N}_{V(b_m)}}{2} \quad (15)$$

4. VERIFICATION EXPERIMENTALE.

A l'aide des essais effectués par JANSS [6, 7], il est aisé de vérifier la validité de la théorie proposée.

Le tableau 1 donne les caractéristiques des trois séries de profils expérimentés. Le tableau 2 donne une comparaison des résultats expérimentaux aux valeurs théoriques calculées :

- sans tenir compte du voilement local (N_1) ;
- en considérant le voilement local sans tenir compte de l'influence du béton (N_2) ;
- en considérant l'influence du béton sur le voilement local des parois du profil creux (N_3).

Profil	A	B	C
a (mm)	331	331	331
t (mm)	4,5	6,35	10,1
f_y (N/mm ²)	372	447	390
f_{ck} (N/mm ²)	30,4	30,4	30,4
A (mm ²)	5807	8108	12614
B (mm ²)	103541	101030	95876

Tableau 1 - Caractéristiques des profils (profils finis à froid).



Profil	$N_{\text{exp.car.}}$ (kN)	N_1 (kN)	N_2 (kN)	N_3 (kN)	$\frac{N_{\text{exp.car.}}}{N_1}$	$\frac{N_{\text{exp.car.}}}{N_2}$	$\frac{N_{\text{exp.car.}}}{N_3}$
A	4194	5308	4008	4108	0,79	1,05	1,02
B	5602	6695	5006	5246	0,84	1,12	1,07
C	7951	7834	7834	7834	1,01	1,01	1,01

Tableau 2 - Comparaison des valeurs calculées aux valeurs expérimentales caractéristiques.

Les résultats du tableau 2 permettent de tirer diverses conclusions :

- pour le profil de type C, qui est un profil à parois épaisses, il n'y a pas de différence entre N_1 , N_2 et N_3 et la corrélation entre théorie et expérience est excellente ;
- le fait de négliger l'effet du voilement local (charges calculées N_1) conduit à une insécurité importante pour les profils à parois minces ;
- la prise en compte du voilement local des parois conduit à un calcul sécuritaire ;
- la prise en compte de l'effet du béton sur le voilement local des parois conduit à une prédiction, à la fois, sûre et précise de la charge de ruine.

5. CONCLUSION.

La méthode proposée permet, sans grande difficulté de calcul, de prendre en compte l'effet du béton sur le voilement local des parois d'un tube en acier, de forme carrée, à parois minces.

BIBLIOGRAPHIE.

1. GRIMAULT J.P., MAQUOI R., MOUTY J., PLUMIER A. et RONDAL J., Stabilité des poutres-poteaux en profils creux à parois minces. Construction Métallique, n° 4, 1984, pp. 33 - 41.
2. CIDECT-CECA, Construire avec des profils creux en acier. Edition en français réalisée par la Chambre Syndicale des Fabricants de Tubes d'Acier et COMETUBE, Paris, 1ère édition, Octobre 1984.
3. AIPC-CEB-CECM-FIP, Projet de code modèle pour constructions mixtes. Construction Métallique, N° 1, 1980, pp. 3 - 99.
4. MATSUI C., Local Buckling of Concrete Filled Steel Square Tubular Columns. IABSE-ECCS Symposium Luxembourg, Symposium Report, IABSE Reports, Volume 48, 1985, pp. 269 - 276.
5. SEIDE P., Compressive Buckling of a Long Simply Supported Plate on an Elastic Foundation. J. Aero. Sc., Vol. 25, N° 6, 1958, pp. 382 - 384.
6. GRIMAULT J.P. et JANSS J., Reduction of the Bearing Capacity of Concrete Filled Hollow Sections due to Local Buckling. ECCS Colloquium on Stability of Steel Structures, Preliminary Report, Liège, 1977, pp. 175 - 179.
7. JANSS J., Charges ultimes des profils creux remplis de béton chargés axialement. Centre de Recherches Scientifiques et Techniques de l'Industrie des Fabrications Métalliques, MT 101, Bruxelles, Novembre 1974.

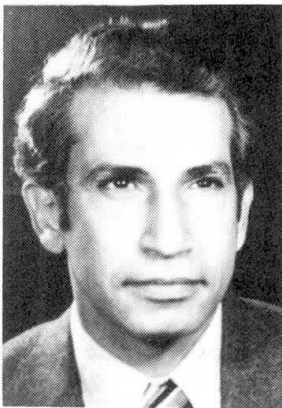
Ultimate Strength of Composite Cold-Formed Steel-Concrete Columns

Résistance ultime des colonnes mixtes composées de profilés formés à froid et de béton

Traglast von Verbundstützen, zusammengesetzt aus kaltverformten Profilen und Beton

George ABDEL-SAYED

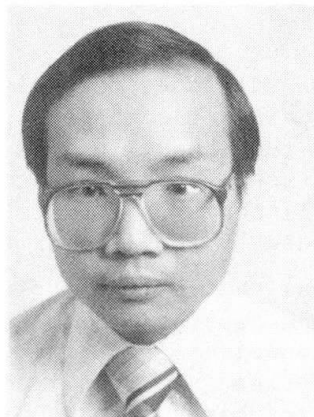
Professor
University of Windsor
Windsor, ON, Canada



Dr. Eng. G. Abdel-Sayed, born in 1933, is a graduate of Cairo University and the Technical University of Karlsruhe, FR Germany. He is involved in research and design of cold-formed steel structures and composite soil-steel structures.

Kwok-Cheung CHUNG

Structural Engineer
Wilson, Dario & Associates
Windsor, ON, Canada



K.C. Chung, born in 1951, is a graduate of the University of Windsor in both Civil Engineering and Commerce. He is active in the field of design of steel and reinforced concrete structures. He also worked for two years as a Research Assistant at the University of Windsor.

SUMMARY

A new system of composite columns is developed using lipped cold-formed steel channels with embossments and cast-in-place concrete. The combined action of the embossments and the channel's lips leads to very good bond characteristics between the steel and the concrete. Experimental study shows that by replacing the standard longitudinal reinforcing bars by cold-formed steel sections of equal areas, the structural performance of the columns is almost unchanged, while considerable savings are achieved in time and material of construction.

RÉSUMÉ

Cette contribution concerne le développement d'un nouveau type de colonnes mixtes composées de profilés minces formés à froid, dont les ailes ont des rebords et l'âme des bosselages, et de béton coulé sur place. L'action conjuguée des bosselages et des rebords conduit à une très bonne solidarisation entre l'acier et le béton. Une étude expérimentale montre qu'en remplaçant l'armature longitudinale classique d'une colonne en béton armé par des profils formés à froid de même aire, la capacité portante est conservée, alors que des économies considérables sont réalisées en temps et matériaux de construction.

ZUSAMMENFASSUNG

Der vorliegende Beitrag befasst sich mit einer neuen Art von Verbundstützen, die aus kaltverformten Profilen und Ortsbeton bestehen. Der Querschnitt der Profile ist \sqsubset -förmig ausgebildet, wobei die Flanschen an ihren Enden nach innen abgebogen sind und der Steg eingepresste Nocken und Rillen aufweist. Die kombinierte Wirkung infolge abgegebener Flanschen und eingepresster Unebenheiten führt zu einem sehr guten Verbund zwischen Profil und Beton. Experimentelle Untersuchungen zeigen, dass die Traglast einer Stütze beim Ersatz der herkömmlichen Längsbewehrung durch ein kaltverformtes Profil fast unverändert bleibt, während wesentliche Einsparungen an Zeit und Material erzielt werden können.



INTRODUCTION

A new system of beams has been developed in which the standard reinforcing bars are replaced by cold-formed steel sections of equal areas [1]. The structural performance of these beams is almost unchanged while saving is achieved in the cost and time of construction.

The present paper deals with a similar system which is applied to build composite columns with cold-formed steel channels placed at two parallel faces, Fig. 1. Herein, considerable savings are achieved in time and material of construction due to the elimination of the steel ties in the column as well as reduction in the form work.

The present paper outlines the main characteristics of the proposed composite columns, as well as an experimental program directed mainly at examining the ultimate load carrying capacity of these columns.

BOND MECHANISM

Steel in the form of stiffened channels with embossments, Fig. 1a performed well as integral parts of composite columns, Fig. 1b. The combined action of the embossments and the channel's lips lead to very good bond characteristics between the steel channel and the concrete. This can be explained, that the concrete has to be lifted up in order to slide over the embossments, while this movement is restrained by the lips of the channel.

By acting as integral part of the column, the channels are prevented from buckling in a mode separate of the column. Therefore, no local supports are required for the channels as in the case of standard reinforced concrete columns in which ties are required in order to avoid local buckling of the individual reinforcing bars.

ANALYSIS

The proposed composite columns are built with the steel components placed at the outside surface of the section, Fig. 1b. Therefore, the compression strain at failure is governed by the yield strain of the steel (usually 0.0015 to 0.002) rather than by the concrete strain at failure (0.003). Therefore, the ultimate strength analysis of the composite column should be based on a trapezoidal shape for the compressive stress block (Jensen's theory [3]). This assumption is the main difference between the composite analysis and that of standard reinforced concrete columns. The latter analysis assumes Whitney's rectangular stress block on the compressive side.

With proper bond between the concrete and channel, strain compatibility is assumed for the analysis of the column. Herein, the ultimate load, P_u , acting at an eccentricity, e , may be computed using the assumed trapezoidal stress block and the equilibrium and compatibility conditions. Details of the analysis of the composite columns are given by Chung [2].

EXPERIMENTAL PROGRAM

An experimental program has been conducted in order to study the behaviour of the proposed composite columns, Fig. 1b.

The dimensions of the tested columns were limited by the load carrying capacities of the available laboratory facilities. The columns were cast vertically to simulate the actual construction process. A minimum dimension of 152 mm (6 in.) was chosen in order to provide clear passage for the vibrator. The steel channel has the following dimensions: $b = 152$ mm (6 in.); $h' = 50.8$

Table 1 Summary of Tests on the Proposed Composite Columns

Column		Eccentricity mm	Steel		Concrete f' _C MPa	Ultimate Load			Expt. Bond Strength (kN)				Remark
No.	Type		t mm	Fy MPa		Expt. kN	Theor. kN	Expt. Theor.	Initial Slip		Ultimate		
									Total	Per Emboss.	Total	Per Emboss.	
Eccentrically Loaded Columns													
A1	U	105	1.83	361	43.4	280	304	92.1%	---	---	---	---	{ Premature bond failure Did not fail
A2	U	26.2	1.91	446	54.8	---	---	---	---	---	---	---	
A2*	U	50	1.91	446	54.8	420	715	58.7%	---	---	---	---	{ Premature concrete crushing Tension steel yielded
A3	B	203.2	1.83	361	37.0	130	127	102.4%	---	---	---	---	
A4	B	105.5	1.83	361	48.9	320	324	98.8%	---	---	---	---	{ Comp. steel buckled Local buckling of comp. steel
A5	B	50.8	1.83	361	47.6	533	576	92.5%	---	---	---	---	
A5*	B	203.2	1.83	361	47.6	120	128	93.8%	---	---	---	---	{ Local buckling of comp. steel Bond failure
Axially Loaded Columns													
B1	B	0	1.83	361	34.3	993	1028	96.6%	---	---	---	---	{ 565 mm long. Gradual failure in concrete and steel
B2	B	0	1.83	361	32.7	844	978	86.3%	---	---	---	---	
Pull-out Test Columns													
C1	B	0	1.83	361	32.9	---	---	---	70	11.67	177	29.26	{ Applied load 20 mm off centre
C2	B	0	1.83	361	32.9	---	---	---	73	12.15	180	30.0	
C3	B	See remark	1.83	361	34.8	---	---	---	111	13.89	210	26.25	
C4	B	0	1.83	361	34.8	---	---	---	120	15.0	183	22.9	
C5	B	0	1.83	361	35.2	---	---	---	120	12.0	260	26.0	
C6	B	0	1.83	361	35.2	---	---	---	110	11.0	264	26.4	

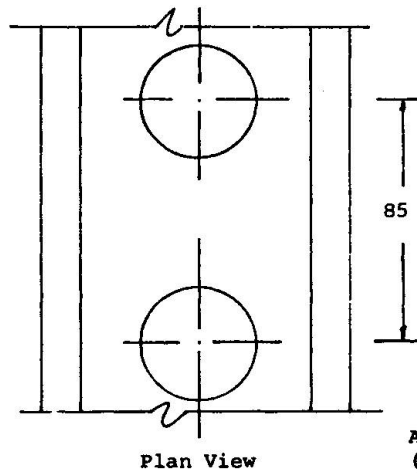
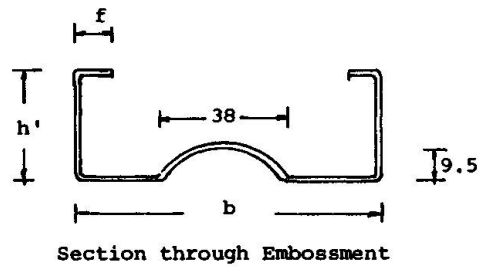
U = Unbattened columns

1 in. = 25.4 mm

B = Battened columns

1 kip = 4.448 kN

1 k.s.i. = 6.895 MPa



All dimensions in mm.
(1 in. = 25.4 mm)

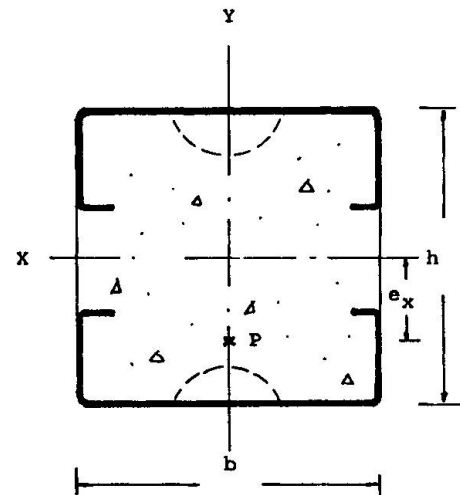


Fig. 1(a) Channels with Round Embossments Fig. 1(b) Proposed Composite Column

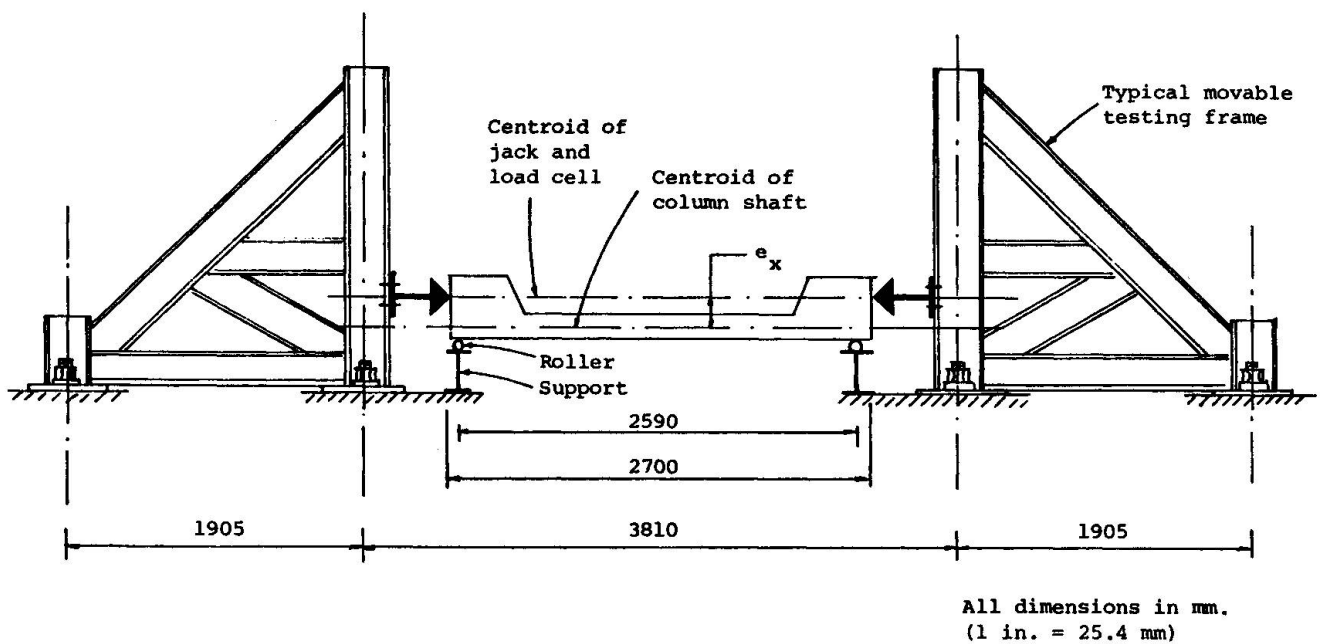


Fig. 2 Set-up of Testing Eccentrically Loaded Columns

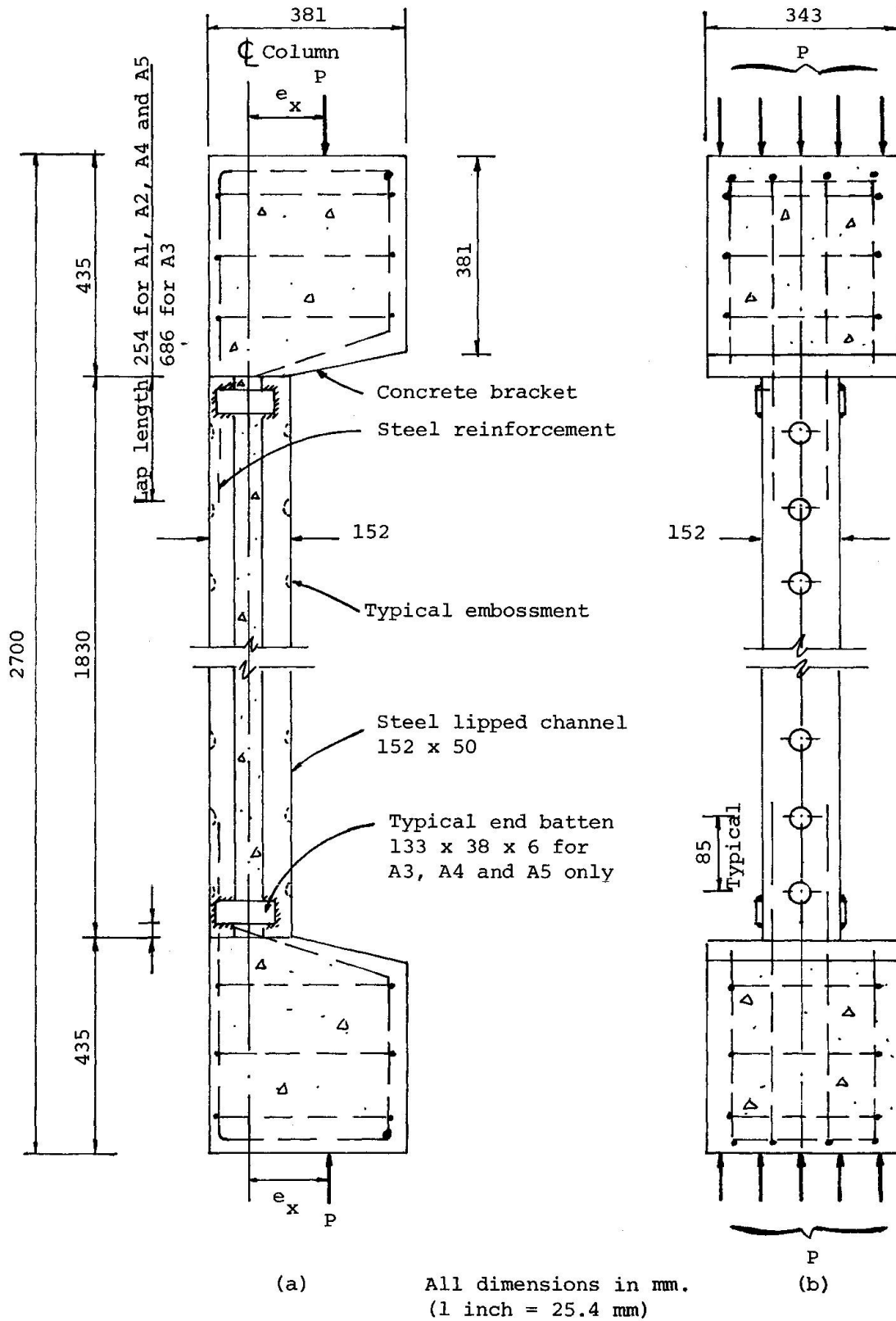


Fig. 3 Typical Eccentrically Loaded Column (Group A)

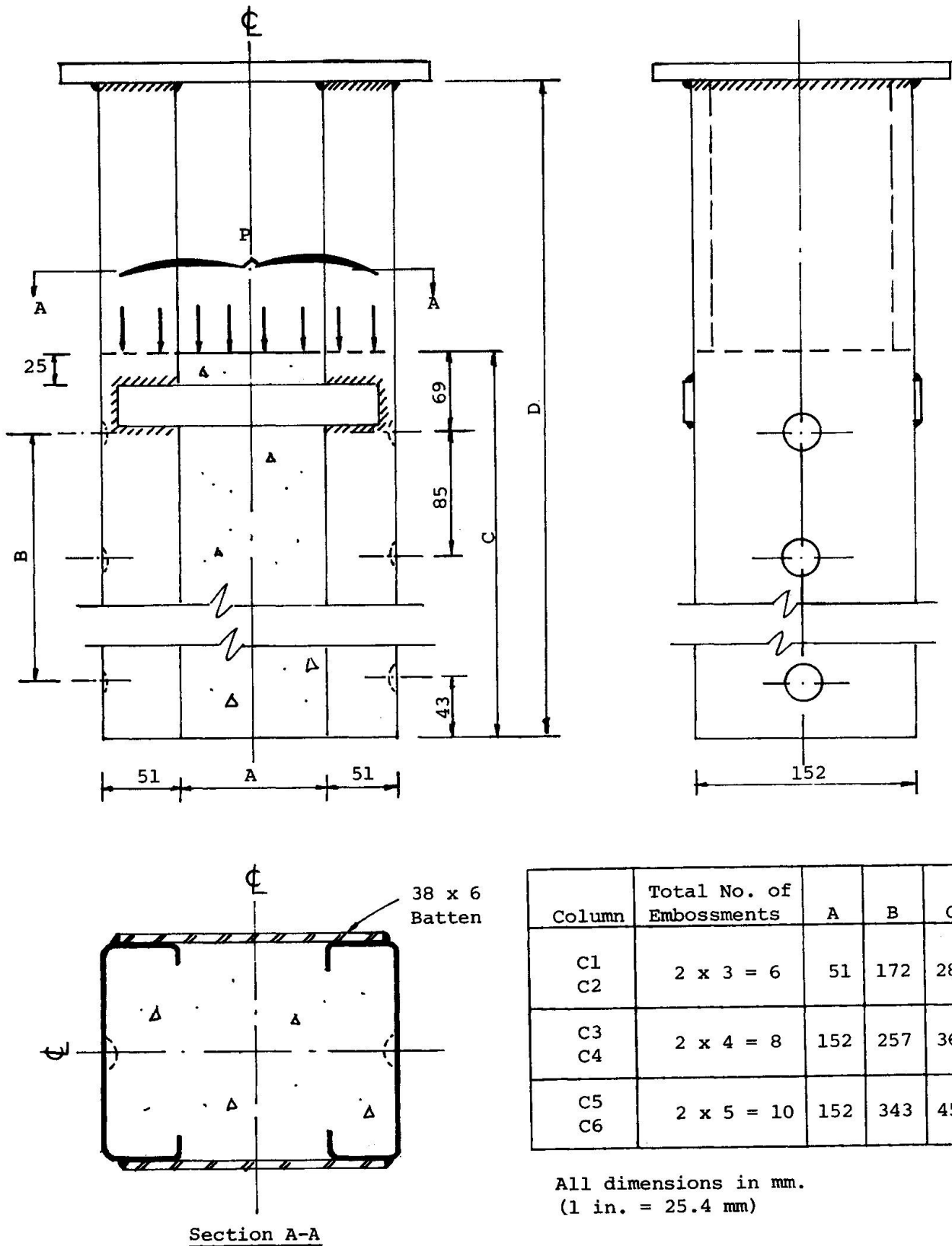


Fig. 4 Typical Pull-out Test Column (Group C)

mm (2 in.); $f = 12.7$ mm (0.5 in.); $t = 1.83$ mm (0.072 in.). The concrete and steel material properties are listed within Table No. 1.

The test specimens are identified by A and B for the eccentrically and axially loaded columns, respectively; and by group C for the pull-out tests. All columns except A_1 and A_2 are provided with two battens at each end, Fig. 3.

Column Tests

The experimental set-up is shown in Fig. 2 while the details of the eccentrically loaded columns are outlined in Fig. 3. Axially loaded columns were built without the end concrete brackets. Strain gauges were placed on the outside face of the exterior channels around an embossment near the mid height of the column. Dial gauges were used to measure the in-plane and lateral mid-height deflections.

Table 1 presents a summary of the ultimate strength of the eccentrically and axially loaded columns. The following has been observed through the test program and by examining Table 1:

- 1 - Comparison between the ultimate load of the tests $A_{1,2}$ and the tests A_3 to A_5 , show that the end battens improve the failure mode and the load carrying capacity of the composite columns. The failure is gradual with end battens, while undesirable sudden split caused the failure in columns with no end battens.
- 2 - Failure of most of the columns was triggered by yielding of the steel section which was observed as the channel web got crippled in the zone between embossments at the compression side. This confirms the assumption that the ultimate load is governed by the yield strain of the steel which is usually lower than the failure strain of concrete (0.003). The ultimate load calculated on the bases of these assumptions is found to be in good agreement with the experimentally obtained load.
- 3 - The combined action of the embossment and the channel's lip lead to very good bond between the channel and the concrete. However, sufficient length of splice should be provided in order to prevent the premature failure at the beam-column connections, as in Test No. A5 (Table 1). This length is determined from pull-out bond tests.

Pull-out Tests

The pull-out test, Fig. 4, is conducted with dial gauges mounted to record any relative displacement (slit or slip) between the concrete and steel. At the pull-out failure, the concrete is displaced forcing the steel to bulge outwards. The concrete surface is scratched by the moving steel embossment. The width and depth of the scratches is maximum near the fully stressed steel section and decreases at the embossments near the stress free end. Such phenomena can explain the observation that the bond strength does not increase proportionally with the increase of number of embossments, Table 1.

CONCLUSION

Lipped channels with embossments performed very well as integral parts of composite columns. No ties were required to prevent the channels from buckling independently of the column leading to savings in time and material of construction. The ultimate load carrying capacity is found to be governed by the yield strain of the steel on either the tension or the compression side.



REFERENCES

1. ABDEL-SAYED, G., Composite Cold-Formed Steel-Concrete Structural System, Proceedings, 6th Specialty Conference on cold-Formed Steel Structures, St. Louis, Missouri.
2. CHUNG, K.C., "Behavior of Composite Concrete Columns With Cold-Formed Steel", M.Sc. Thesis, Dept. of Civil Eng., Univ. of Windsor, Windsor, Ontario, Canada, 1985.
3. JENSEN, V.P., The Plasticity Ratio of Concrete and Its Effect on the Ultimate Strength of Beams, ACI Journal, Vol. 14, No. 6, June 1943, pp. 565-582.
4. LIN, T.Y. and LAKHWARA, T.R., Ultimate Strength of Eccentrically Loaded Partially Prestressed Columns, PCI Journal, Vol. 11, No. 3, June 1966, pp. 37-49.

Sandwich Panels with Cold-Formed Thin Facings

Panneaux sandwich à parements en tôle mince formée à froid

Sandwichplatten mit dünnwandigen kaltgeformten Verkleidungen

Ken P. CHONG

Professor
Univ. of Wyoming
Laramie, WY, USA



Ken P. Chong, F.ASCE, born in 1942, got his Ph.D. degree from Princeton University, NJ, 1969, majoring in structures/solid mechanics. He pioneered the R&D of sandwich panels with cold-formed facings starting in 1970. He is Chairman-elect of ASCE Stability Committee, serves as control member of 3 ASCE committees, and serves on 2 editorial boards of journals.

SUMMARY

Sandwich panels with thin-walled cold-formed facings and rigid foamed insulating core are becoming more and more popular as enclosures for system buildings. In this paper, the structural behavior, including flexural stresses/deflections, axial stability, and thermal stresses, is presented, summarizing more than a decade of research. Methods used are analytical (boundary-valued approaches), numerical (finite-strip, finite-layer, finite prism approaches) and experimental (full-scale testings). Key equations are formulated, and results by different methods are compared.

RÉSUMÉ

Les panneaux sandwich à parements en tôle d'acier et âme en mousse isolante rigide deviennent de plus en plus utilisés comme enveloppes de bâtiment. Dans cet article est présenté le comportement structural des panneaux sandwich à la flexion, à la compression axiale et sous contraintes thermiques, résumant plus de dix ans de recherche. Les méthodes utilisées sont analytiques, numériques et expérimentales. Les équations déterminantes sont formulées et les résultats des différentes méthodes sont comparés.

ZUSAMMENFASSUNG

Sandwichplatten bestehend aus dünnwandigen kaltgeformten Stahlverkleidungen und einer versteifenden Schaumisolierung werden als Fassadenelemente für Fertigteilbauten immer beliebter. In dieser Arbeit wird das strukturelle Verhalten solcher Platten unter Biegebeanspruchung, Axialstabilität und Temperaturbeanspruchung dargestellt. Damit wird mehr als ein Jahrzehnt der Forschung auf diesem Gebiet zusammengefasst. Die verwendeten Untersuchungen basieren auf analytischen (Grenzwertanalysen), numerischen (finite Streifen-, finite Schichten-, finite Prismen-Analyse) und experimentellen (ausführliche Tests) Methoden. Die hauptsächlichsten Gleichungen werden angegeben und die Resultate der verschiedenen Methoden verglichen.



1. INTRODUCTION

Sandwich construction has been widely applied in aircraft and structural engineering since before the Second World War. The structural analysis of sandwich panels with thin flat facings has been investigated as early as the 1940's, particularly for aeronautical applications [1-3]. However, research and development of architectural sandwich panels with formed facings (Fig. 1) began only in the early 1970's, pioneered by Chong and his associates. These panels are becoming popular due to their superior structural efficiency, mass productivity, insulation qualities, transportability, fast erectability, prefabricatability, durability, and reusability. The formed facings serve two purposes: architectural appearance and structural stiffness. In 1972, Chong and Hartsock [4,5] presented a method to predict the localized wrinkling instability of such panels. Subsequently, Chong and his associates have investigated flexural behavior [6,7,8] and thermal stresses [9,10,11] for both simple and continuous spans, axial stability [8,12,13] and vibration [14]. The classical references for flat-faced sandwich panels are given by Allen [1] and Kuenzi [15], and ASCE conducts regular literature surveys [16] including sandwich panels under the composite construction heading.

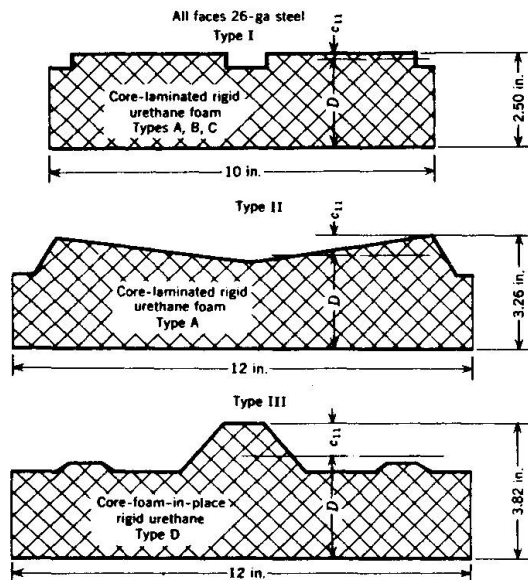


Fig. 1. Panel Geometry [5]
(Note: 1 in = 25.4 mm)

2. FLEXURAL BEHAVIOR

The flexural behavior of sandwich panels subject to bending is investigated analytically [7,17], experimentally [7], and numerically [8].

2.1 Analytical Studies

The basic assumptions are: Young's moduli of the faces are large compared to that of the core; and adequate adhesion exists between the faces and the core. The total moment, M , is equal to the sum of the moment due to composite action, M_c , and the moment due to bending of the faces about their own centroidal axis, M_o . Incorporating flexural and shear deformations, the resulting governing differential equation is:

$$\frac{d^4 y}{dx^4} - C_y \frac{d^2 y}{dx^2} = -\frac{C_y}{E_1 I} M + \frac{dV}{dx} \frac{1}{E_1 I_o} \quad (1)$$

where, C_y = panel properties [7]; E_1 = Young's modulus of face 1; I, I_o = composite moment of inertia and moment of inertia of faces, respectively, normalized with respect to E_1 ; V = shear force. Integrating twice,

$$\frac{d^2 y}{dx^2} - C_y y = -\frac{C_y}{E_1 I} \iint M dx^2 + \frac{M}{E_1 I_o} + C_1' x + C_o \quad (3)$$

C_1' and C_o can be determined from boundary conditions [7,17]. In actual cases, M is a known function and Eq. 3 can be put in a generalized form:

$$\frac{d^2 y}{dx^2} - C_y y = C_4 x^4 + C_3 x^3 + C_2 x^2 + C_1 x + C_o \quad (4)$$

The solution is:

$$y = D_4 x^4 + D_3 x^3 + D_2 x^2 + D_1 x + D_o + F_1 e^{\sqrt{C_y} x} + F_2 e^{-\sqrt{C_y} x} \quad (5)$$

To find the coefficients, F_1 and F_2 , boundary conditions [6,7] are used; e.g.

for simple spans under symmetrical loads: at $x = \frac{L}{2}$: $\frac{dy}{dx} = 0$; and at $x = 0$: $y = 0$;

in which L denotes the length of the span. The results are

$$F_2 = \frac{D_4 \frac{L^3}{2} + 3D_3 \frac{L^2}{4} + D_2 L + D_1 - D_0 C_y^{1/2} e^{\sqrt{C_y} L/2}}{C_y^{1/2} (e^{\sqrt{C_y} L/2} + e^{-\sqrt{C_y} L/2})} \quad (6)$$

$$F_1 = -D_0 - F_2 \quad (7)$$

D_0 , D_1 , D_2 , D_3 , and D_4 can be expressed in terms of C_y , C_0 , C_1 , C_2 , C_3 , and C_4 . For the stress in face 1

$$S_{11} = \frac{- (M - E_1 I_o \frac{d^2 y}{dx^2})}{a_1 D} - E_1 c_{11} \frac{d^2 y}{dx^2} \quad (8)$$

where, a_1 = cross-sectional area of Face 1; c_{11} = distance from neutral axis of face 1 to outside fiber; D = distance between neutral axes of faces 1 and 2, and

$$\frac{d^2 y}{dx^2} = 12D_4 x^2 + 6D_3 x + 2D_2 + C_y (F_1 e^{\sqrt{C_y} x} + F_2 e^{-\sqrt{C_y} x}) \quad (9)$$

Stress at other locations in the profile of face 1 can be found similarly using other values in place of c_{11} . For the shear stress carried by the core

$$S_{sc} = (V - E_1 I_o \frac{d^3 y}{dx^3}) / (bD) \quad (10)$$

$$\text{in which } \frac{d^3 y}{dx^3} = 24 D_4 x + 6D_3 + C_y^{1.5} (F_1 e^{\sqrt{C_y} x} - F_2 e^{-\sqrt{C_y} x}) \quad (11)$$

b = width of the panel.

2.2. Experimental

The two test panel profiles (Types I and III) are shown in Fig. 1. Strain gages were mounted at the highest parts of the profiles (No. 1) at sixth, third, and midspan. At midspan, gages were also located at the bottom of the grooves of the laminated panels and at different elevations of the foam-in-place panel (gages Nos. 2 and 3). The panels were tested in a suction box. The 1,220 mm long samples were mounted on 25.4 mm diameter pipe supports with a 1,140 mm span. The formed faces were facing up. The box was covered with a 0.15 mm polyethylene film which was taped to the sides of the box. Deflection was measured by means of dial indicators located over one support and at sixth, third, and midspan. Suction was applied by a vacuum pump through a hole in one side of the box and controlled by means of a small damper. Pressure was measured with a water manometer.

2.3. Theoretical vs. Experimental Results

Theoretical computations were made on a computer. The properties of the faces were calculated from conventional methods assuming the full cross-sectional areas of the faces were effective. The core thickness, D_c , applies more directly to panels with thick faces rather than to formed faces of light gage sheet metal. Therefore, the mean core thickness was used. Computed deflections are in good agreement with the experimental values. The moduli are reasonable, and the shapes of the computed deflection/span curves are in good agreement with the experimental. In conclusion, within the buckling loads, the methods outlined herein provide a reasonably accurate method of calculating the deflections and



stresses in sandwich panels with formed faces. There is good agreement between experimental and theoretical values. The theory is applicable to combinations of formed and flat faces, and to faces of different or the same material, subjected to flexural loading.

2.4. Numerical Method

The finite strip method and the finite prism method are especially efficient in analyzing prismatic members such as these architectural sandwich panels, whereas it would be prohibitive in cost and time to apply the finite element method [18]. The pioneering papers on the finite strip method were written by Cheung on plate bending problems [19,20] and had been applied in the analysis of flat-faced sandwich plate [21]. The finite prism method was described by Cheung, et al. [22]. The various applications of the finite strip method, the finite prism method, and in addition to the finite layer method are discussed comprehensively in a paper by Cheung [23].

In this article, the finite prism method, in combination with the finite strip method, are used. Results are compared with those obtained analytically by Hartsock and Chong [7] for flexural bending. The general equilibrium matrix equation is

$$S\delta = F \quad (12)$$

where, S = stiffness matrix; F = load vector; and δ = displacement vector.

2.4.1 Finite-Strip-Prism Model for Sandwich Construction

Thin faces are approximated by the finite shell strip, whereas the weak core is modelled by the finite prism. The detail formulation for the above matrices is given in texts [21], and only germane points are outlined here.

2.4.1.1. Finite Strip for Modelling the Thin Face

Both in-plane and bending action of the strip are considered, and the shape functions for the simply supported strip (Fig. 2) are given as

$$u = \sum_{m=1}^r [1 - \bar{x}, \bar{x}] \begin{bmatrix} u_1 \\ u_2 \end{bmatrix}_m \sin \frac{m\pi y}{L} \quad (13)$$

$$v = \sum_{m=1}^r [1 - \bar{x}, \bar{x}] \begin{bmatrix} v_1 \\ v_2 \end{bmatrix}_m \cos \frac{m\pi y}{L} \quad (14)$$

$$w = \sum_{m=1}^r [(1 - 3\bar{x}^2 + 2\bar{x}^3), (x - 2\bar{x}x + \bar{x}^2x), (3\bar{x}^2 - 2\bar{x}^3), (\bar{x}^2 x - \bar{x}x)] \begin{bmatrix} w_1 \\ \theta_1 \\ w_2 \\ \theta_2 \end{bmatrix}_m \sin \frac{m\pi y}{L} \quad (15)$$

where $\bar{x} = x/b$ and b, L are the width and length of the strip, respectively.

In the linear analysis, the in-plane and bending terms are decoupled, and the stiffness matrices for each action can be formed separately. The in-plane and bending stiffness matrices of the bending strip are given by Cheung [21].

2.4.1.2 Finite Prism Modelling the Weak Core

Referring to Fig. 2, it can be seen that a suitable set of displacement functions for a straight prism is

$$u = \sum_{m=1}^r C_k U_{km} \sin \frac{m\pi y}{L} \quad (16)$$

$$v = \sum_{m=1}^r C_k V_{km} \cos \frac{m\pi y}{L} \quad (17)$$

$$w = \sum_{m=1}^r C_k W_{km} \sin \frac{m\pi y}{L} \quad (18)$$

where C_k is the shape function of the isoparametric element (Fig. 3) for interpolation in the x - z direction. The shape functions for the isoparametric quadrilateral with 4 corner nodes (ISW4 model [8]) are

$$C_1 = \frac{1}{4} (1 + \eta_1 \eta) (1 + \xi_1 \xi) \quad (19)$$

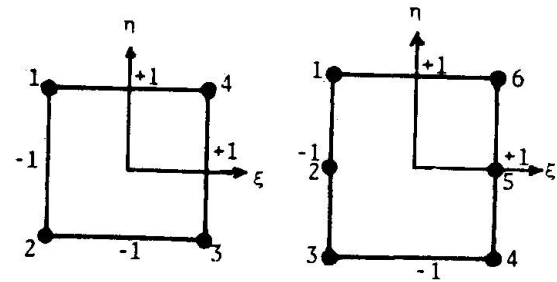
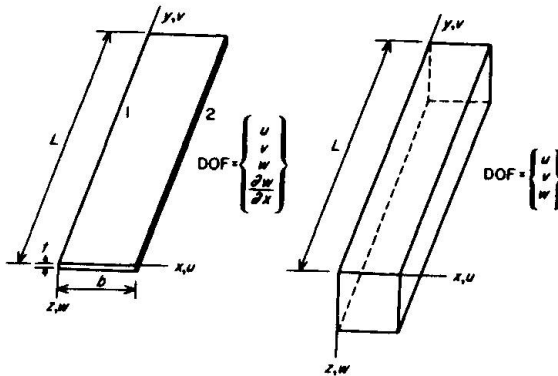


Fig. 2. Rectangular strip and prism [8] Fig. 3. ISW4 and ISW6 models [8]

The shape functions for the isoparametric quadrilateral with 6 nodes (ISW6 model [8]) are

$$\text{Corner Nodes: } C_1 = \frac{1}{4} \eta_1 \eta (1 + \eta_1 \eta) (1 + \xi_1 \xi) \quad (20)$$

$$\text{Mid-Side Nodes: } C_1 = \frac{1}{2} (1 + \xi_1 \xi) (1 - \eta^2) \quad (21)$$

ξ and η are localized coordinates of x and z . The stiffness matrix is given as

$$P_{S_{ijmn}} = \int P_{B_{im}}^T P_D P_{B_{jn}} d(\text{vol}) \quad (22)$$

where $P_{B_{im}}$ = the gradient matrix [8]

and P_D = the elasticity matrix for isotropic materials. (23)

The geometric transformation from the natural coordinate (x - z) to the local coordinate (ξ - η) can be carried out as in the standard finite element method, and the stiffness matrix can be obtained accordingly.

2.4.1.3 Coupling of the Thin Face and the Weak Core

The thin face is assumed to be in contact with the weak core throughout the loading history; hence, the stiffness matrices can be assembled easily. With the above choice of harmonic series, the stiffness matrices are zero for unequal m and n , and they are decoupled. The static equilibrium equation is

$$s_{S_{mm}}^P s_{\delta_m}^P + s_{S_{mm}}^B s_{\delta_m}^B + P_{S_{mm}} P_{\delta_m} = F_m \quad (24)$$



where s^p is the in-plane stiffness matrix of the bending strip; s^B is the bending stiffness matrix of the bending strip; p_s is the stiffness matrix of the finite prism; s^p and s^B are the in-plane and bending interpolating parameters of the bending strip; p_s is the interpolating parameters of the finite prism; δ_m is the total interpolating parameters; F_m is the loading vector.

The superscript s indicates strip variables and p , those of the finite prism. Also, the load vector (F_m) of the out-of-plane loading (q is the load intensity) can be expressed in terms of the displacement parameters of the prism, that is

$$F_m = \int q C_k W_{km} \sin \frac{m\pi y}{L} d(\text{vol}) \quad (25)$$

2.4.1.4. Numerical Examples

(a) In Fig. 4, the depth of corrugation of face 1, Y , is a variable to investigate the influence due to the degree of forming. The properties of this panel are: Young's modulus of thin faces = 1000.0 units; Poisson ratio of thin faces = 0.0; thickness of thin faces = 0.02 units; and Young's modulus of core = 1.0 units. The ISW6 model is used in the analysis, and the results for bending are depicted in Fig. 5. The results compared favorably with Hartsock and Chong's analytical solutions [7].

(b) A commercial type of formed-face sandwich panel (Type II, Fig. 1) is investigated. The properties and dimensions are:

Properties of Core: $E_c = 4685 \text{ kN/m}^2$; $\nu_c = 0.177$.

Properties of Top and Bottom Faces: $E_f = 203,550 \text{ MPa}$; $\nu_f = 0.267$; $t_f = 0.51 \text{ mm}$. Span = 1143 mm; Loading = 4.79 kN/m^2

The midpoint deflection (4.47 mm) is compared with Hartsock and Chong's analytical solution [7] of 4.55 mm, which are very close.

The formed face sandwich panel has been modelled by the finite-prism-strip model. Such method saves considerable computing or experimental cost and effort and can easily be applied for the analysis of formed face panel. The ISW6 model is more accurate than that of the ISW4 and is recommended for such analysis.

3. AXIAL STABILITY

3.1 Numerical Analysis

The buckling of sandwich panels due to axial compression is investigated using the finite-strip-prism model as described in Article 2.4. Buckling is usually preceded by wrinkling instability [4]. Similar to Eq. 12, the equilibrium matrix equation for a stable loaded system is

$$S\delta + G\delta = F \quad (26)$$

where G = geometric stiffness matrix.

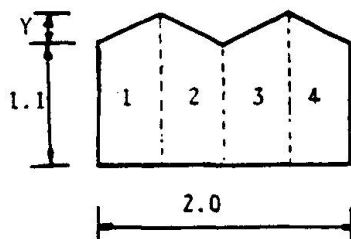


Fig. 4. Mesh details [8]

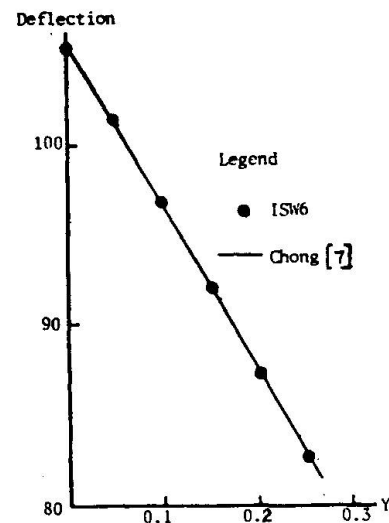


Fig. 5. Deflection vs. Y [8]

The stability analysis of the system is equivalent to finding a set of non-

trivial solutions to the set of homogeneous equations (a generalized eigen-value problem) of the form

$$(S + \lambda G^*)\delta = 0 \quad (27)$$

where G^* is the geometric stiffness matrix corresponding to the fixed preimposed stress distribution σ_{ij} . The finite-strip-prism model has been described in Eqs. 13-22.

In the stability analysis of strut, it is obvious that instability can only arise due to the action of axial stress σ_{yy} . The geometric stiffness of the strip element can then be shown to be [8]

$$G_{mn}^* = \begin{bmatrix} G_{mn}^P & 0 \\ 0 & G_{mn}^B \end{bmatrix} \quad (28)$$

$$\text{in which, } G_{mn}^P = t \sigma_{yy} \int g_{um}^T g_{un} d(\text{area}) + t \sigma_{yy} \int g_{vm}^T g_{vn} d(\text{area}) \quad (29)$$

$$G_{mn}^B = t \sigma_{yy} \int g_{wm}^T g_{wn} d(\text{area}) \quad (30)$$

where g_u , g_v , and g_w are slope matrices associated with displacement variables u , v , and w , respectively, and t is the thickness of the strip. They are,

$$g_{um} = [(1 - \bar{x}) \frac{m\pi}{L} \cos \frac{m\pi y}{L}, \quad \bar{x} \frac{m\pi}{L} \cos \frac{m\pi y}{L}] \quad (31)$$

$$g_{vm} = [-(1 - \bar{x}) \frac{m\pi}{L} \sin \frac{m\pi y}{L}, \quad -\bar{x} \frac{m\pi}{L} \sin \frac{m\pi y}{L}] \quad (32)$$

$$g_{wm} = [(1 - 3\bar{x} + 2\bar{x}^3), (x - 2\bar{x}x + x^2\bar{x}), (3\bar{x}^2 - 2\bar{x}^3), (\bar{x}^3x - \bar{x}x)] \frac{m\pi}{L} \cos \frac{m\pi y}{L} \quad (33)$$

Coupling the faces and the core, the equilibrium equation for the stability analysis is [8]

$$s_{S_{mm}}^P s_{\delta_m}^P + s_{S_{mm}}^B s_{\delta_m}^B + P_{S_{mm}} P_{\delta_m} + \lambda G_{mm} \delta_m = 0 \quad (34)$$

where G_{mm} = global geometric stiffness matrix; and the rest of matrices have been defined in Eq. 24.

3.2 Numerical Examples

(a) Panel is the same as Example (a) in Article 2.4.1.4. ISW6 model was used, and it compared favorably with solution presented in Allen's book [1]. Results are shown in Fig. 6.

(b) Panel is the same as Example (b) in Article 2.4.1.4. The ISW6 model gives a buckling load of 12.07 kip (53.71 kN).

Again, it is found that the ISW6 model is more accurate than the ISW4 model. For flat-faced

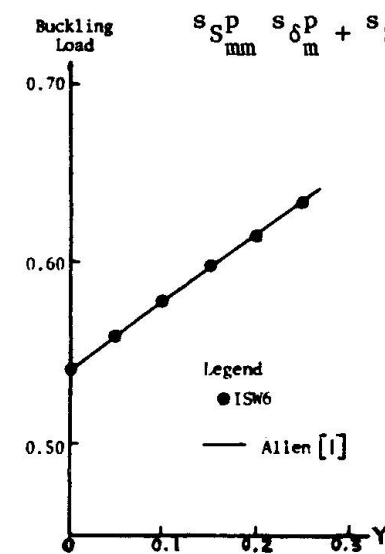


Fig. 6. Buckling load vs. Y.



sandwich panels, the ISW4 model gives satisfactory results.

3.3 Cores with Variable Stiffnesses

Due to uneven curing or other reasons, the sandwich cores may have variable stiffnesses [12] throughout the thickness. In this article, sandwich panels with flat faces and variable core stiffnesses are investigated by the finite layer method [12,21,24]. The formulation is similar to Eqs. 26 - 34.

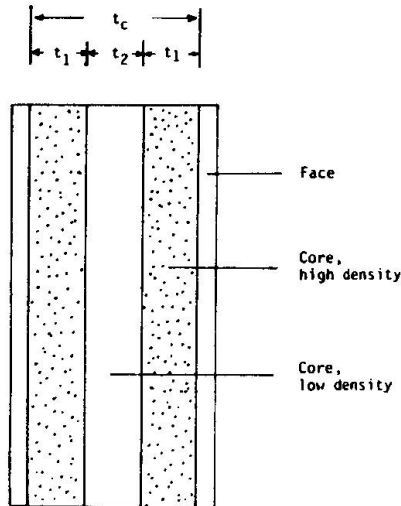


Fig. 7. Variable core densities

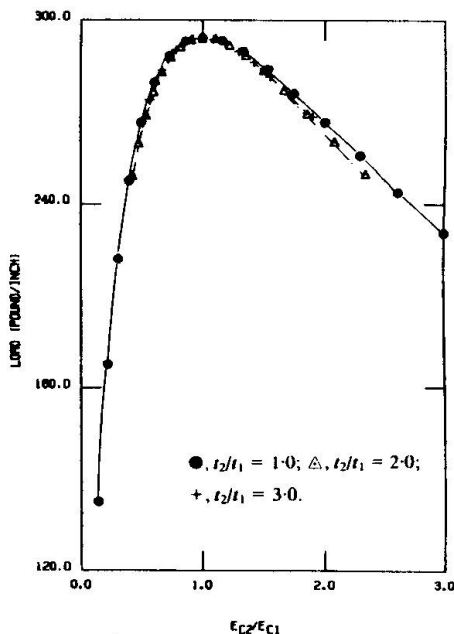


Fig. 8. Buckling load of short panels

A typical sandwich rectangular plate is divided into a number of layers (Fig. 7) which are simply supported at boundaries. The faces of the sandwich plate are assumed to be isotropic and equal in thickness. The stiffness of the core follows the distribution assumption

$$E_c t_c = \sum E_i t_i \quad (35)$$

where E_c is the mean Young's modulus of the core, t_c is the thickness of the core, E_i is the Young's modulus of each layer of the core, and t_i is the thickness of each layer of the core.

The buckling loads of a sandwich square plate with homogeneous core material are studied. The core is polyurethane with a Poisson's ratio of 0.25, and the Young's modulus is 5175 kNm^{-2} , with a density of about 40 kg m^{-3} . The Poisson's ratio and Young's modulus of each steel face are 0.3 and 207 GPa, respectively. Thicknesses of each face and core are 0.508 mm and 12.7 mm, respectively. All of the sandwich plates are divided into five layers (Fig. 7). The buckling load for $L_x = L_y = 51 \text{ cm}$ is 1.31 kN as compared with Allen's result [1] of 1.34 kN.

For variable core density of square sandwich plate, the results are given in Fig. 8 in which the mean Young's modulus is 5175 kNm^{-2} . Similar results are obtained for longer panels, 3 m long, 1 m wide, and 7.7 cm thick.

For variable stiffness of the core of sandwich plates, the optimal results are when the stiffness ratios of the outer layers to the inner layers are equal to 1, which means the core material is homogeneous through the thickness of the core. Thus, it is best to have a homogeneous core in any fabrication process. If the core is cured improperly, the outer layers tend to be different in stiffness compared with the inner layers. The strong outer layer or strong inner layer will reduce the strength of the plate. This article presented quantitative data on the buckling strength due to uneven core stiffnesses. Qualita-

tively, it can be seen if any part of the core is weakened or strengthened at the expense of the overall core stiffness (Eq. 35), then the buckling strength is lowered. Intuitively, efficient sandwich columns should have stiff faces and weak cores such that the radii of gyration (by the transformed area concept) are maximized.

4. THERMAL STRESSES AND DEFLECTIONS

Due to the superior insulation quality of sandwich panels, they have been used in places of extreme climates. It is not unusual that the temperature difference between the inside and outside wall surfaces may exceed 100°F (55.6°C). Due to the flexural rigidity of cold-formed facings, thermal stresses [10] are present even in simple span conditions.

In this investigation, a series of experiments was conducted to study the stresses and deflection induced when a sandwich panel was exposed to a temperature gradient between the two faces. The sandwich panels were tested for both single and two-span conditions, with the temperature difference between the two faces reaching up to 55.6°C (100°F).

Formulated as an ordinary fourth-order differential equation with suitable boundary conditions, theoretical expressions [10] were derived for deflection, flexural stresses in the facings, and shear stresses in the core. Numerically, finite-prism-strip method [11] is used. Experimental data, numerical analysis, and theoretical predictions are found in reasonable agreement. Due to the lack of space, details of this Article are omitted.

5. CONCLUSIONS

Structural behavior of sandwich panels with cold-formed facings is investigated analytically, experimentally, and numerically. Close agreements among these independent methods show that the results are reliable. Since experiments usually consume much time, theoretical (analytical) and/or numerical analyses are preferred for the designing and optimization of such panels. If necessary, confirmatory tests can be performed.

ACKNOWLEDGMENTS

The author would like to thank his former colleague, Mr. John A. Hartsock; graduate assistants, Messrs. K. A. Wang, K. O. Engen, B. Lee, P. A. Lavdas, et al.; and expert typing by Mrs. A. Biggs. He would also like to express his sincere appreciation to Prof. Y. K. Cheung and Dr. L. G. Tham with whom he collaborated during his stay at the University of Hong Kong as an Honorary Professor.

REFERENCES

1. ALLEN, H. G., Analysis and Design of Structural Sandwich Panels, New York, Pergamon Press, Inc., 1969.
2. GOUGH, C.S., ELAM, C.F., and De BRUYNE, N. A., The Stabilization of a Thin Sheet by a Continuous Supporting Medium, J. of the Royal Aeron. Soc., 1940.
3. HOFF, N. J., and MAUTNER, S.E., The Buckling of Sandwich-Type Panels, Journal of the Aeronautical Sciences, 12, 285-297, 1956.
4. CHONG, K. P., and HARTSOCK, J. A., Flexural Wrinkling Mode of Elastic Buckling in Sandwich Panels, Proceedings of ASCE Specialty Conference on Composite Materials, Pittsburgh, PA, 1972.
5. CHONG, K. P., and HARTSOCK, J. A., Flexural Wrinkling in Foam-Filled Sandwich Panels, J. Engr.Mech. Div., Vol. 100, No. EM1, ASCE, 95-110, 1974.
6. CHONG, K. P., et al., Analysis of Continuous Sandwich Panels in Building System, Building and Environment, 14, 125-130, 1979.
7. HARTSOCK, J. A., and CHONG, K. P., Analysis of Sandwich Panels with Formed Faces, Journal of the Structural Division, ASCE, Vol. 102, No. ST4, Proc. Paper 12058, 803-819, 1976.



8. THAM, L. G., CHONG, K. P., and CHEUNG, Y. K., Flexural Bending and Axial Compression of Architectural Sandwich Panels by Combined Finite-Prism-Strip Method, J. Reinforced Plastic and Composite Materials, 1, 16-28, 1982.
9. CHONG, K. P., ENGEN, K. O., and HARTSOCK, J. A., Thermal Stress in Determinate and Indeterminate Sandwich Panels with Formed Facings, ASCE-EMD First Specialty Conference, Waterloo, Canada, 1976
10. CHONG, K. P., ENGEN, K. O., and HARTSOCK, J. A., Thermal Stress and Deflection of Sandwich Panels, J. Structural Division, 103, ST1, 35-49, 1977.
11. CHONG, K. P., THAM, L. G., and CHEUNG, Y. K., Thermal Behavior of Foamed Sandwich Plate by Finite-Prism-Strip Method, Computers and Structures, 15, (3), 321-324, 1982.
12. CHONG, K. P., LEE, B., and LAVDAS, P. A., Analysis of Thin-Walled Structures by Finite Strip and Finite Layer Methods, Thin-Walled Structures, 2, 1984.
13. CHEUNG, Y. K., CHONG, K. P., and THAM, L. G., Buckling of Sandwich Plate by Finite Layer Method, Computers and Structures, 15 (2), 131-134, 1982.
14. CHONG, K. P., CHEUNG, Y. K., and THAM, L. G., Free Vibration of Foamed Sandwich Panel, J. Sound and Vibration, 81, (4) 575-582, 1982.
15. KUENZI, E. W., Structural Sandwich Design Criteria, National Academy of Sciences-National Research Council, Publication 798, pp. 9-18, 1960.
16. ASCE Subcommittee on Literature Survey of Cold-Formed Structures (K. P. Chong, Chairman), Literature Survey of Cold-Formed Structures, Preprint 3762, 1979; and Preprint 2807, 1976.
17. HARTSOCK, J. A., Design of Foam-Filled Structures, Technomic Publishing Co., Stamford, CT, 1969.
18. ZIENKIEWICZ, O. C., and CHEUNG, Y. K., The Finite Element Method in Structural and Continuum Mechanics, McGraw-Hill, 1967.
19. CHEUNG, Y. K., Finite Strip Method in the Analysis of Elastic Plates with Two Opposite Simply Supported Ends, Proc. Inst. Civil Eng., 40, 1-7, 1968.
20. CHEUNG, Y. K., Finite Strip Method Analysis of Elastic Slabs, Journal of Engineering Mechanics, ASCE, Vol. 94, EM6, pp. 1365-1378, 1968.
21. CHEUNG, Y. K., Finite Strip Method in Structural Analysis, Pergamon, 1976.
22. CHEUNG, Y. K., YEO, M. F., and CUMMING, D. A., Three-Dimensional Analysis of Flexible Pavements with Special Reference to Edge Loads, Proc. 1st Conf. of the Road Engineering Assoc. of Asia and Australia, Bangkok, 1976.
23. CHEUNG, Y. K., Finite Strip Method in Structural and Continuum Mechanics, Int'l. Journal of Structures, Vol. 1, No. 1, pp. 19-37, 1981.
24. CHEUNG, Y. K., THAM, L. G., and CHONG, K. P., Buckling of Sandwich Plate by Finite Layer Method, Computers & Structures, 15, (2), 131-134, 1982.
25. AHMED, K. M., Free Vibration of Curved Sandwich Panels by the Method of Finite Elements, Journal of Sound and Vibration, 18, 61-74, 1971.
26. Academia Sinica, Solid Mechanics Group, Bending, Stability and Vibration of Sandwich Plates (in Chinese), Beijing, China, 1977.

Load Bearing Strength of Sandwich Panel Walls with Window Openings

Résistance ultime des panneaux sandwich de façade
comportant des ouvertures

Tragfähigkeit von Wänden aus Sandwichelementen mit Fensteröffnungen

Torsten HÖGLUND

Professor
Royal Inst. of Technology
Stockholm, Sweden



Torsten Höglund, born 1936, received his civil engineering degree 1963 and his doctors degree 1972 at the Dep. of Structural Mechanics and Engineering at the Royal Institute of Technology, Stockholm. After eight years as a consulting engineer, he is since 1982 professor of steel structures. He has been involved in local buckling problems in thin-walled steel structures.

SUMMARY

Sandwich panel elements used as walls of buildings are often weakened by holes for windows. In this paper is discussed the design of vertically and horizontally placed sandwich elements with openings for windows in different positions.

RÉSUMÉ

Les panneaux sandwich utilisés comme éléments de façade de bâtiment sont souvent affaiblis par les ouvertures nécessitées par les fenêtres. Cet article traite du dimensionnement des panneaux sandwich disposés verticalement ou horizontalement et comportant des ouvertures pour fenêtres en différents emplacements.

ZUSAMMENFASSUNG

Sandwichkonstruktionen, die als Wandelemente benutzt werden, weisen häufig Schwächungen infolge der Anordnungen von Fenstern auf. In diesem Beitrag wird der Entwurf und die Berechnung senkrecht und waagrecht eingebauter Sandwichelemente mit Fensteröffnungen in verschiedenen Positionen behandelt.



1. INTRODUCTION

Sandwich panel elements with foam-in-place cores and light-gauge cold-formed metal skins are becoming more and more popular as external walls of buildings both in Sweden and in many other countries. As often as not it is necessary to fit windows, vents and doors into the panel wall. Door and larger openings normally need to be strengthened by using, for example, a steel frame. It is, however, not necessary to strengthen openings for windows if the sandwich element is designed so that it may cope with the extra forces, especially those at the corners of the window.

Numerous alternative solutions are possible for the fitting of sandwich elements and the positioning of windows. The sandwich elements may be horizontal or vertical, simply supported or continuous. The windows may occasionally be symmetrically placed in the element, but are normally placed independently of the element joints. Fig. 1 shows some typical window positions in industrial building walls.

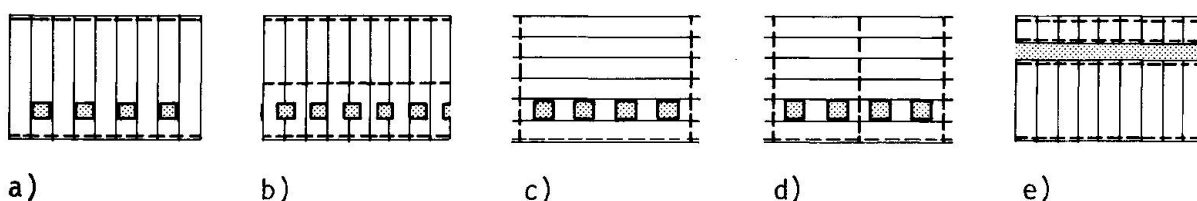


Fig. 1 Example of window positions in sandwich element walls

In many cases the windows are so close to each other, e.g. case b) and e) in Fig. 1, that the sandwich elements and windows must be supported by special beams.

In the following it is assumed that the window frames are fastened in the corners only and that no composite action with the sandwich elements exists.

2. SIMPLY SUPPORTED VERTICAL ELEMENTS

2.1 Windows in every second element

The element between two windows in Fig. 1 a) will be acted upon by symmetrical forces, wind load on the element itself, shear forces from the adjacent elements above and below the windows and shear forces from the adjacent windows. If the bending stiffness in the transverse direction is slightly less than that in the longitudinal direction (for example sandwich elements with flat or linear skins as in Fig. 2) and if the element length is large compared to the element width, the element can simply be designed for the maximum bending moment in a section through the upper corners of the window opening and the shear force in a section through the lower corners. Furthermore the shear force in the element joints close to the corners must be checked, see below.

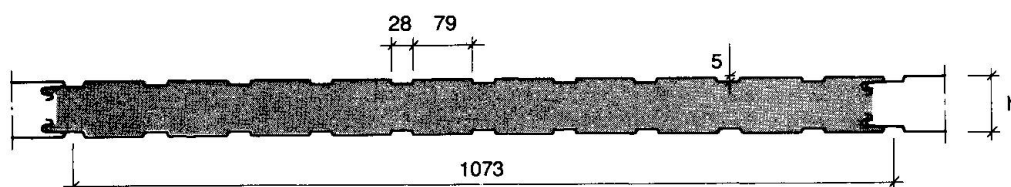


Fig. 2 Sandwich element with linear skins

2.2 Torsional rigidity

When there is more than one element between the windows, the elements between the windows will be acted upon by asymmetrical forces. The distribution of the

loads from the windows and from the elements above and below the windows depend on the bending, shearing and torsional rigidity of the elements. According to Timoshenko [1] all values of torsional rigidity D_{xy} based on purely theoretical considerations should be regarded as a first approximation, and a direct test must be recommended in order to obtain more reliable value. Therefore, two simple torsional tests according to Fig. 3 and two bending-torsional tests according to Fig. 4 were made. The torsional tests gave

$$GK_V = 84 \text{ kNm}^2 \text{ and } 147 \text{ kNm}^2$$

for 55 and 85 mm thick elements with the cross section shown in Fig. 2 and skins of 0.42 mm steel sheet.

These values may be compared with values according to a modified Bredt's formula, compare Fig. 5,

$$GK_V = \frac{4 (2b_s/3)^2 h^2}{2 (2b_s/3 G_f t + 3h/G_c b_s)}$$

which, for $G_f = 81000 \text{ N/mm}^2$ for the sheet, $G_c = 8 \text{ N/mm}^2$ for the core, $t = 0.42 \text{ mm}$ and $b_s = 1083 \text{ mm}$, gives

$$GK_V = 78 \text{ kNm}^2 \text{ and } 148 \text{ kNm}^2 \quad (1)$$

for $h = 55$ and 85 mm respectively.

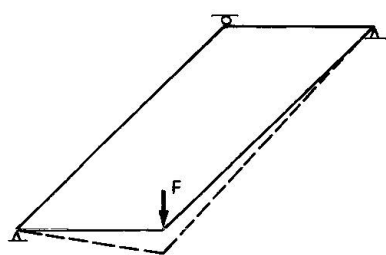


Fig. 3 Sandwich element in torsion

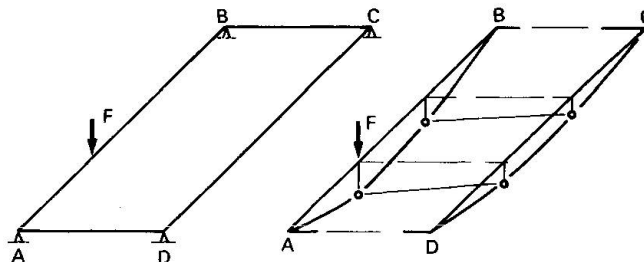


Fig. 4 Sandwich element in bending and torsion

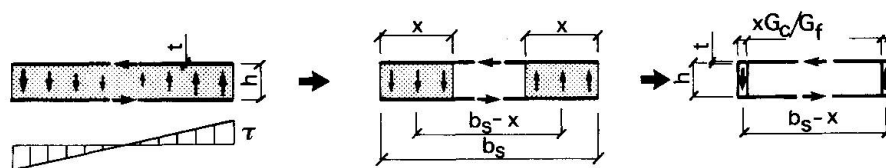


Fig. 5 Model for calculating the torsional rigidity GK_V . $x = b_s/3$.

The deflection of the torsional-bending test elements of Fig. 4 were compared with a finite element calculation based on 24 elements in the longitudinal direction and 2 elements in the transverse direction. Isoparametric, orthotropic plate elements taking into account shear deformation (Mindlin-theory) with four nodes were used. The torsional rigidity was supposed to be $D_{xy} = GK_V/2b = 37 \text{ kNm}$.

It can be seen in Fig. 4 that the agreement between tests and calculations was good.



2.3 Windows in every third element

A finite element calculation was carried out for the example in Fig. 6 a) where, by using geometrical symmetry, one whole element and half of the element above and below the window were studied. The window was assumed to have the same width as the sandwich elements.

Calculated deflection, bending moments and shear forces in the element joint are shown in Fig. 6 c), d) and e) respectively.

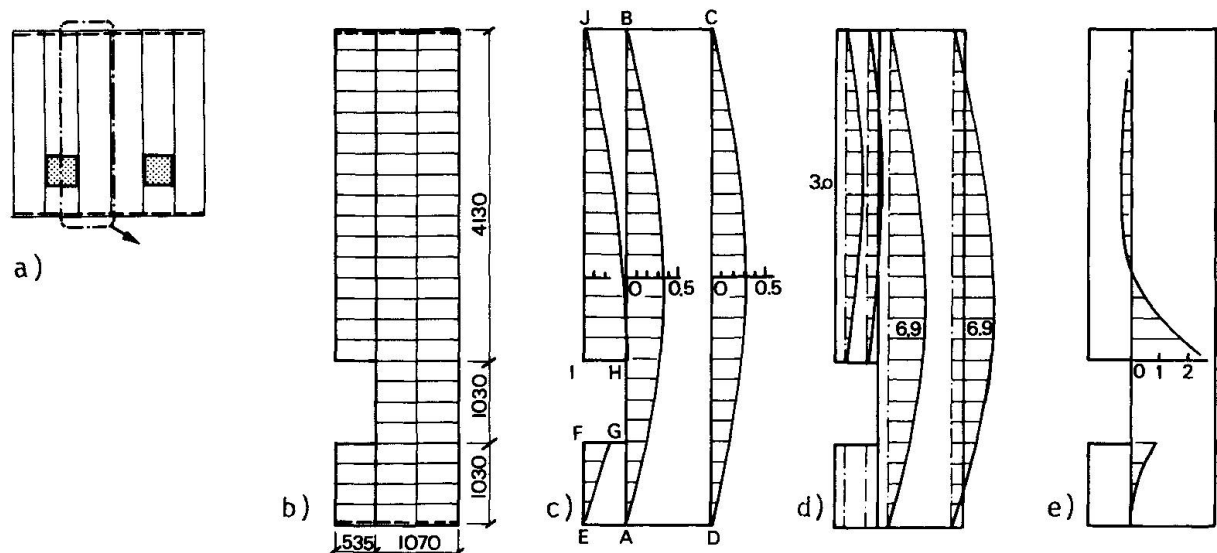


Fig. 6 a) Window in every third element
b) Finite element mesh
c) Deflection
d) Bending moment
e) Shear force in element joint

Fig. 6 c) shows that torsion in the element ABCD is small. Therefore, the bending moment on both sides of the element is almost the same. The bending moment in the element above the window is about 1.5 times that of an element which was supposed to be simply supported on the window. The maximum bending moment is only slightly larger than $1.5 M_0$ where M_0 is the moment at a section through the upper corner of the window for one isolated element. This result was used when the approximate formulae in 2.6 were derived.

The shear force in the joints between the elements has a marked peak at the upper corner of the window opening. A very rough estimate for the peak value is

$$V = 2.5 q b_w. \quad (2)$$

2.4 Test on joints between elements

The shear capacity of the joints depends, of course, on the shape of the joints. Tests on joints shown in Fig. 7 gave shear strengths which were 55 to 70 % of the shear capacity of the element in the longitudinal direction. During testing crack 1 in Fig. 6 a) appeared at 60 to 80 % of the collapse load (which occurred when crack 2 arose). In the rules in Fig. 8 the shear strength of the joints were, on the safe side, supposed to be half of the shear strength of the element.

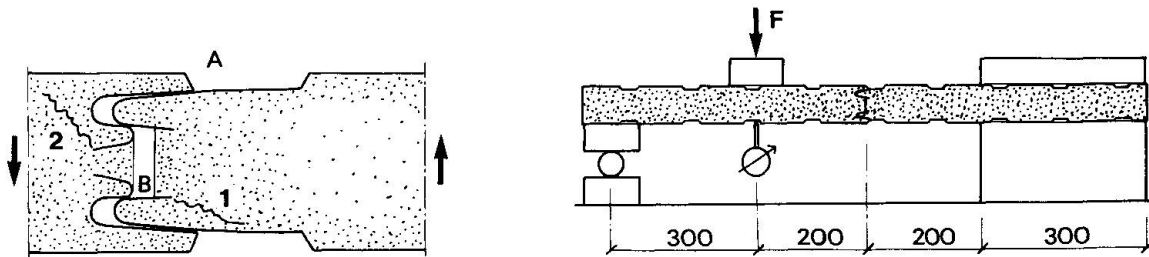


Fig. 7 Testing of the joints between sandwich elements

2.5 Two or more elements between windows

When there are two or more elements between the windows the bending moment in the element next to the window will decrease. The reduction depends on the relation between the bending, torsional and shear rigidity of the element.

For the type of element shown in Fig. 2 the following reduction factor for the bending moment can be used

$$\kappa = 0.6 + 1.6/n^2 \quad (3)$$

where n is the number of elements between the windows.

The shear forces will not decrease to the same extent, which is why no reduction is recommended.

2.6 Design formulae

Proposed design formulae for the type of elements shown in Fig. 2 are given in Fig. 8. As was pointed out in the introduction the formulae are valid for the case where the window frames have been fastened in the corners only. The formulae are conservative if there is composite action between the window frames and the sandwich panels.

Simply supported vertical elements

$u > 2 t_s$
 $v > 2 t_x$
 $b_w < 1.2 b_s$

Bending moments and shear forces according to the following formulae shall be less than allowable values for the actual sandwich panel:

$$M = M_0 \left(1 + \frac{0.58 b_f}{b_s + t_s} \right) \cdot \left(0.6 + \frac{1.6}{n^2} \right) \text{ for } n \geq 2$$

$$M = 2 M_0 \text{ for } n = 1$$

$$M_0 = \frac{q \ell g}{2} \left(1 - \frac{g}{\ell} \right)$$

Furthermore $M \geq q \ell^2 / 8 \text{ kNm/m}$

$$V = 5 q b_w \geq q \ell^2 / 2 \text{ and}$$

$$\geq q (\ell / 2 - g + h_w) (1 + 1.2 b_w / a) \text{ kN/m}$$

where

q = wind load (kN/m^2)
 t_s = element thickness (m)
 n = number of whole elements between windows
 b_s = element width

Fig. 8 Proposed design rules for vertical sandwich elements with flat or creased skins



3. SIMPLY SUPPORTED HORIZONTAL ELEMENTS

It is assumed that the windows are so close to each other that the wind load on the windows will be almost evenly distributed along the adjoining sandwich elements, see Fig. 9.

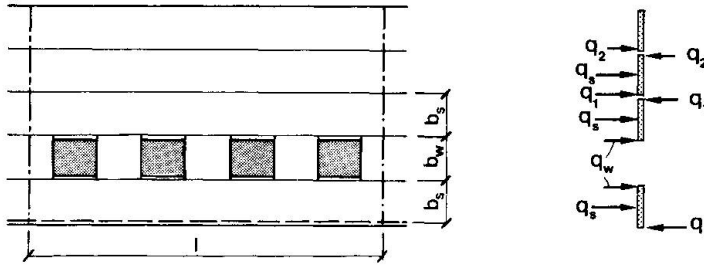


Fig. 9 Windows in horizontal elements

3.1 Sandwich element supported on three edges

The deflection v of the element below the windows is the sum of v_b due to bending moments, v_s due to shear forces and v_t due to torsional moments.

$$v_b = B (q_w + q_s - q_r) \quad \text{where } B = 5 \ell^4 / (384 EI) \quad (4)$$

$$v_s = S (q_w + q_s - q_r) \quad S = \ell^2 / (8 GA_w) \quad (5)$$

$$v_t = T (q_w + q_r) \quad T = \ell^2 b_w / (16 GK_v) \quad (6)$$

At the lower edge of the element below the window the deflection $v = v_b + v_s - v_t = 0$ which gives

$$q_r = q_w (1 - 2\beta) + q_s (1 - \beta) \quad \text{where} \quad (7)$$

$$\beta = T / (B + S + T) \quad (8)$$

The above is strictly correct only if the distribution of the bending deflection is affined to the shear and the torsional deflection. The maximum deflection, bending moment, shear forces and torsional moment is then

$$v_{\max} = (2 q_w + q_s)(B + S) 2\beta \quad (9)$$

$$M_{\max} = (2 q_w + q_s) \beta \ell^2 / 8 \quad (10)$$

$$V_{\max} = (2 q_w + q_s) \beta \ell / 2 \quad (11)$$

$$T_{\max} = (2 q_w + q_s)(1 - \beta) b_s \ell / 4 \quad (12)$$

The torsional moment gives shear stresses which shall be added to the stresses due to the shear forces. The shear stresses due to the torsional moment are derived according to the model in Fig. 5.

$$\tau_c = \frac{T \cdot 1.5}{2 (2b_s/3)h (b_s/3)} = \frac{T}{0.30 h b_s^2} \quad (13)$$

where the factor 1.5 accounts for the peak value of the shear stress in Fig. 5 a).

A fictitious shear force can be derived

$$T_{eq} = \tau h_{bs} = \left[\frac{V_{max}}{hb_s} + \frac{T_{max}}{0.30 hb_s} \right] hb_s \quad (14)$$

which, with V_{max} and T_{max} according to (11) and (12) and $q_w = Q b_w/2$ and $q_s = Q b_s$ gives

$$T_{eq} = qb_s \ell (1 + b_w/b_s)(0.833 - 0.33 \beta)$$

where q is the wind load.

3.2 Sandwich elements elastically supported along one longitudinal edge

The element above the windows in Fig. 9 is supported by the other elements above the windows. If the upper edge of the top element is simply supported, then the direct wind load on the elements gives no torsional moments. The shear stresses are then less than in the element below the windows while the bending moment is larger.

The deflection of the elements caused by the load on the window can be written

$$v_1 = (q_w - q_1)(B + S) - (q_w + q_1) T = (q_1 - q_2)(B + S) + (q_1 + q_2) T \quad (15)$$

which with regard to eqn (8) gives

$$q_1 = (q_w + q_2)(1/2 - \beta) \quad (16)$$

and similarly

$$q_2 = (q_1 + q_3)(1/2 - \beta) \quad (17)$$

If there are only two elements, then $q_2 = 0$ and the total load on the element above the window will be

$$\Sigma q = q_s + q_w - q_1 = q_s + q_w (1 + \beta)/2$$

If there are three elements $q_r = 0$, $q_2 = (0.5 - \beta) q_1$ and from eqn (16)

$$q_1 = q_w (1/2 - \beta)/(1 - (1/2 - \beta)^2) \quad (18)$$

β is often close to $1/2$ which is why the denominator for practical design can be put equal to unity. The design formulae can then be summarized as in Fig. 10.

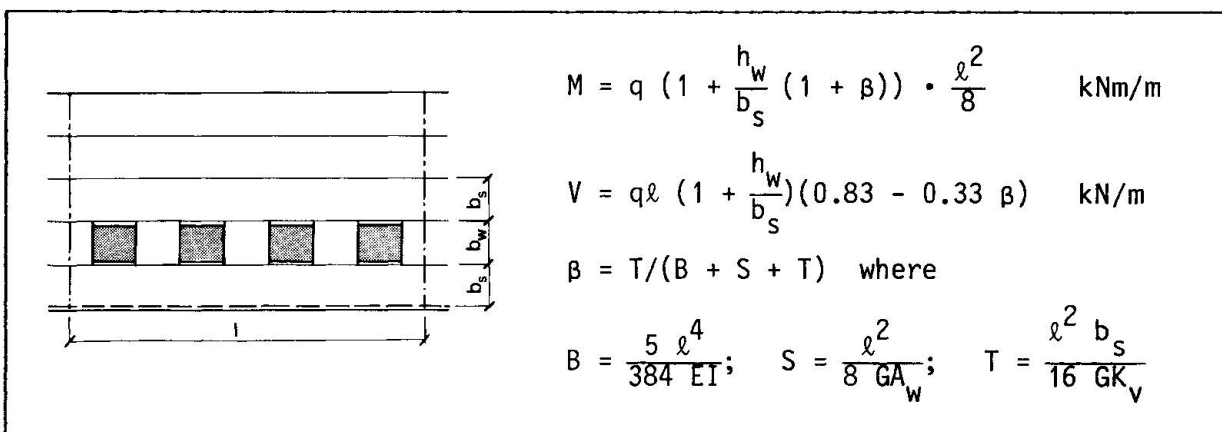


Fig. 10 Proposed design rules for horizontal sandwich elements with flat or lined facing



4. CONTINUOUS ELEMENTS

The temperature difference between the inside and outside of the sandwich elements can be considerable. If the elements are continuous, then restraining forces must be considered in design. Even if higher permissible stresses are used for the combination of forces due to temperature differences and wind load, this load combination is governing. Testing of two continuous elements subjected to a combination of distributed load and temperature difference has shown that elastical behaviour can be supposed.

Despite the simplification of design methods the calculation involved for the design of continuous elements with window openings is considerable. The design tables for permissible loads have therefore been constructed for a number of spans, window positions and window sizes, compare Fig. 11 a) and b). As these tables are applicable for specific products only, they are not included here.

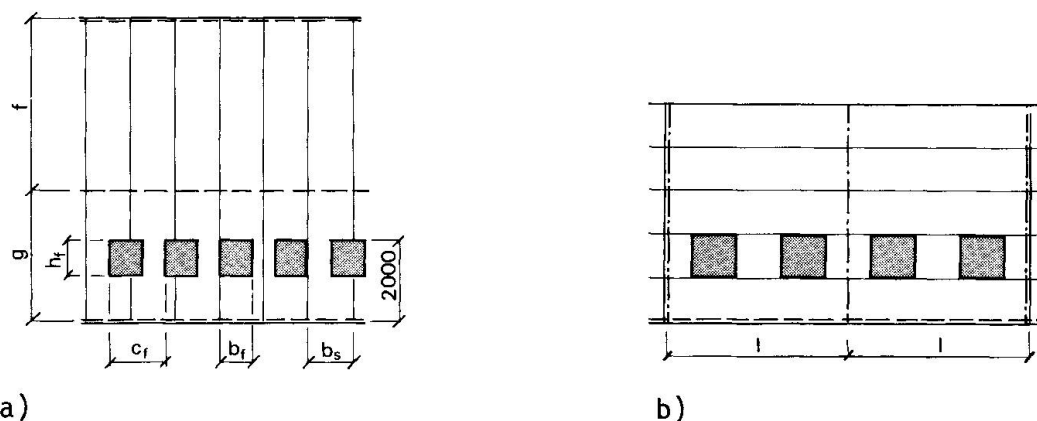


Fig. 11 Continuous sandwich elements with windows

ACKNOWLEDGEMENT

This report is a summary of work financed by Ahlsell Profil AB, Anderslöv, Sweden.

REFERENCES

1. TIMOSHENKO S. & WOINOWSKY-KRIEGER S., Theory of Plates and Shells. Mc Graw-Hill, 1959.
2. PLANTEMA F.J., Sandwich Construction. John Wiley & Sons, 1966.

Biege- und Membrantragwirkung von ebenen Fassadenelementen unter Windlasten

Transmitting Wind Loads on Flat Facade Plates by Bending and Membrane Effects

Éléments de façade plans sous charges de vent résistant par flexion et effet de membrane

Gerhard VÖLKE

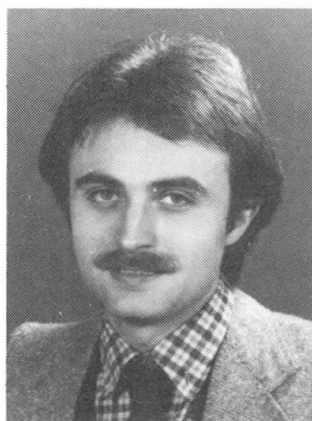
Dr. Ing.
Otto-Graf-Institut
Stuttgart, BR Deutschland



G. Völkel, geb. 1936; 1964 Dipl.-Ing.; 1970 Dr.-Ing., TH Darmstadt; 1971-1976 Beratender Ing. v. Tetra Darmstadt; 1976-1982 Referatsleiter, Gerüstbau beim IfBt; 1982-heute Leiter der Abt. Baukonstruktionen, FMFA B.W.

Hans Georg SCHIEBL

Dipl.-Ing.
Otto-Graf-Institut
Stuttgart, BR Deutschland



H. G. Schiebl, geb. 1955; 1981 Dipl.-Ing. für Bauwesen von der Univ. Karlsruhe; 1983 Dipl.-Wirtschaftsing. von der TFH Berlin; 1983-heute Wissenschaftlicher Angestellter an der FMFA B.W.

ZUSAMMENFASSUNG

Für dünnwandige, zweiseitig und vierseitig gelagerte rechteckige und ebene Fassadenplatten werden analytisch geschlossene Lösungen der Differentialgleichung für das Gleichgewicht am verformten System unter Berücksichtigung von nichtlinearer Geometrie bei den Verträglichkeitsbedingungen vorgestellt. Ergebnisse aus Rechnung und Versuch werden verglichen.

SUMMARY

For thin-walled rectangular and flat facade plates which are supported along two or four edges, complete analytical solutions of the differential equation for equilibrium of the deformed system are presented, including the non-linear geometry in the conditions of compatibility. Results of calculation and of tests are compared.

RÉSUMÉ

Cette contribution présente des solutions analytiques complètes de l'équation différentielle exprimant l'équilibre des systèmes déformés d'éléments de façade plans, rectangulaires et à parois minces appuyés sur deux ou quatre bords. Cette analyse prend en compte dans les conditions de compatibilité la non-linéarité géométrique des éléments. Les résultats de l'analyse sont finalement comparés à des résultats d'essais.



1. EINLEITUNG

Großflächige, rechtwinklige und ebene Fassadenplatten aus den Werkstoffen Aluminium, Stahl, Kunststoff, Keramik und aus Verbundwerkstoffen werden insbesondere in Kombination als Sandwichelemente in zunehmendem Maße für Außenwandbekleidungen von Bauwerken eingesetzt. Diese Platten werden in der Regel neben ihrem Eigengewicht und evtl. Schnee- und Eislasten hauptsächlich durch Windlasten und durch Zwängungen infolge Temperatur beansprucht und sind als in statischer Hinsicht untergeordnete Bauteile relativ schlank und biegeweich ausgelegt.

Großflächige und biegeweiche Platten erreichen bei den nach den Regeln der Technik anzusetzenden Windlasten oft Feldmittendurchbiegungen, die das Vielfache ihrer Dicke erreichen. Um den Schnittgrößenverlauf in einer Platte mit einer im Verhältnis zur Plattendicke großen Durchbiegung wirklichkeitsnah erfassen zu können und um die Horizontalkräfte in den Befestigungsmitteln überhaupt bestimmen zu können, müssen die üblichen Näherungen der Statik aufgegeben werden. Es wird erforderlich, das Gleichgewicht am verformten System aufzustellen und bei den Verträglichkeitsbedingungen Anteile aus nichtlinearer Geometrie zu berücksichtigen.

Bei einer einachsrig gespannten Fassadenplatte, die z.B. mit Nieten oder Schrauben an der Unterkonstruktion befestigt ist, werden sich mit steigender Querbelaastung und damit zunehmender Durchbiegung infolge der in Längsrichtung elastisch gehaltenen Plattenrändern Membrankräfte aufbauen, siehe Bild 1.

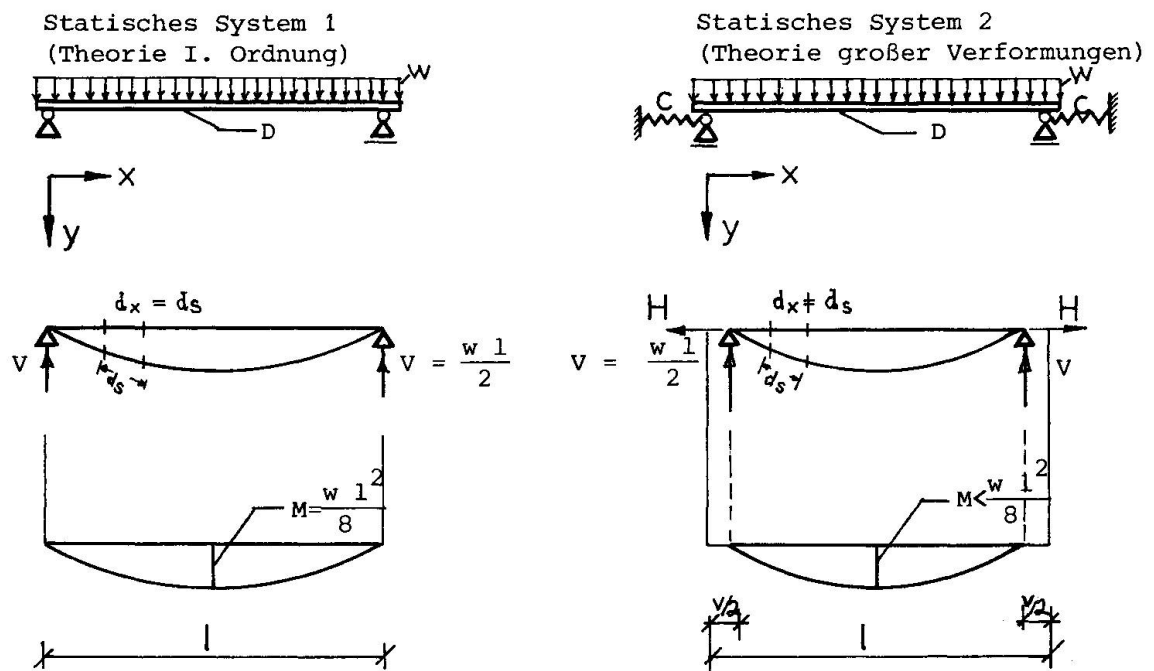


Bild 1. Einachsrig gespannte Platte unter Windlast w

Ähnlich verhält es sich bei der vierseitig liniengelagerten Platte. Durch die großen Durchbiegungen der Platte werden ihre Ränder zur Feldmitte gezogen. Im Gegensatz zur einachsrig gespannten Platte werden hier nicht Befestigungsmittel zur Aufnahme der entstehenden Zugkräfte benötigt.

Durch die Linienlagerung bleiben die Randbereiche der Platte weitgehend eben und wirken als ringförmig aussteifende Scheiben, in die sich die biegeweiche Membran hineinhängen kann (innere Membrantragwirkung). In Bild 2 sind Verformungen, in Bild 3 der resultierende Druckring und die Hauptrichtungen der Zug-



2.2 Differentialgleichung (DGL) und deren Lösung

Die Differentialgleichung eines Stabes mit konstanter horizontaler Zugkraft am Stabende und mit konstanter Streckenlast querbelastet, entsprechend Bild 5,

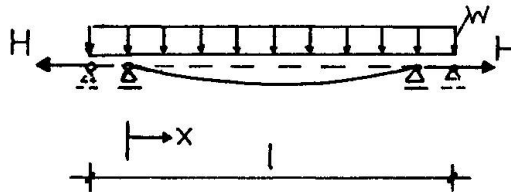


Bild 5. Statisches System eines mit einer konstanten Zugkraft H und einer konstanten Streckenlast w querbelasteten Stabes

lautet bei der Aufstellung des Gleichgewichts am verformten System:

$$\text{DGL: } y''''(x) - \alpha^2 \cdot y''(x) + \frac{M_0(x)}{D} = 0 \quad (1)$$

$$\alpha^2 = H/D, \quad \xi^2 = H \cdot l^2/D = \alpha^2 \cdot l^2$$

$M_0(x)$ = Momentenverlauf nach Theorie I. Ordnung

Die allgemeine Lösung der DGL lautet:

$$y(x) = C_1 \cdot \sinh(\alpha \cdot x) + C_2 \cdot \cosh(\alpha \cdot x) + \frac{1}{H} \cdot (M_0(x) + \frac{M_0''(x)}{\alpha^2} + \dots) \quad (2)$$

Die Berücksichtigung der Randbedingungen und der speziellen Last für das in Bild 5 dargestellte System ergibt die folgende Lösung:

$$y(x) = \frac{w \cdot l^4}{D \cdot \xi^4} \left[\gamma \cdot \cosh(\alpha \cdot x) + \sinh(\alpha \cdot x) + \frac{\xi^2}{2} \cdot \frac{x}{l} \cdot (1 - \frac{x}{l}) - 1 \right] \quad (3)$$

mit $\gamma = \frac{1 - \cosh \xi}{\sinh \xi}$

Die Verkürzung des Stabes infolge seiner Durchbiegung $y(x)$ ergibt sich entsprechend Bild 6 wie folgt:

$$\begin{aligned} dx &= ds \cdot \cos \beta \\ dv &= ds - dx \\ &= (1 - \cos \beta) \cdot ds \end{aligned}$$

für $y_1'^2 \ll 1 \rightarrow 1 - \cos \beta = 1 - 1 + \frac{y_1'^2}{2!} + \frac{y_1'^4}{4!} - \dots \approx \frac{y_1'^2}{2}$

$$v = \int_0^l dv = \int_0^l \frac{y'^2}{2} ds \quad (4)$$

Bild 6. Geometrischer Zusammenhang zwischen Durchbiegung und Auflagerver-schiebung

Differenzieren von Gleichung (3) und Einsetzen in Gleichung (4) ergibt:

$$v = \frac{1}{4} \cdot \frac{w^2 \cdot l^7}{D^2 \cdot \xi^2} \left[\frac{\xi^3}{12} + (\gamma^2 - 5) \cdot \frac{\xi}{2} - 5 \cdot \gamma \right] \quad (5)$$

Die Erfüllung der Verträglichkeitsbedingungen zu den Längsfedern am Stabende erfordert:

$$\frac{H}{C} = V(w, l, D, \xi) \quad (6)$$

w kann damit in Abhängigkeit von den anderen Parametern explizit dargestellt werden:

$$w \cdot l^3 \cdot \sqrt{\frac{C}{D^3}} = 2 \cdot \sqrt{\frac{12 \cdot \xi^9}{\xi^3 + 6 \cdot (\gamma^2 - 5) \cdot \xi - 60 \cdot \gamma}} \quad (7)$$

Der funktionale Zusammenhang von Gleichung (7) ist in Bild 7 dargestellt.

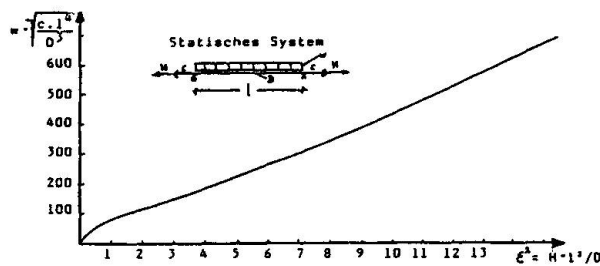


Bild 7. Grafische Darstellung des funktionalen Zusammenhangs der Gleichung (7)

2.3 Vergleich der Ergebnisse aus Rechnung und Versuch an einigen Beispielen

In Bild 8 sind Last-Auflagerverschiebungskurven für ein System wie in Bild 4 abgebildet für unterschiedliche Lochspiele (Lose), v_0 , Federsteifigkeiten c und Biegesteifigkeiten D dargestellt. Vergleichsrechnungen mit der Methode der Finiten Elemente für geometrisch nichtlineare Systeme ergaben im Vergleich zu der hier vorgestellten Lösung bis zu einer Feldmittendurchbiegung $\max f/h = 9,2$ bei den Verformungen in Feldmitte keine größeren Abweichungen als 1,8 %, bei den maximalen Spannungen keine größeren als 3,3 % und bei den Auflagerverschiebungen keine größeren als 4,0 %.

Bild 9 zeigt eine Last-Durchbiegungskurve für die Plattenmitte und eine Last-Auflagerverschiebungskurve, wie sie mit dem hier vorgestellten Modell errechnet wurden, und an 5 Stellen, welche mit Kreisen gekennzeichnet sind, in Bauteilversuchen gemessene Werte. Zum Vergleich wurden die Werte der Durchbiegung in Feldmitte nach Theorie I.O. berechnet und mit einer unterbrochenen Linie eingezeichnet. Weiter ist in Bild 9 der Lastabtragungsanteil der Biegetragwirkung bezogen auf die Gesamtlast dargestellt.

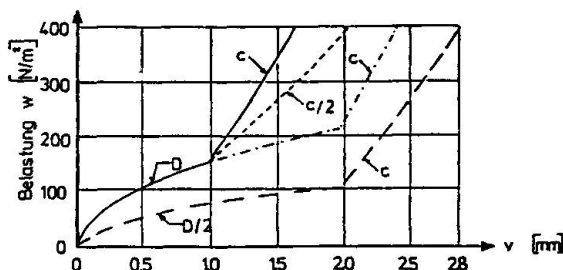


Bild 8. Last-Auflagerverschiebungskurven für verschiedene v , c und D

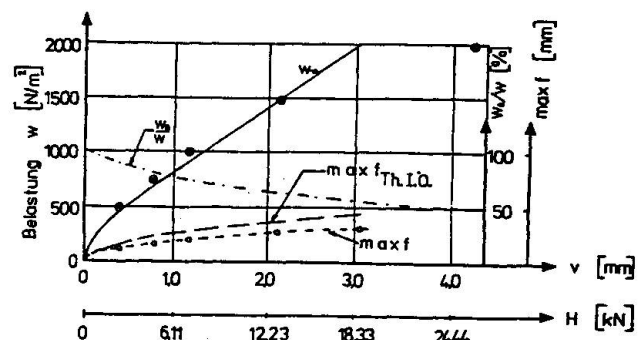


Bild 9. Theoretisch berechnete Kurven und einzelne Meßwerte (O, O) aus Bauteilversuchen



3. NÄHERUNGSLÖSUNG FÜR EINE ZWEIACHSIG GELAGERTE PLATTE MIT INNERER MEMBRAN-TRAGWIRKUNG

3.1 Analytische Lösung des Biege-Membran-Problems

Gleichung (8) gibt eine Näherungslösung für die freidrehbar und in der Platten-ebene verschieblich liniengelagerte Platte nach Barés [1] wieder, die insbesondere auf die Anwendung für Sandwichplatten hin modifiziert wurde.

$$\frac{16 \cdot w \cdot a^4}{\pi^6 \cdot D \cdot h} = (\gamma^2 + 1)^2 \cdot f/h + \frac{2,00 \cdot \gamma^2 \cdot (1 - \mu^2)}{(\gamma^2 + 0,6 + \frac{1}{\gamma^2})} \cdot \frac{t \cdot f^3/h}{h^3 - (h-t)^3} \quad (8)$$

mit w = gleichmäßige Flächenlast

γ = Seitenverhältnis der Platte ($\gamma = a/b$)

a = kurze Seite der Platte

t = Dicke der beiden Deckbleche

h = Höhe des Sandwichelements

f = Plattenmittendurchbiegung

d = Plattensteifigkeit ($D = EI/(1-\mu)^2 = E \cdot \frac{h^3 - (h-t)^3}{12(1-\mu^2)}$)

Spaltet man die Gleichung (8) nach ihrem Linearanteil, welcher die Biegetragwirkung berücksichtigt, und kubischen Anteil, welcher die Membrantragwirkung beinhaltet, auf, so erhält man Gleichung (9) und (10).

$$w = w_B + w_M \text{ oder } 1 = w_B^* + w_M^*, w_{B,M} = \frac{w \cdot 16 \cdot a^4}{\pi^6 D h} \cdot w_{B,M}^*$$

$$\Rightarrow w_B^* = (\gamma^2 + 1)^2 \cdot \frac{\pi^6 \cdot D}{16 \cdot a^4} \cdot \frac{f}{w} \quad (9)$$

$$w_M^* = \frac{2,00 \cdot \gamma^2 \cdot (1 - \mu^2)}{\gamma^2 + 0,6 + \frac{1}{\gamma^2}} \cdot \frac{\pi^6 D}{16a^4} \cdot \frac{1}{w} \cdot \frac{t \cdot f^3/h}{h^3 - (h-t)^3} \quad (10)$$

In Bild 10 sind die Lastanteile für zwei unterschiedlich hohe Belastungen w_1^* und w_2^* in Abhängigkeit vom Seitenverhältnis wiedergegeben.

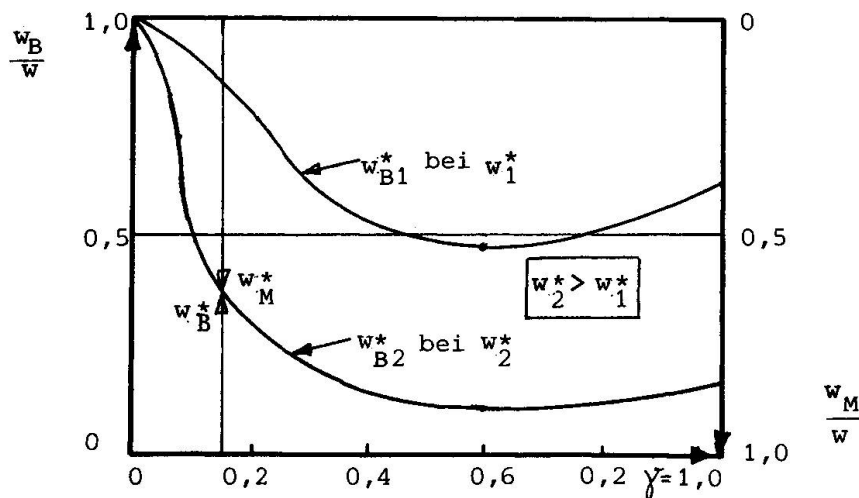


Bild 10. Lastabtragungsanteile aus Membran- und Biegetragwirkung (qualitativer Verlauf) in Abhängigkeit von Plattenseitenverhältnis γ und der Lasthöhe w^* (Die Summe aus w_B^* und w_M^* gibt immer 1)

3.2 Vergleich der Ergebnisse aus Rechnung und Versuch für einige Beispiele

In Bild 11 sind die Mittendurchbiegungskurven von vierseitig gelagerten Sandwichplatten für zwei verschiedene Kernschichtdicken h ; ($h_1 = 4 \text{ mm}$, $h_2 = 6 \text{ mm}$) und jeweils zwei verschiedene Seitenverhältnisse γ_i

$$\gamma_{11} = \frac{1,22 \text{ m}}{1,22 \text{ m}}, \gamma_{12} = \frac{1,22 \text{ m}}{3,66 \text{ m}}, \gamma_{21} = \frac{1,47 \text{ m}}{1,47 \text{ m}}, \gamma_{22} = \frac{1,47 \text{ m}}{3,66 \text{ m}}$$

angegeben. Ferner sind die Versuchswerte an einzelnen Laststufen durch Symbole gekennzeichnet.

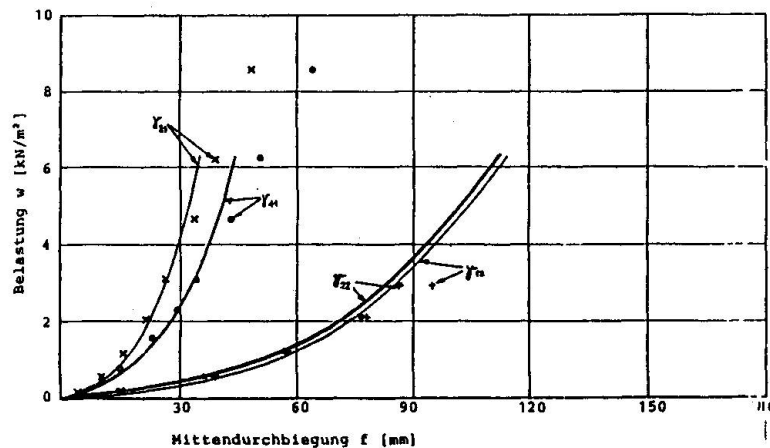


Bild 11. Last-Verformungskurven von Sandwichplatten, die mit einer gleichmäßigen Flächenlast w beaufschlagt werden.

Krümmungen bzw. Spannungen lassen sich jedoch nach dieser Formel wegen der sinusförmigen Ansatzfunktion der Lösung nur sehr ungenau, aber meist auf der sicheren Seite liegend, angeben.

4. SCHLUSSBEMERKUNGEN

Für den mit konstanter Flächenlast querbelasteten Plattenstreifen, der an den beiden liniengelagerten Rändern in Plattenebene elastisch gehalten ist, wird eine analytisch geschlossene Lösung angegeben. Ferner wird eine analytische Näherungslösung für die Last-Mittendurchbiegungsbeziehung einer vierseitig liniengelagerten und mit einer konstanten Flächenlast querbelasteter, rechteckiger Platte angegeben, welche die innere Membrantragwirkung der Platte berücksichtigt.

Meßwerte aus Bauteilversuchen werden mit Hilfe der angegebenen Gleichungen berechneten Werten gegenübergestellt. Versuchswerte und berechnete Werte stimmen gut überein.

Die angegebenen analytischen Lösungen ermöglichen somit, die Membrankrafteffekte von den genannten Plattentypen mit großen Durchbiegungen wirklichkeitsnah und im Vergleich zu numerischen Berechnungsverfahren wie z.B. mit der Methode der Finiten Elemente und mit dem Differenzenverfahren ohne Computereinsatz relativ einfach für praktische Fälle genügend genau zu berechnen.

LITERATUR

- [1] BARÈS, RICHARD, Berechnungstabeln für Platten und Wandscheiben. Bauverlag GmbH, Wiesbaden und Berlin (Germany), 3. Auflage, 1979, Seite 549.

Leere Seite
Blank page
Page vide

Compression Strength of the Profiled Face in Sandwich Panels

Résistance à la compression des parements profilés en acier
de panneaux sandwich

Druckwiderstand der profilierten Deckschicht von Sandwichbalken

Paavo HASSINEN

Civil Engineer
Technical Research Center
Espoo, Finland



Paavo Hassinen, born 1952, received his M.Sc. Eng. degree in civil engineering at Helsinki University of Technology. Since 1978 he has been working at Technical Research Centre of Finland in the Laboratory of Structural Engineering. In 1982–83 he worked as a post-graduate student at the Swiss Federal Institute of Technology in Zürich.

SUMMARY

In sandwich panels the foamed core effectively stabilizes the faces against buckling. The compression strength of the thin-walled metal face can be further increased by profilation. If, however, the widths of the flanges in the profiled face exceed a limit, local buckling becomes governing. Experimental and theoretical results for nonlinear behaviour of profiled steel face of sandwich panels with polyurethane core are presented.

RÉSUMÉ

Dans les panneaux sandwich, l'âme en mousse rigide assure la stabilité au voilement des parements en tôle d'acier. La résistance à la compression de ces derniers peut être augmentée par utilisation d'une tôle profilée. Cependant, si la largeur des ailes de la tôle profilée dépasse une certaine limite, le voilement local devient déterminant. Dans cet article sont présentés les résultats théoriques et expérimentaux de l'étude du comportement non-linéaire de la tôle d'acier profilée constituant le parement des panneaux sandwich à âme en mousse rigide de polyuréthane.

ZUSAMMENFASSUNG

In den Sandwichtragwerken stabilisiert die Kernschicht Deckschichten gegen das Beulen. Der Druckwiderstand der dünnen metallischen Deckschicht kann mit einer Profilierung noch erhöht werden. Falls die Breite des Flansches in der profilierten Deckschicht eine bestimmte Grenze überschreitet, wird das örtliche Beulen massgebend. In diesem Artikel werden experimentelle und theoretische Resultate über das nichtlineare Verhalten von Sandwichkonstruktionen mit einer profilierten Deckschicht und einem Polyurethan-Hartschaum-Kern dargestellt.



1. INTRODUCTION

One of the most important criteria in the design of sandwich panels is the compression strength of the faces. If the faces are flat the compression strength or so called wrinkling stress can be calculated by assuming the faces to be beams on a Winkler foundation or on an elastic half space (1). Depending on these assumptions and Poisson's ratio of the core the parameter k in the equation varies theoretically between 0.54 and 0.65.

$$\sigma_{kr} = k \cdot (E_c^2 E_f)^{1/3} \quad (1)$$

where E_c is Young's modulus for the core and E_f for the face material.

If the faces are slightly profiled the profilation can be taken into account in the parameter k or equation (1) can be changed to the form

$$\sigma_{kr} = \frac{k_1}{A_f} (E_c^2 B_f)^{1/3} \quad (2)$$

where A_f and B_f are the area and the bending rigidity of the face. Here the unit width has to be considered. Theoretically calculated k_1 varies between 1.34 and 1.44.

Because of the greater bending stiffness, in many roof panels one face or both are profiled (fig. 4). The behaviour of the flanges and the web of the profile can be studied by assuming them to be plates instead of a beam on a Winkler foundation or an elastic half space. Linke /3/ has based his geometrically nonlinear analysis on the Karmans equations of sheet and plate and further on the principle of the minimum of the total potential energy:

$$\sigma_u = f(b, t, E_f, E_c, f_y) \quad (3)$$

where b and t are the width and thickness of the profile and f_y the yield strength of the material. For compression strength the value of the stress can be chosen which on the most compressed fibers of the plate or of the foundation produces a stress the value of which is equal to that of yield strength.

The behaviour of the flange or the web of the profile can be studied using numerical methods and finite element codes too. Here it is possible to take into account geometrical and material nonlinearities of different kinds. Often all the material properties and imperfections of the structures are not known or they are too complicated to take into account in calculations. So experimental research for determining the parameters in calculation models are needed.

2. EXPERIMENTAL RESULTS

2.1 Test arrangements

For the study the behaviour of the thin steel face, sandwich panels with cross section shown in fig. 1 have been tested at the Laboratory of Structural Engineering in Technical Research Centre of Finland. The core in the panels was made of polyurethane foam. Its modulus of elasticity in flatwise direction was measured by repeated loading, which gave the average modulus $E_c = 3.2$ MPa

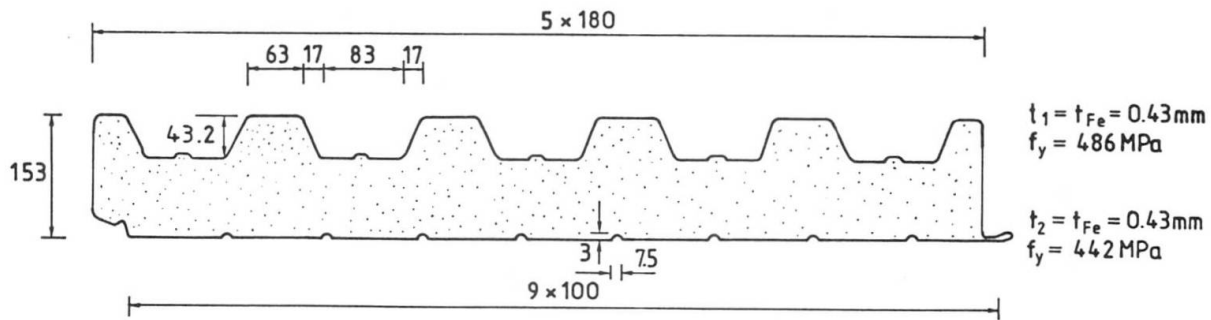


Fig. 1 Cross section of the sandwich panel used in the tests.

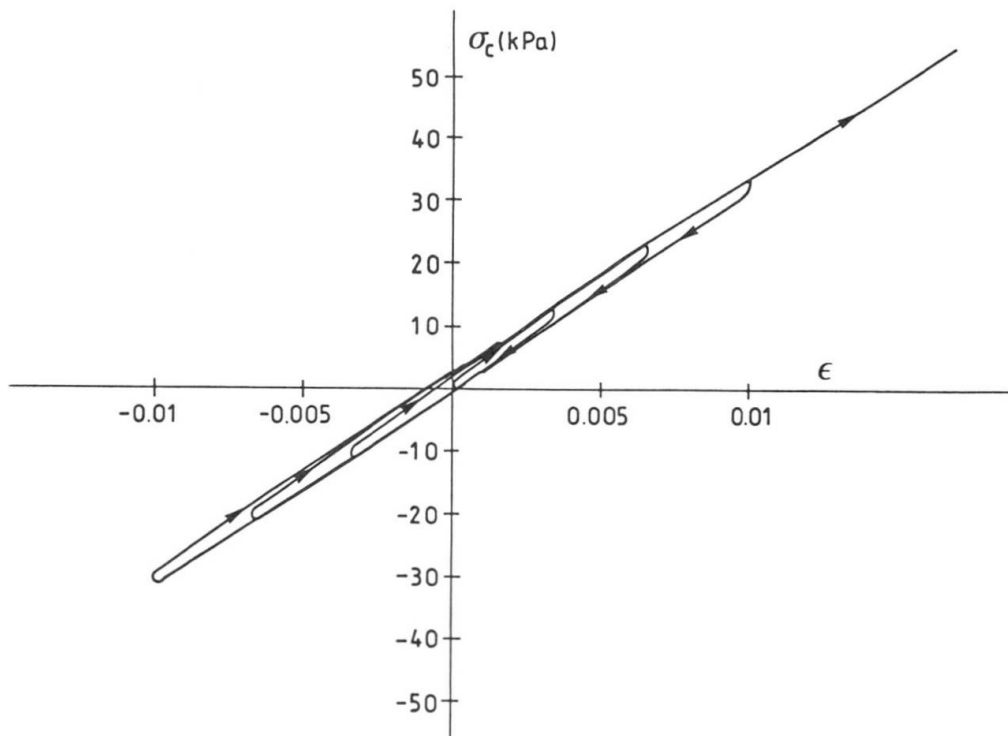


Fig. 2 The modulus of elasticity for the polyurethane core was tested by repeated loading.

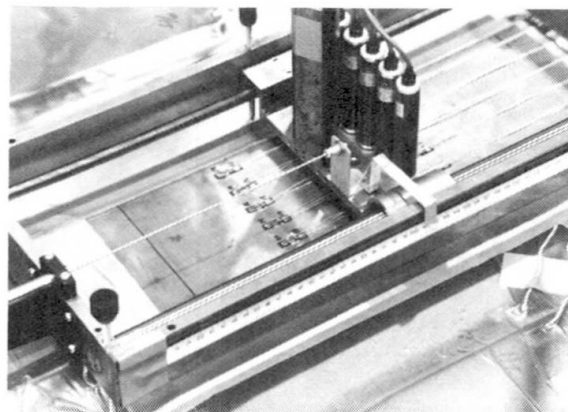


Fig. 3 The equipment for measuring the mode and amplitude of buckling wave in the compressed flange of a sandwich panel.

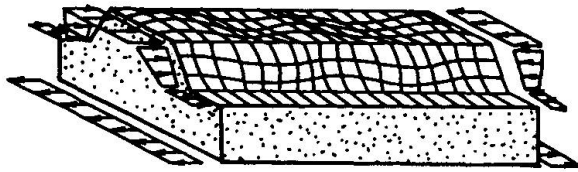


Fig. 4 Local buckling waves in the profiled face of a sandwich panel.

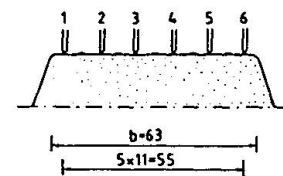
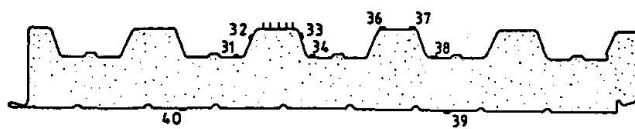
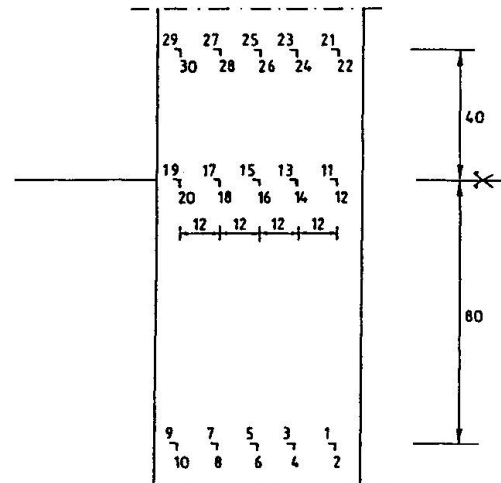


Fig. 5 The location of strain gauges and inductive displacement transducers for measuring the global and local deformations.

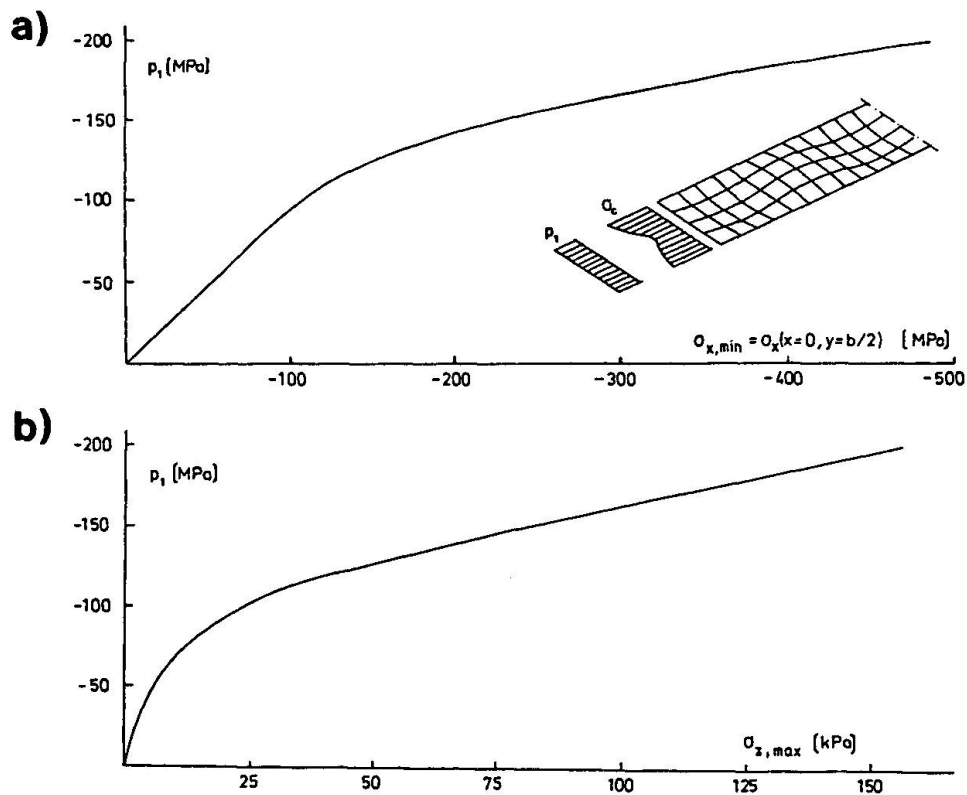


Fig.8 a) The computed compressive stress of the flange and b) the tensile stress of the joint of the tested sandwich panel using the method presented by Linke /3/. The initial deflection is $w_0 = 0.1 \cdot t$.

(fig. 2). The average tensile strength in flatwise direction was 180 kPa and Poisson's ratio 0,26. The panels were loaded as single span beams and the load was applied by a vacuum.

2.2 Results for the flat face

The compression strength of the very slightly profiled face was tested by three panels and the tests gave for the ultimate compression strength the average value of 218 MPa. Using the formula (1) and given modulus of elasticity for the core the value of the parameter k can be calculated. In this case k exceeds the value 1.68. If we take the slight profiles into account and use the formula (2) we get $k_1 = 1.32$.

The value of k is far above the evaluated theoretical limit and an apparent reason for that are the slight profiles. The value of k_1 is suitable regarding the theoretical values but in practice it is quite high, too. Polyurethane foam is a highly ortotropic material. Its properties depend on the orientation of ellipsoidal cells and the distribution of density. If the local buckling phenomenon is studied, the most important part of the cross section lies near the face, where normally the modulus of elasticity can be threefold compared to the average modulus. This increases the values of k and k_1 if the average modulus of elasticity is used. For a greater accuracy the distribution of the elastic properties of the core in the direction of height should be taken into account.

2.3 Results for the profiled face

The static behaviour of profiled face was tested by seven panels. A special measuring equipment was built for registration of the modes and amplitudes of local buckling waves (fig. 3). With a net of strain gauges measurements on the distribution of normal stresses over the cross section and especially in one compressed flange were carried out (fig. 5).

The displacements at four measuring lines and seven load levels for one element are presented in fig. 6. Using the data we can calculate the length of the half buckling wave to be 48 - 50 mm. The flange tends to buckle upwards from the initial flange level. The greatest amplitudes on the load level $F = 0.88 \cdot F_u$ are 2.5 mm and these are local displacements. This means that the core hardly can elongate as much below the elastic limit but the ultimate tensile strength of the the joint between the face and core is reached. The average ultimate tensile strains in flatwise direction over the whole height for this polyurethane core was found to be 2 - 3 %.

On the basis of measured strains it can be said that the flange begins to buckle on the load level $F = 0.30 F_u$ (fig. 7a). If the load has reached the level $F = 0.42 F_u$ the stresses in the corners between the flange and web begin to decrease. It means that somewhere in that flange the corners of the flange are loosing their stability too. If the load is still increased the resultant of compressive force tends to move from the upper flange to the lower flange of the upper profiled face (fig 7b). The reduction of the compressive rigidity of the upper flange and that of the whole upper face can be seen in the curves for global deflections. These curves are loosing their linearity on the load level $F = 0.6 F_u$ (fig. 7c). The ultimate load bearing capacity of the tested sandwich panel was $F_u = 27.0$ kN.



Using the nonlinear analysis presented by Linke /3/ and the given modulus of elasticity ($E_c = 3.2 \text{ MPa}$) and Poisson's ratio ($\nu = 0.26$) computed values for the length of buckling wave are 28 mm and for the critical stress 138 MPa. The first value is lower and the second higher than the corresponding measured ones, 48 - 50 mm and app. 80 - 90 MPa. The nonlinear analysis gives the curves for the maximum compressive stress of the flange and the tensile stress of the joint (fig. 8). According the results the yield strength of the face (fig. 1, $f_y = 486 \text{ MPa}$) is reached on the stress level $p = 200 \text{ MPa}$ (fig. 8a). If we utilize the experimental linear distribution of stresses at the beginning of the loading (fig. 7a, b, $F < 0.3 F_u$) we get the value for the ultimate load; $F_u = F (p = 200 \text{ MPa} = 0.00095 \cdot E_f) = 19.2 \text{ kN}$, which value is far below the experimental capacity $F_u = 27.0 \text{ kN}$. The stress level $p = 200 \text{ MPa}$ gives the value for the maximum tensile stress in the joint $\sigma = 155 \text{ kPa}$ (fig. 8b), which corresponds a local tensile strain $\epsilon = 4 \%$ in the core.

On the basis of the results it can be concluded that the flange of the profile should be analysed as a plate on a tensionless foundation. But because of the nonlinear behaviour of the upper face it is even with the results of this analysis not possible to evaluate exactly the ultimate capacity of the panel. In calculation we should take the decrease of the compressive and bending rigidity of the profiled face into account.

3. CONCLUSIONS

The compressive strength of flat and profiled faces in sandwich panels are studied on the basis of theoretical calculation models and experiments. If the flat or slightly profiled face of the panel is subjected to compressive stress, the behaviour of the panel is quite linear up to the compressive strength or the wrinkling stress of the face. In the case where profiled face is compressed the behaviour of the face and so the whole panel is quite complicated. The compressive and bending rigidities of the thin-walled face tend to decrease with the load because of the local buckling, which further depends on the tensile strength of the joint between the face and core layers. As an extreme case the compressed profiled face can be assumed to consist only of the lower flange of the profile in the ultimate limit state.

4. ACKNOWLEDGEMENT

The research concerning the theoretical analysis of sandwich panels has been made at Swiss Federal Institute of Technology in Zürich under the guidance of Prof. Dr. P. DUBAS and under the financial support of the SWISS GROUP of IABSE. The author wants to express appreciation of the valuable help. The author would also thank FOUNDATION OF TECHNOLOGY IN FINLAND for the grant for financing the experimental research.

5. REFERENCES

1. Stamm, K., Witte, H., Sandwichkonstruktionen. Berechnung, Fertigung, Ausführung. Springer Verlag, Wien 1974. 337 s.
2. Allen, H.G., Analysis and design of structural sandwich panels. Pergamon Press 1969. 283 s.
3. Linke, K-P., Zum Tragverhalten von Profilsandwichplatten mit Stahldeckschichten und einem Polyurethan - Hartschaum - Kern bei kurz- und langzeitiger Belastung. Dissertation, Technische Hochschule Darmstadt, Darmstadt 1978.

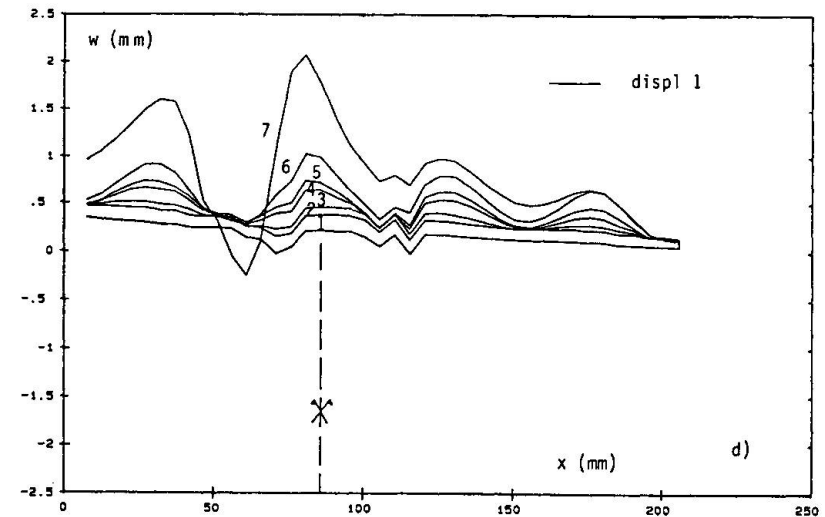
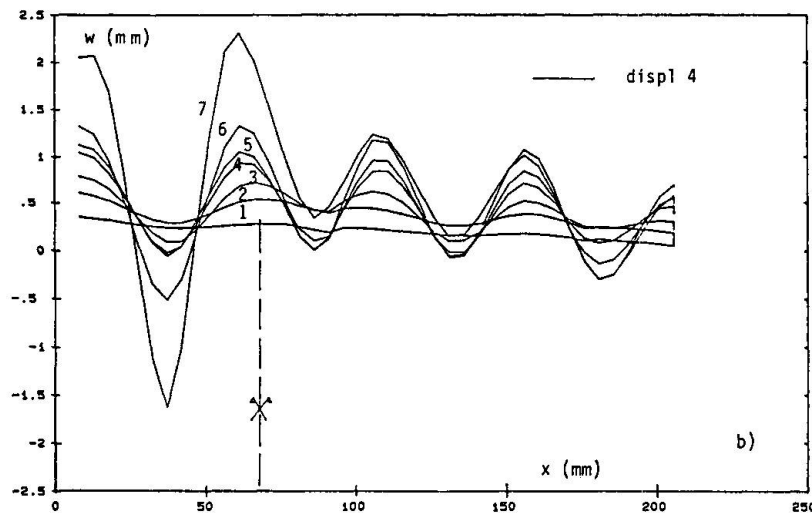
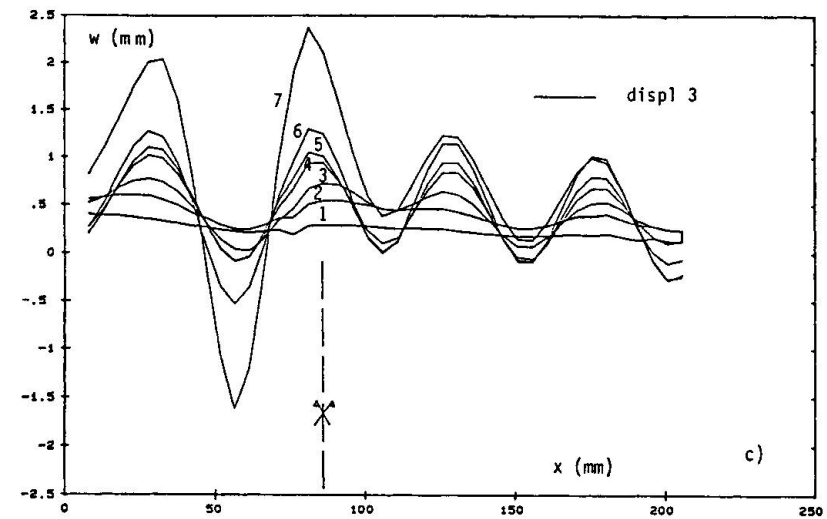
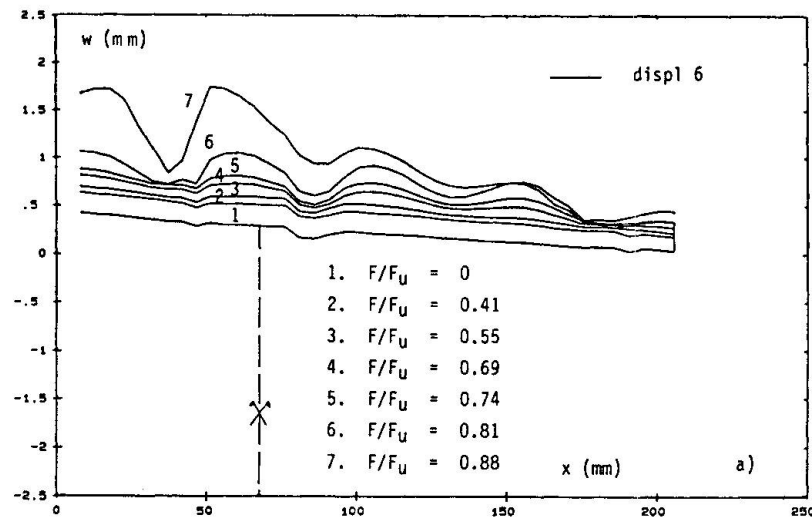


Fig. 6 Measured modes and amplitudes of buckling waves in the upper flange of the profiled face along four different measuring lines on seven different load levels. The locations of transducers see fig. 5.

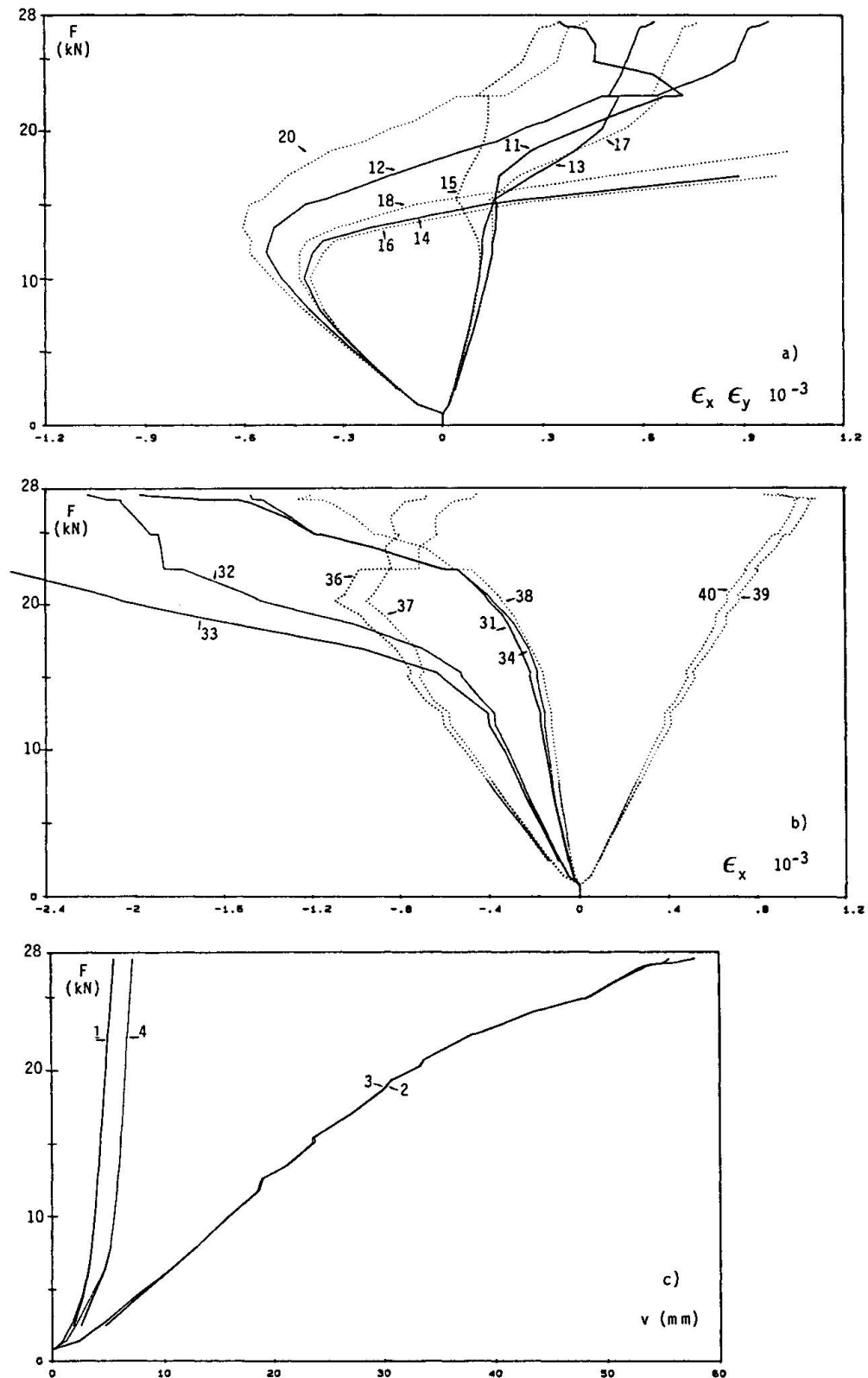


Fig. 7 Measured results for the sandwich panel:
a) strains ϵ_x and ϵ_y in five different locations on the upper flange in the centre of the element,
b) strains ϵ_x in different points of cross section in the centre of the element and
c) global displacements on the supports (1, 4) and in the centre (2, 3) of the element.

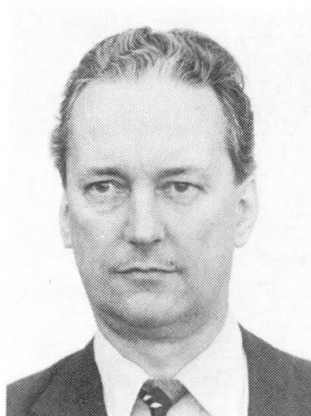
Built Up Roofs – Wind Uplift Resistance

Construction de toiture – Résistance de soulèvement au vent

Festigkeit gegen Windsaugkräfte von Dächern

Germund JOHANSSON

Assist. Prof.
Chalmers Univ. of Technology
Göteborg, Sweden



Germund Johansson, born 1937, received his civil engineering degree at Chalmers Univ. of Technology in 1962. After some years at a consulting firm for geotechnical problems he joined the Dep. of Steel and Timber Structures at Chalmers Univ. of Technology. His research interests are, among others, steel structures, roofs, and structural damage (due to snow, wind).

SUMMARY

Results from laboratory and in situ tests with glued fasteners (steel deck – insulation – roofing felt) are presented. It is shown how to predict the «strength on the roof» from the laboratory test results. The roofs tested have been retested 8 years later with the same equipment and these results show that the strength has been reduced – in some cases to a very low level. The paper includes a theoretical analysis of the behaviour of mechanical fasteners and a comparison with tests.

RÉSUMÉ

Les résultats d'essais en laboratoire et in situ sur des toitures collées (tôle profilée – isolation – étanchéité) sont présentés. On y montre comment prévoir la résistance in situ à partir d'essais en laboratoire. Les toits testés ont été soumis à de nouveaux essais huit ans plus tard, avec le même équipement; les résultats montrent que la résistance a diminué dans certains cas jusqu'à un niveau très faible. Cette contribution comprend une analyse théorique du comportement des attaches mécaniques ainsi qu'une comparaison avec les essais.

ZUSAMMENFASSUNG

Labor- und Feldversuche mit Klebverbindungen (Stahlblech – Isolation – Dachhaut) werden beschrieben. Die Ergebnisse zeigen, dass es möglich ist, eine wirklichkeitsnahe Voraussage der Festigkeit mit Hilfe der Laborversuche zu machen. Die Dächer sind acht Jahre später noch einmal getestet worden. Diese Versuchsergebnisse zeigen eine Reduktion der Festigkeit. In einigen Fällen war diese Reduktion ganz erheblich. Schliesslich wird eine theoretische Berechnungsmethode mechanischer Verbindungsmittel und ein Vergleich mit Versuchen angegeben.



1. INTRODUCTION

An externally insulated sheet metal roof consists of load-bearing trapezoidal metal sheet, thermal insulation and a covering surface. The insulation and the surface covering can be fixed to the sheet either by means of mechanical fasteners or by asphalt. Earlier the insulation were traditionally fixed to the sheet metal by bonding with warm asphalt. Nowadays often mechanical fasteners are used. In the case of mineral-wool insulated roofs the washers for these fixing devices are placed on the lower felt layer or, in certain cases, directly on the insulation.

A lot of tests have been carried out during the last decade – both laboratory tests and in situ tests. Due to the large number of tests it has been possible to predict the "strength on the roof" from the laboratory test results. The roofs tested have been retested 8 years later with the same equipment and these results show that the strength has been reduced – in some cases to a very low level.

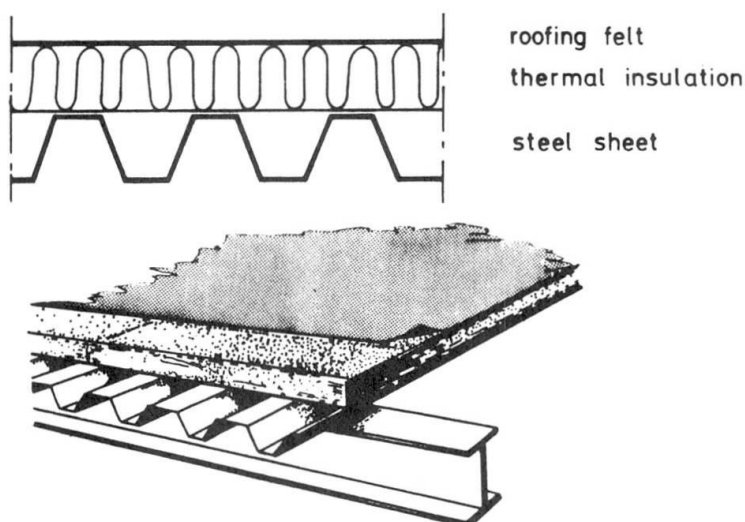


Fig.1 Built up roof

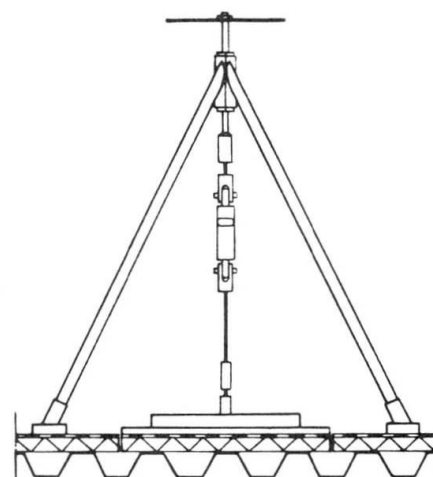


Fig.2 Test equipment for wind uplift testing

2. TEST EQUIPMENT AND TESTING PROCEDURE

The test equipment used consists of three main parts – a stand with lift outfit, a frame to be attached to the specimen and a dynamometer between the stand and the frame, fig.2. The stand is made of aluminium and wood. The lifting force is achieved via screw in the top of the stand. A 22 mm thick slab of chipboard was bonded with hot asphalt to the surface of the roofing felt. The width of the chipboard slab is 500 mm and the length is governed by the pitch of the steel sheet. After having glued the board slab and screwed the frame to the slab, the insulation and the roofing felt were cut along the slab lines. The test method is easy to handle but it has some disadvantages – the test surface is disturbed by cutting and by gluing with hot asphalt. However, some test roofs which showed very low strength have later blown off during storms and the roofs with high values for the strength have not done so.

It must be remembered that the test results are no more than values of the strength obtained by this test method. As far as reliability is concerned there is no doubt that roof with low measured strengths are exposed to a higher risk of damage than roofs with high measured strengths. Classification on the basis of the test results into roofs conforming to certain specifications and those which do not is a very doubtful procedure, and may easily lead to the wrong conclusions.

3. TEST RESULTS

In the middle of the 70's several roofs were tested with the equipment described. Twentyfive different roofs with insulation of fiber glass or mineral wool were tested with about ten specimens on each roof (200 in situ tests). The results showed a very large scatter, the maximum strength value obtained was more than twenty times the minimum value. The results are presented as a histogram in fig.3. The conclusion to be drawn is that the material quality and workmanship is not always what it ought to be. For instance, on one roof the lowest strength measured was 0.4 kN/m^2 and the highest 9.1 kN/m^2 , a difference as high as 8.7 kN/m^2 .

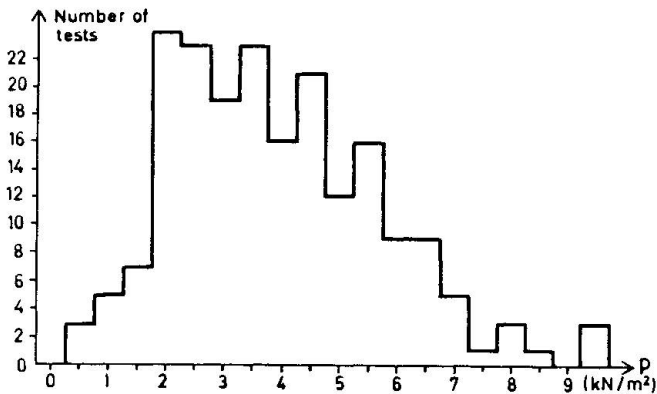


Fig.3 Measured strength of roofs with glass wool and mineral wool

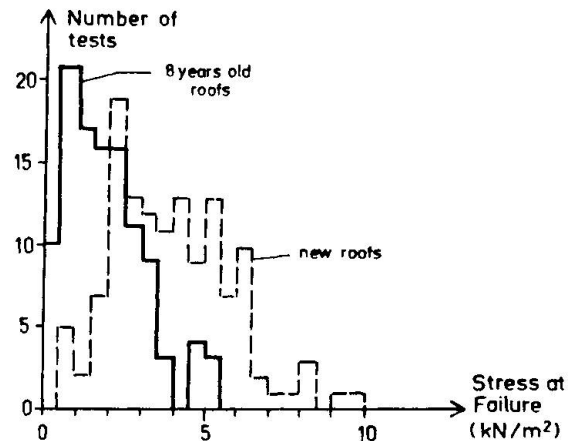


Fig.4 Measured strength of roofs with glass wool and mineral wool - comparison between old and new strength,

4. RETESTING

Eight years later, in the beginning of the 1980's, 13 of the roofs have been re-tested using the same equipment and the same technique. Some of the other roofs were "not available" for tests or they had blown off or they had been destroyed by fire. The results from the tests are a little bit frightening - there is a very large strength reduction. In table 1 some of the results are shown. After eight years the mean strength is reduced to about 50% of the original strength. The two histograms in fig.4 correspond to the measured strengths at all the roofs in table 1. The field tests show that for a new roof the fracture usually occur in the lower part of the insulation or between the insulation and the steel deck. Older roofs nearly always break in the upper part of the insulation just under the roofing felt.

5. THE SHEETING SURFACE

Unevenness of the sheeting surface has some effect on the strength. There does not seem to be a definite relationship, but approximate scatter range can be discerned. The relationship between strength and the measured deviation over three corrugations, Δ_3 , are plotted in fig.5 for 18 roofs. The conclusion which can be drawn from these figures is that a more even roof surface may increase the short-term strength, but need not necessarily do so.

Table 1 Measured wind uplift strength in kN/m^2 on roofs. The ratio in column (4) indicates the long-term strength reduction.

Roof no.	Mean uplift strength 1974-75	Mean uplift strength 1982-83	Ratio (3)/(2)
(1)	(2)	(3)	(4)
1	3,0	1,8	0,58
2	3,4	1,8	0,52
3	5,6	3,8	0,68
4	4,9	0,8	0,17
5	5,4	1,2	0,23
6	3,2	1,2	0,36
7	6,4	3,2	0,50
8	3,2	1,2	0,36
9	3,4	2,6	0,75
10	3,9	2,0	0,51
11	2,7	1,7	0,64
12	2,8	2,8	1,00
13	2,4	1,2	0,51
14	4,4	1,2	0,26



6. DIFFERENT TEST METHODS

The wind uplift strength depends mainly on two parameters - the strength of the insulation and the strength of the bonding between the insulation and the steel deck/roofing felt.

In pure material oriented laboratory tests only the insulation values are given. Several laboratory tests have also been made on specimens representing a cut-out part of a full roof.

It may be stated that a more realistic test method will lead to a lower measured strength. From several tests (≈ 200 specimens or more per group) the approximate relationship as shown in fig.6 were obtained. This means that after some years in service one may expect a rather low strength of the roof. If the initial strength is 10 kN/m^2 this value is reduced to about 1.5 kN/m^2 after a period of approximately 10 years in service. The risk for storm damages increases. The figures given above are mean values.

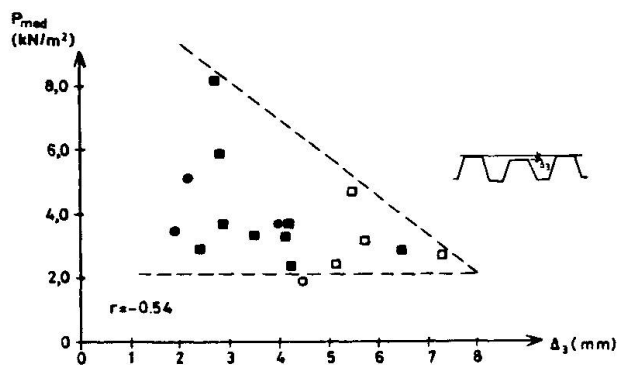


Fig.5 Relationship between measured strength (failure at sheeting - insulation interface) and measured flatness deviation Δ_3 for roofs insulated with mineral wool.

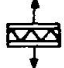

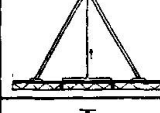
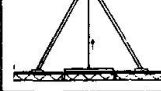
TEST METHOD	RELATIVE STRENGTH
 Material test	1.0
 Laboratory test	0.6
 Field test new roofs	0.3-0.35
 Field test old roofs	0.15

Fig.6 Dependence of strength on the test method

7. MECHANICAL FASTENERS

Storm damages due to the low strength have led to a new concept. Instead of using asphalt bonding most of the roofs nowadays have mechanical fasteners. This means that the requirements on the steel deck have been reduced and that the roof behaves in a different way. The use of mechanical fasteners on roofs have led to very few storm-damaged roofs. There are many different types but most of them consist of a screw and a washer. The fasteners are placed in a rectangular net, fig.7.

"Full scale tests" with suction box have shown that there is not linear relationship between the limit load and the number of screws mer m^2 if fracture occurs in the attachment between the water proofing membrane and the fastener. Usually fracture appears to be a combination of bending in the washer and punching of the membrane. The washer and its perimeter can be divided in four different parts where

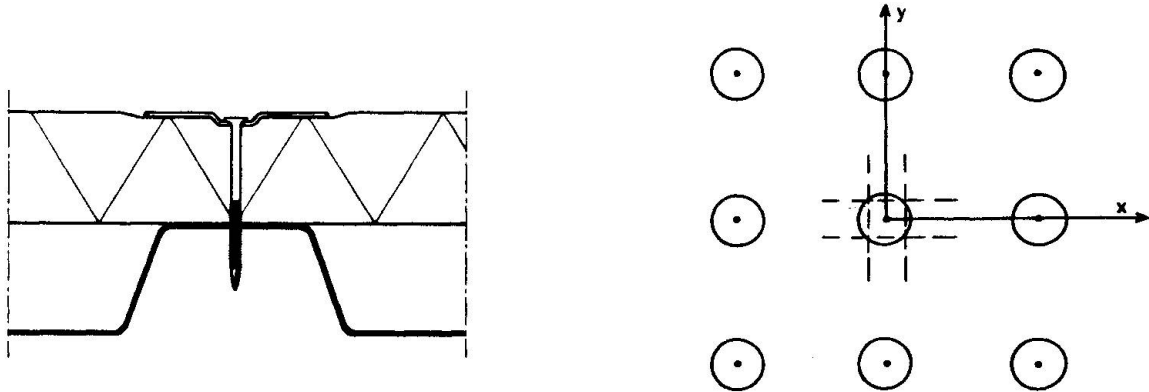


Fig.7 Mechanical fasteners. Possible folding lines for the washers are indicated.

the boundary between the areas inclines 45° degrees to the attachment lines. The load on the screw, the total force, is the sum of all the loads on the different areas, I-IV, fig.8. The maximum load of the fastener occurs when the load on any of the perimeters I, II, III, IV reaches its maximum (fracture) level. If the exterior load is assumed to be carried the nearest way from the membrane to the fastener we get the influence areas shown in fig.9. When the external load q causes fracture in the fastener the load on perimeter II is

$$P_{II} = q \cdot \frac{a}{2} (b - \frac{a}{2}) \quad (1)$$

The corresponding load at perimeter I is

$$P_I = \frac{a/2}{(b-a/2)} P_{II} \quad (2)$$

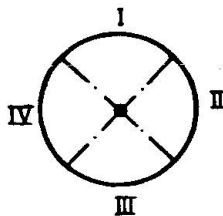


Fig.8 Washer

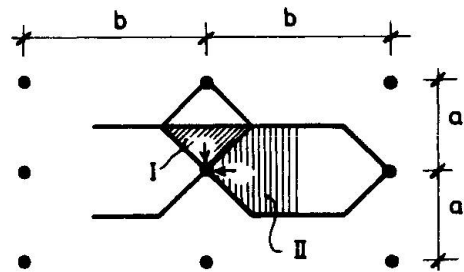


Fig.9 Influence areas. Area I = $a^2/4$

The total load on the fastener at rupture can be expressed as

$$P_{fast} = P_{II} (2 + a/(b - 0.5 a)) \quad (3)$$

The maximum load for the fastener is reached for $a = b$ and P_{max} is $4P_{II}$. The ratio a/b is governing the maximum load in the fastener and in fig.10 the ratio P_{fast}/P_{max} is shown.

$$P_{fast}/P_{max} = 0.5 + 0.5/(2 b/a - 1) \quad (4)$$

From eq (4) you will find that doubling the number of fasteners by changing from a quadratic net $a \times a$ to a rectangular net $\frac{a}{2} \times a$ will raise the external load by 33%. (P_{fast}/P_{max} decreases from 1 to 0.67) There have been conducted tests [2] on



different types of membranes and different spacings. Those results can be said to confirm the thoughts behind equation (4). In table 2 are given the theoretical and measured load ratios for four different membranes with the results from the specimen with $a = 0.4$ m as reference value. The theoretical values are the ratios between the influence areas. The membrane types 2 and 3 are fastened in a different way - that is why the ratios differ a little even for the same values of a and b . With regard to the fact that the number of tests is small one must say that there is a fairly good agreement between theory and practice.

Table 2 Comparison between calculated and measured load ratios, P_{fast}/P_{max} . The results from the specimen with $a = 0.4$ are used as reference values.

Membrane	b m	a m	Theory	Measured
Type 1	0.9	0.4	(1.0)	(1.0)
		0.6	1.29	1.31
		0.8	1.43	1.62
Type 2	0.9	0.4	(1.0)	(1.0)
		0.6	1.21	1.21
		0.8	1.31	1.34
Type 3	0.9	0.4	(1.0)	(1.0)
		0.6	1.21	1.24
		0.8	1.31	1.40
Type 4	1.2	0.4	(1.0)	(1.0)
		0.6	1.35	1.27
		0.8	1.6	1.53

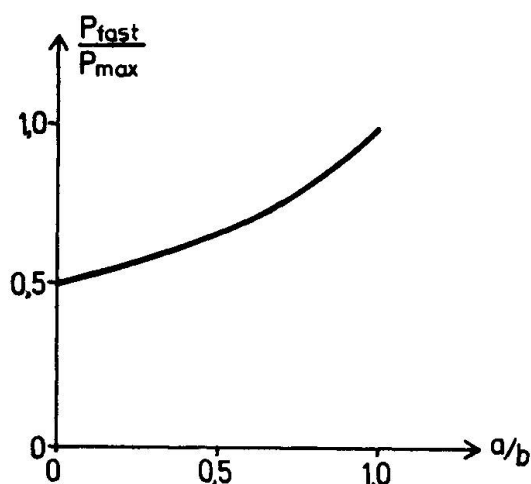


Fig.10 Maximum load in the fastener as a function of a/b

8. CORROSION

Fasteners on 14 different roofs, all situated on the Swedish West Coast have been examined. Totally 134 ($\approx 10/\text{roof}$) screws + washers have been removed and examined. The average age of these roofs was five years. Some little rust was found on 5% of the examined screws but no serious corrosion was found. No corrosion at all was found on the steel deck. The investigation indicates that corrosion of screws is not a great problem.

9. CONCLUSION

This paper is a summary of several research projects into the strength of built-up roofs against wind suction. The main conclusion is: Be careful with asphalt glued design — use mechanical fasteners (if possible equally spaced) instead.

10. REFERENCES

1. GULLBRANDSON B. - JOHANSSON G., Field investigation of externally insulated sheeting roofs. Document D15:1978. Swedish Council for Building Research.
2. NILSSON S., Roof membranes, mechanically fastened (in Swedish). Report R17:1985. Swedish Council for Building Research, Stockholm 1985.